NTNU
Det skapende universitet

Modellering av YPL Fluid Strømning i Eksentrisk Annulus med Borestrengsrotasjon

Henrik Sehested Næsgaard

Geofag og petroleumsteknologi
Innlevert: Juli 2012
Hovedveileder: Pål Skalle, IPT
Medveileder: Ramadan Ahmed, University of Oklahoma, Mewbourne School of Petroleum and Geological Engineering

Norges teknisk-naturvitenskapelige universitet
Institutt for petroleumsteknologi og anvendt geofysikk

LIST OF FIGURES **4**

LIST OF TABLES **6**

ACKNOWLEDGEMENT **7**

ABSTRACT **8**

SHORT SUMMARY IN NORWEGIAN/KORT SAMMENDRAG PÅ NORSK 9

1. INTRODUCTION **10**

1.1. OVERVIEW 10
1.2. STATEMENT OF THE PROBLEM 11
1.3. OBJECTIVES 12
1.4. APPROACH 13
1.5. SCOPE 14

2. LITERATURE STUDY **15**

2.1. OVERVIEW OF PREVIOUS STUDIES 15
2.2. EXPERIMENTAL STUDIES 17
2.2.1. Concentric annulus *17*
2.2.2. Eccentric annulus *17*
2.3. THEORETICAL AND NUMERICAL STUDIES 20
2.3.1. Concentric annulus *20*
2.3.2. Eccentric annulus *20*

3. THE FUNDAMENTALS IN ANNULAR FLOW OF DRILLING FLUIDS **25**

3.1. THE BEHAVIOUR OF ANNULAR FLOWS AFFECTED BY PIPE ROTATION 25
3.1.1. Drillstring Motion and Vibration *25*
3.1.2. Secondary Flows and Taylor Vortices *25*
3.1.3. Shear-Thinning Effects *27*
3.1.4. Geometric Irregularities and Inertial Effects *28*
3.2. THEORETICAL MODELING OF ANNULAR FLOWS 30

4. DEVELOPMENT OF NEW MODEL BASED ON THE DIRECT NUMERICAL SOLUTION, THE DIVIDING OF AN ECCENTRIC ANNULUS INTO SEVERAL CONCENTRIC ANNULUS AND A CORRELATION FOR INERTIAL EFFECTS **33**

4.1. CONCENTRIC ANNULI WITH ROTATION 34
4.2. REPRESENTING AN ECCENTRIC BOREHOLE BY SEVERAL CONCENTRIC BOREHOLES 36
4.3. EMPIRICAL CORRELATION FOR INERTIAL EFFECTS 38
4.4. THE CODE PROCEDURE 39

5. VALIDATION OF THE MODEL **40**

5.1. COMPARISON TO NUMERICAL MODELS 40
5.1.1. Comparison to Escudier et al. (2000) for Newtonian fluid *40*
5.1.2. Comparison to Escudier et al. (2002) for Power Law fluid *42*
5.2. COMPARISON TO LABORATORY MEASUREMENTS 44
5.2.1. Comparison to Walker and Al-Rawi *44*
5.2.2. Measurements by Ahmed and Miska (2008) *52*
5.3. TEST RUNS-STUDY 64

6. DISCUSSIONS **69**

6.1. LIMITATIONS 69

6.1.1. Limitations of the model *69*

6.1.2. Limitations of the data *73*

6.2. RECOMMENDATIONS FOR FUTURE WORK ON THE NEW MODEL 74

7. CONCLUSIONS **75**

NOMENCLATURE **76**

REFERENCES **79**

APPENDIX A – DATA FROM WALKER AND AL-RAWI (1970) **86**

APPENDIX B – DATA FROM ESCUDIER ET AL. (2000) **89**

APPENDIX C – DATA FROM ESCUDIER ET AL. (2002) **91**

APPENDIX D – PROGRAM CODE OF THE NEW MODEL **95**

APPENDIX E – ERROR SOURCE FOR NO CONVERGENCE OF LOW FLOWRATES **120**

List of figures

Figure I- Slot equivalents of concentric and eccentric annuli, Iyoho and Azar (1981). 18
Figure II- Pressure gradients in eccentric annular flow of Power-Law fluids (left) and Bingham-plastic fluids 18
Figure III - Influence of inertia on the pressure drop, Ooms et al. (1999). 21
Figure IV - Ratio of friction factors as a function of eccentricity, Ooms et al. (1999). 21
Figure V - Variation of frictional pressure loss as a function of eccentricity and Taylor number (κ=0.2) 22
Figure VI- The effect of eccentricity on the stream function (ψ) and axial velocity (w/wm) distribution 23
Figure VII-The effect of radius ratio on the stream function (ψ) and axial velocity (w/wm) distribution 23
Figure VIII- Schematic of the Taylor-Couette system. The outer cylinder is not rotating, Avila (2012). 25
Figure IX -Flow with rotating inner cylinder, Hussain (1999). 26
Figure X-Taylor vortices, Yamada (1962). 26
Figure XI- Axisymmetric Taylor vortices and wavy vortices 27
Figure XII- Shear-thinning Non-Newtonian flows (dotted line) and Newtonian flows (full line) 27
Figure XIII - Viscosity distribution in eccentric borehole (Power Law fluid, n=0,75), Elias (2004). 28
Figure XIV - From left to right: concentric borehole, partially eccentric borehole and fully eccentric borehole . 29
Figure XV - Streamline distribution in eccentric borehole (Power Law fluid, n=0,75), Elias (2004). 29
Figure XVI – Newtonian turbulent velocity distribution (NRe=20 000, D=1 in., water at 20°C) 31
Figure XVII – Newtonian fractional flow contribution, Dodge and Metzner (1959). 31
Figure XVIII- Chart of the development steps in the creation of the new model. 33
Figure XIX- YPL flow in concentric annulus, Ahmed and Miska (2008). 34
Figure XX- Eccentric Annuli, Luo and Peden (1990). 36
Figure XXXII- Calculated fRe against true fRe for Newtonian flow. 40
Figure XXXIII- Calculated fRe against true fRe for Power Law flow. 42
Figure XXXIV- Calculated fRe against true fRe for both Newtonian and Power Law flow. 43
Figure XXIV- Comparison to data from Table 2 by Walker and Al-Rawi for velocity equal to 11.2 ft/min 44
Figure XXV- Comparison to data from Table 2 by Walker and Al-Rawi for velocity equal to 6.8 ft/min 45
Figure XXVI- Comparison to data from Table 3 by Walker and Al-Rawi for velocity equal to 17.7 ft/min 46
Figure XXVII- Comparison to data from Table 3 by Walker and Al-Rawi for velocity equal to 14.2 ft/min 47
Figure XXVIII- Comparison to data from Table 3 by Walker and Al-Rawi for velocity equal to 10.7 ft/min 47
Figure XXIX- Comparison to data from Table 4 by Walker and Al-Rawi for velocity equal to 18.0 ft/min 49
Figure XXX- Comparison to data from Table 4 by Walker and Al-Rawi for velocity equal to 14.6 ft/min 50
Figure XXXI- Comparison to data from Table 4 by Walker and Al-Rawi for velocity equal to 7.3 ft/min 51
Figure XXXV- Comparison to Table 4 from Ahmed and Miska (2008). 52
Figure XXXVI- Comparison to Figure 4 from Ahmed and Miska (2008). 53
Figure XXXVII-Comparison to Figure 11 from Ahmed and Miska (2008). 54
Figure XXXVIII- Comparison to Figure 5 from Ahmed and Miska (2008). 55
Figure XXXIX- Comparison to Figure 7 from Ahmed and Miska (2008). 56
Figure XL-Comparison to Figure 8 from Ahmed and Miska (2008). 57
Figure XLI-Comparison to Figure 12 from Ahmed and Miska (2008). 58
Figure XLII- Comparison to Figure 9 from Ahmed and Miska (2008). 59
Figure XLIII- Comparison to Figure 13 from Ahmed and Miska (2008). 60
Figure XLIV- Comparison to Figure 10 from Ahmed and Miska (2008). 61
Figure XLV-Comparison to Figure 14 from Ahmed and Miska (2008). 62
Figure XLVI-Comparison to Figure 15 from Ahmed and Miska (2008). 63
Figure XLVII- Pressure loss versus eccentricity for a PL fluid 65
Figure XLVIII-Pressure loss versus rotation speed for PL fluid 65

Figure XLIX- Pressure loss versus eccentricity for a YPL fluid 66
Figure L- Pressure loss versus rotation speed for Yield-Power Law fluid 67
Figure LI-Pressure loss versus fluid behavior index for PL fluid 67
Figure LII - Pressure loss versus flow behavior index for YPL fluid 68
Figure XXI- The function of $fRew/fRe0$ against eccentricity for different Taylor numbers for κ=0.2. 70
Figure XXII- The function of $fRew/fRe0$ against eccentricity for different Taylor numbers for κ=0.5. 70
Figure XXIII- The function of $fRew/fRe0$against eccentricity for different Taylor numbers for κ=0.8. 70
Figure LIII- Change in Reynolds number with rotation speed for a specific case 94
Figure LIV - Flowrate versus Pressure Loss in the case of no convergence 120

List of tables

Table A- Summary of previous investigations on the effect of pipe rotation on annular pressure loss 16
Table B- Typical drillpipe and hole sizes, Aadnoy et al. (2009). 31
Table C- Error table for calculated fRe against true fRe for Newtonian flow. 41
Table D- Error table for calculated fRe against true fRe for Power Law flow. 42
Table E- Error table for calculated fRe against true fRe for both Newtonian and Power Law flow. 43
Table F- Inputs for the Power Law and Yield-Power Law fluid 64
Table G – Calculated flowrate against pressure loss in the case of no convergence 121

Acknowledgement

I would like to greatly thank my advisors Ramadan Ahmed, Assistant Professor at the Mewbourne School of Petroleum & Geological Engineering (MPGE), University of Oklahoma (OU), Oklahoma, United States and Pål Skalle, Associated Professor of the Department of Petroleum Engineering and Applied Geophysics (IPT), Norwegian University of Science and Technology (NTNU), Trondheim, Norway.

I would also like to thank the faculty and staff at the Mewbourne School of Petroleum & Geological Engineering for welcoming me as an exchange student and for their support throughout the academic school year of 2011/2012.

My appreciation goes out to the employees at NTNU that supported me in my choice of leaving the country during the final year of my Master degree studies, including the staff at IPT NTNU and at the International Section NTNU.

Abstract

The drilling of slimholes, extended reach wells and deepwater wells requires accurate bottomhole pressure (BHP) predictions because of the small annular clearance, long horizontal departure, and narrow operating pressure window. The effect of drill string rotation on pressure loss has been investigated before and the general consensus is that pipe rotation has a positive effect on pressure drop. In several numerical and theoretical studies, the effect has been found to mainly show the opposite effect, namely a decrease in pressure drop. Numerical and theoretical approaches to model the annular flow in eccentric annulus with inner pipe rotation is made especially difficult because of the inertial effects associated with pipe rotation.

In this thesis, theoretical modeling of the pressure loss in eccentric annulus with pipe rotation has been conducted. The approach was to use an existing model for concentric boreholes with drill string rotation and systematically incorporate the effects of eccentricity and acceleration of the flow. Eccentricity of the annulus was approximated by several sectors of concentric annuli with varying radii. For the inertial effects, a correlation was developed based upon analysis of published numerical data on Newtonian and Non-Newtonian flows. The model was programmed into a code, which can give pressure loss as an output, with flow rate, rotation speed, rheological parameters, annulus size and eccentricity as inputs.

Simulations with the program were compared with published field and laboratory data. Compared to a set of data from a study on concentric boreholes with pipe rotation, the results are excellent. In comparison to numerical data on the calculation of frictional pressure loss of Newtonian and Power-Law fluids, the results are satisfying. The model captures the pressure loss trends of measured experimental data well. The new model is recommended for field use due to its simplicity and fast calculations.

Short summary in Norwegian/Kort sammendrag på norsk

Stadig flere slimholes, ERD og dypvanns-brønner blir boret. Disse typer brønner stiller store krav til kontroll av trykk i ringrommet. Rotasjon av borestreng er en spesielt vanskelig effekt å modellere på grunn av dets konsekvenser som inkluderer skjær-fortynnende effekter og akselerasjon av strømningen.

Denne oppgaven omhandler teoretisk modellering av trykktap grunnet rotasjon i eksentriske borehull med Herschel-Bulkley strømning. En eksisterende modell for trykktap for konsentriske borehull ble videreført til å inkorporere borerrørets eksentrisitet ved å fremstille ett konsentrisk borehull med flere konsentriske borehull med varierende radier. Gjennom å studere numeriske resultater for trykktap for både Newtonske og ikke-Newtonske strømninger i ringrommet, ble en korrelasjon for trykktap grunnet akselerasjon av strømningen laget som en funksjon av viktige parametere. Disse inkluderer Taylor nummer, eksentrisitet og radiusforhold (borerør- mot ringrom-radius). Den nye modellen kan altså beregne trykktap i ringrommet i eksentriske borehull med effekten av rotasjon (skjær-fortynnende og akselerasjon av strømmen inkludert); eller enklere scenarioer hvis det er ønskelig.

Modellen ble skrevet til et enkelt program som kan brukes i felten. Programmet ble videre validert mot eksisterende numeriske data og feltdata. Resultatene var svært gode for konsentriske borehull og trendene ble riktig regnet. Trendene for Herschel-Bulkley strømninger var ikke like gode som for de andre fluidene i eksentriske borehull, men anses fortsatt som tilfredsstillende.

1. Introduction

1.1. Overview

Field measurements show that there is an increase in bottomhole pressure with pipe rotation and this effect needs to be analyzed and modeled. Accurate prediction will allow for better planning of slimholes, extended reach wells and deepwater wells; in which the small annular clearance, long horizontal departure, and narrow operating pressure window significantly affect downhole hydraulics.

In this thesis, theoretical modeling of Yield-Power Law (YPL) flow in eccentric annulus has been conducted. The approach was to adopt the existing numerical solution for YPL flows in concentric annulus with drillpipe rotation for eccentric annulus. This model was extended systematically to include eccentricity of the inner pipe by dividing the eccentric annulus into several sectors of concentric annuli with varying radii. Correlations from available numerical and theoretical data were developed to account for the inertial effects due to acceleration of the flow for both Newtonian and Non-Newtonian fluids. A program was created to run simulations with these assumptions. It was then possible to evaluate the accuracy of this theoretical approach by comparing with laboratory and field data published in the literature.

1.2. Statement of the Problem

The modeling of the flow in the annulus is important in order to accurately predict the pressure loss, and subsequently, the bottom hole pressure. The borehole geometry is usually eccentric due to inclination and the swirling movement of the drillpipe. The rotation of the drill string also creates a flow that is superimposed on the axial, pressure-driven flow from the mud pumps. It is generally believed in the industry that drillstring rotation has a positive effect on cuttings transport. The movement of the pipe stirs the mud and stimulates movement of the particles. However, the effect of rotation is more complicated and is a combination of several effects: shear thinning, flow regime transition from laminar to turbulent, formation of Taylor vortices, inertial/acceleration effects, secondary flows, drill pipe eccentricity and wobbling effects, suspension of cuttings and tool joint effect. It is of importance to model bottomhole pressure (BHP) changes due to this effect. New technology and methods like casing while drilling and slimhole drilling are strongly relying on accurate prediction of BHP, because of the very small annular clearance.

The challenge in modeling the shear-thinning contribution due to pipe rotation is due to the inertial effects (acceleration of the flow). The inertial effects will counteract the decrease in pressure loss and are difficult to model. The approach was to come up with a correlation based upon an analysis of available numerical data on pressure loss.

To date, there is no simple model to calculate pressure drop in an eccentric annulus with drillpipe rotation and bulk YPL fluid flow. It is desired to create a field-friendly model, thus complex calculations in spherical coordinates was avoided. The model was neither made too simple, as not to overlook a hydraulic effect that influences BHP significantly. Therefore, the model accounted for drill string rotation and eccentricity, and works for YPL fluid flows, which is the most common rheology model for drilling muds. By studying the results from the new model, a better understanding of inertial effects can be obtained. Few studies have concentrated on quantifying these effects.

1.3. Objectives

When drilling a well with narrow pore pressure window (small difference between pore pressure and fracture pressure) reliable BHP predictions are needed, for example for deepwater operations.
It has already found out that there is considerable difference between theoretical representation of the annular flow and laboratory or field experiments, which involves more complex flow patterns such as wobbling, whirling, formation of secondary flows and turbulence. In order to develop a better understanding of this effect, it is imperative to achieve the following goals:

1. Develop an accurate model to predict pressure loss in the eccentric annulus with inner pipe rotation for YPL fluid.
2. Better understand the effects of rotation, eccentricity, shear-thinning and inertial effects on the pressure drop.
3. Optimize wellbore hydraulics, especially for boreholes with small annular clearances.
4. Manage ECD (Equivalent Circulating Density) within narrow pressure windows.
5. Create a simple field-friendly model for calculation of pressure loss.

1.4. Approach

Recently, a hydraulic model (Ahmed and Miska 2008) for YPL fluids in concentric borehole with drillpipe rotation has been developed. This model is based on Coleman and Noll's (1959) analytical solution for helical flow of generalized fluids, which had no other assumptions than fluid incompressibility. Ahmed and Miska's (2008) solution was specified for YPL flow.

In this study, the concentric model was adopted to provide hydraulic predictions for eccentric boreholes by approximating the eccentric annulus with several sectors of concentric annuli of different radii, an approach developed by Luo and Peden (1990).

The concentric annulus-based model does not account for inertial effects, a phenomenon, which only occurs in eccentric annular flows. In order to account for inertial effects, a correlation was derived from analyzing data from Escudier et al. (2000, 2002) for both Newtonian and Non-Newtonian flows. Newtonian flows are not affected by shear-thinning and are therefore best suited for studying these inertial effects. Most drilling fluids are non-Newtonian however, so the correlation was adopted for Non-Newtonian fluids.

The final model was programmed to run several simulations to compare its validity with published numerical results and measurements. By nullifying shear-thinning effects, it is possible to observe the impact of the flow acceleration on pressure drop, and vice-versa.

1.5. Scope

The scope of this work includes theoretical modeling studies of YPL fluid flow in eccentric boreholes to be able to accurately predict pressure loss in the annulus of a drilling bore well. A special focus was given towards modeling and quantifying separately the inertial effects and shear-thinning effects due to pipe rotation.

A program created using the model was utilized to validate the approach with available numerical and theoretical solutions in the literature.

The successful completion of the project and achievement of these objectives would offer the industry with a new means to procure reliable prediction of downhole pressures, thus reducing dangers related to drilling in zones with narrow pressure window. It will also help understand the impact of inertial effects on pressure loss.

2. Literature Study

2.1. Overview of Previous Studies

A number of previous studies have been published that focused on the theoretical and computational analysis of the flow of generalized fluids in annulus. Many earlier studies described flow in pipe and a concentric annulus without inner pipe rotation. Later, when it was discovered inherent to include drillpipe rotation, a number of papers have been written on helical flow. The focus has also been toward the effects of eccentricity and drill pipe rotation on the wellbore design. More recently, the situation that is the most comparable to the field conditions has been investigated, namely flow through an eccentric annulus with drillpipe rotation.

It has already been found out that there is substantial difference between flow conditions in laboratory pilot tests and field operations. Laboratory setups have a tendency of minimizing inertial effects, while field conditions favor inertial phenomena such as wobbling, whirling, agitation of cuttings, geometric irregularities and axial reciprocation. A summary of results (Table A) from a previous study by Ahmed and Miska (2008) on the effect of pipe rotation, show an increase in pressure loss. Wobbling is especially difficult to model and may be the reason for the discrepancies between the theoretical/lab results and the measurements experienced in the field. These trends have been pointed out by Cartalos et al. (1992) and Marken et al. (1992).

Field measurements that demonstrate that the frictional pressure drop is dependent on drillpipe rotation are several (Luo and Peden 1990; Bailey and Peden 1997; Ward and Adreassen 1998; Isambourg et al. 1998; Charlez et al. 1998; Green et al. 1999; Wang et al. 2000; Diaz 2002; Diaz et al. 2004; Hemphill et al 2007). The same deductions were made for field measurements for slimholes (see Bode et al. 1991; Marken et al. 1992; Delwiche et al. 1992; McCann et al. 1995).

Table A- Summary of previous field and laboratory investigations on the effect of pipe rotation on annular pressure loss. Ahmed and Miska (2008).

Year	Reference	Annular Geometry	Eccentricity	Fluid	Flow Rates	Length	RPM	Test	Conclusion
1962	Yamada[1]	$\kappa = 0.90$ to 0.99, $D_o = 2.5$"	0.0	Water	Re: 100 to 30,000	1.1 ft	90 to 5000	Lab	+
1970	Walker and Al-Rawi[2]	1.75" X 1.9"	0.0	Bentonite	Up to 0.4 gpm	3 ft	0 to 300	Lab	-
1991	Bode et al.[8]	3.7" X 4.4" & 2.8" X 3.1"	Vertical Wells	WBM/OBM	Up to 50 gpm	6500 ft	0 to 600	Field	+
1992	Delwiche et al.[9]	3.5"x3.9", 3.5" x 4.4", 3.5" x 5" & 5"x13.4"	Vertical	Polyglycerol & K_2CO_3 Muds	160 gpm	4000 ft	0 to 370	Field	+
1993	Marken et al[10]	9.6" × 5.0" (DP) and 9.6" × 6.5" (DC)	Vertical/Inclined Well	OBM	238 to 476 gpm	984 ft to 4904 ft	0 to 120	Field	+
1993	McCann et al.[11]	3.7" X 4.4" 1.25" X 1.5"	Vertical 0 to 1.0	Water/Gel Rev dust/HEC	Up to 150 gpm 12 gpm	1424/2417 ft 4 ft	0 to 600 0 to 900	Field Lab	+ ±
1994	Nouri, and Whitelaw[3]	0.79" x 1.59"	0.0	Glycerol and CMC solutions	Up to 31.70 gpm	≈ 10 ft	0 to 300	Lab	+
1995	Hansen et al.[4]	1.25" × 1.57"	0.1 to 0.5	CMC	4 to 63 gpm	13 ft	0 to 700	Lab	±
1997	Wei[5]	4.5" x 8"	0.0 – 0.75	PAC, HEC & XG	150 to 350 gpm	85 ft	0 to 120	Lab	±
1999	Hansen et al.[6]	2.0" X 1.75"	0 to 0.7	CMC & XG	Up to 132 gpm	13 ft	0 to 600	Lab	±
2000	Wang et al.[12]	6" X 3.5" 5" X 3.5" & 5" X 3.0"	Inclined Well 0.0 to 0.6	- MMH Fluids	Up to 266 gpm Up to 308 gpm	5660 ft 20 ft	Up to 270 Up to 200	Field Lab	+ +
2004	Diaz et al.[13]	12.42" X 11.75" 4.5" X 6.37" & 5" X 6.25"	Vertical/S. Inc. Vertical	- Bentonite	- 350 to 550 gpm	- 300 - 500 ft	- 0 to 180	Field Field	+ +
2005	Woo et al.[7]	$\kappa = 0.52$, 0.8 & 0.9	0.0	CMC & Bentonite	Re: 100 to 5000	1.7 ft	0 to 500	Lab	+

The importance of accurate prediction of friction pressure loss was pointed out by Bode et al. (1991) in their work about slimhole wells. Slimholes have smaller annular clearances than conventional wellbores and may experience higher frictional pressure loss. During conventional drilling, frictional pressure drop is said to account for 10 %, however Bode et al. (1991) reported that for slimhole wells this number could be as high as 90 %. Cartalos and Dupuis (1993) studied the flow in an eccentric annulus with inner pipe rotation, with a special focus on slimhole drilling. Slimhole drilling was made popular for its cost advantages, being more compact and easier to transport to rigs and accelerated drilling programs. The reduced borehole diameter raises new hydraulic issues. The specific geometry also poses restrictions to the drilling fluid design.

In addition to its hydrodynamic effects, the rotation of the inner pipe produces centrifugal action that may cause flow instabilities, which can generate secondary flows such as Taylor vortices. As a result, the study of flow instability due to inner pipe rotation has received great attention, since Lord Rayleigh (1880) discovered the existence of flow instabilities in annular flow with inner string rotation. The flow separation that occurs, and the kidney-shaped vortex that is created by eccentric annular flow with drillstring rotation, were studied by several authors (Kamal 1966; Ballal and Rivlin 1976; San Andres and Szeri 1984; Ho Tung et al. 1993; Siginer and Bakhtiyarov 1998).

Takeuchi and Jankowski (1982) and Lockett (1992) demonstrated that the onset of Taylor vortices can be delayed to higher Taylor numbers by bulk axial flow. Besides this, Lockett (1992) also showed through his numerical work that the occurrence of Taylor vortices can be suppressed by eccentricity of the pipe. His results were consistent with previous experimental observations reported by Kamal (1966), Cole (1968), Vohr (1968) and Castle and Mobbs (1968).

2.2. Experimental studies

2.2.1. Concentric annulus

Helical flow of non-Newtonian fluids in concentric and eccentric annuli has been studied in the laboratory (Yamada 1962; Walker and Al-Rawi 1970; Nouri and Whitelaw 1994; Hansen and Sterri 1995; Wei 1997; Hansen et al. 1999; Woo et al. 2005; Ahmed and Miska 2008) to evaluate the effect of pipe rotation on pressure loss. Most of these studies showed mixed trend (i.e. both positive and negative effects of pipe rotation on annular pressure loss).

Yamada (1962) conducted an earlier experimental study on concentric annulus with inner pipe rotation using water as test fluid. Very narrow annular clearance ($1 > \kappa \geq 0.897$) was considered for the investigation. Higher values of hydraulic resistance (fRe) for increasing rotation speed was reported. A more advanced experimental study (Escudier and Gouldson, 1995, 1997) was performed to study the velocity profile and friction factor in annulus with fixed diameter ratio (κ=0.506) while varying the pipe eccentricity. The frictional pressure loss was reported to increase with rotation speed. A similar study (Nouri and Whitelaw, 1994), conducted using a different annular geometry showed an increase in the friction factor with inner pipe rotation under laminar flow conditions. However, a study (Walker and Al-Rawi, 1970) conducted using highly shear thinning bentonite slurry demonstrated a decrease in annular pressure losses with the increase in rotation speed for a laminar helical flow. These results were regarded as a confirmation of the exact solution by Coleman and Noll (1959). More recently, Ahmed and Miska (2008) corroborated all the previous studies to confirm that pressure loss could increase or decrease with increasing drillpipe rotation speed.

2.2.2. Eccentric annulus

An analytical solution for eccentric annular flow is only available for Newtonian fluids. An analytical solution for non-Newtonian fluids is difficult to develop due to non-linearity of the model equations. To better understand the flow and to develop an approximate model, several investigators (Mitsuishi and Aoyagi 1973; Iyoho and Azar 1981; Luo and Peden 1990; Walton and Bittleston 1991) studied the effect of eccentricity on annular pressure loss in eccentric annulus with non-Newtonian fluids. The pressure drop was observed (Mitsuishi and Aoyagi, 1973) to be decreasing with increased eccentricity. An approximate model (slot model shown in Figure I) was developed (Iyoho and Azar,1981) using an analytical approach to the problem of non-Newtonian fluid flow through eccentric annuli. Results indicated that local velocity values greatly reduce in the narrow region of an eccentric annulus. The overall effect showed (Figure II) reduction in pressure loss with eccentricity. Following a similar approach, Luo and Peden (1990) analyzed the flow by representing an eccentric annulus by an infinite number of sectors of concentric annuli with variable outer radii. The analytical solutions for the shear stress, shear rate, and volumetric flow rate/pressure gradient were obtained for both Power Law and Bingham-plastic fluids. The pressure gradients of both flows were found to decrease with increasing eccentricity.

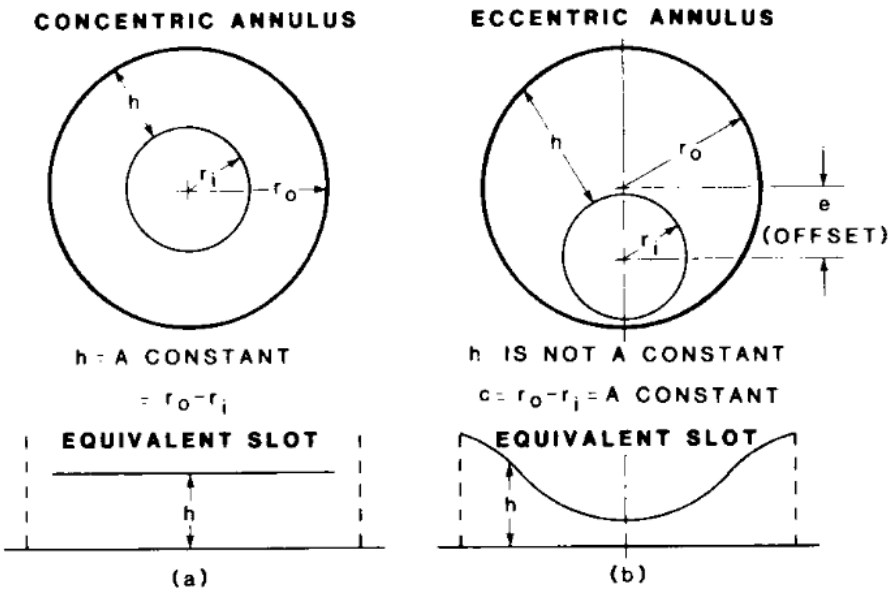

Figure I- Slot equivalents of concentric and eccentric annuli, Iyoho and Azar (1981).

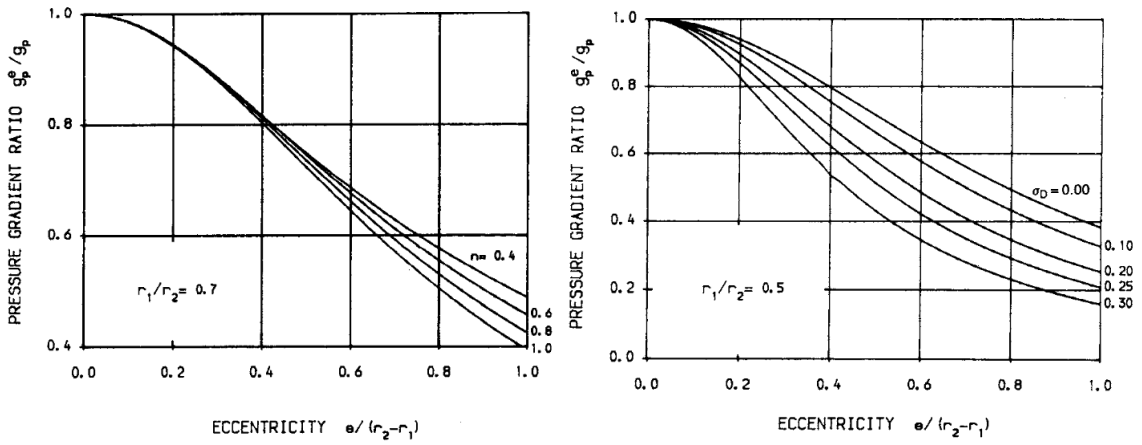

Figure II- Pressure gradients in eccentric annular flow of Power-Law fluids (left) and Bingham-plastic fluids (right), Luo and Peden (1990).

Theoretical analysis of helical flow in eccentric annulus is very challenging. As a result, a number of studies (Hansen and Sterri,1995; Wei, 1997; Hansen et al., 1999; Woo et al., 2005) on helical flow of non-Newtonian fluid in eccentric annuli were based on experimental approaches. The experimental work of Nouri and Whitelaw (1997) were focused on turbulent flows in eccentric annulus with rotation. Their results built on a previous study by the same authors in 1994 where the flows of Newtonian and non-Newtonian fluids in concentric annulus were examined with rotation. They reported an increase in pressure drop with pipe rotation. Their findings were supported by another study (Sterri et al., 2000) conducted in partially eccentric annulus with diameter ratio of 80 %. Despite this, other experimental studies (Hansen and Sterri, 1995, 1999; McCann et al., 1995) showed mixed results (i.e. pressure loss may increase or decrease with the rotation). Experimental studies (Hansen and Sterri, 1995, 1999) on the effect of pipe rotation and eccentricity on pressure losses in narrow annuli showed the pressure loss could increase or decrease with increased rotation speed. Another similar experimental investigation (McCann et al., 1995) on the effects of pipe rotation found an increase in pressure loss for Power Law fluids in narrow annuli with the increase in

pipe rotation under turbulent flow condition. Nevertheless, under laminar flow condition the trend changed; pressure loss decreased with increasing pipe rotation.

2.3. Theoretical and numerical studies

2.3.1. Concentric annulus

The first paper to be published about the flow of a non-Newtonian fluid through an annulus was written by Volarovich and Gutkin (1946). They also presented an approximate analytical solution for the axial flow of a Bingham fluid in a concentric annulus. Following their work, a number of studies were conducted to develop hydraulic models for annular flow of non-Newtonian fluids. Laird (1957) developed an exact solution for laminar flow of Bingham fluid in a concentric annulus. He related flow rate to frictional pressure loss. Fredrickson and Bird (1958) also presented their approach which was perceived to be better for routine uses because of the quick use of their charts. They proposed solutions for both Bingham and Power Law fluids.

Other studies on generalized Newtonian fluids in concentric annuli include the work conducted by Bird (1965), Rotem (1962), Kozicki et al. (1966), Nebrensky and Ulbrecht (1968), Shul'man (1970), Nebrensky et al. (1970), Russell and Christiansen (1974), Hanks (1979) and Fordham et al. (1991). Several of the models developed in these studies were upgraded (Rivlin, 1956; Rigbi and Galili, 1971; Batra and Eissa, 1994) to handle flow through a concentric annulus with inner pipe rotation.

Drilling fluids often used in the industry are non-Newtonian. Consequently, most of the early theoretical studies (Coleman and Noll, 1959; Savins and Wallick, 1966; Chin, 1992) focused on the helical flow of non-Newtonian fluids in concentric annulus. Coleman and Noll (1959) presented an exact analytical solution for helical flow of generalized incompressible fluid in a concentric annulus. Their mathematical model is accurate for laminar flow in concentric annulus without the formation of secondary flows such as Taylor vortices .

2.3.2. Eccentric annulus

Purely axial flow of Newtonian fluid in eccentric annulus was theoretically analyzed by Piercy et al. (1933). Applying a complex coordinate transformation method, they developed an exact solution for Newtonian fluid. Later, theoretical studies (Vaughn, 1965; Mitsuishi and Aoyagi, 1973; Guckes, 1975; Haciislamoglu and Langlinais, 1990; Pham and Mitsoulis, 1998) were continued on the flow of non-Newtonian fluids in eccentric annuli. Earlier studies (Tiedt, 1966 and 1967) for the case of no rotation presented analytically, obtained fRe (hydraulic resistance) values that indicated a decrease in frictional pressure loss due to eccentricity for annulus with a constant diameter ratio. In addition to the theoretical study, numerical solutions (Manglik and Fang, 1995) were also obtained for the situation of no inner cylinder rotation. Results showed the formation of a stagnant region in the narrow section of the annulus and a high-velocity core in the wide section.

For eccentric annulus with pipe rotation, it was not possible to obtain exact solutions before the finite-difference and finite element methods were applied to provide exact numerical solutions to the complex equations. Examples of such studies include Locket (1992) and Meuric et al. (1998) who presented solutions for Power Law, Bingham and Herschel-Bulkley fluids.

There are conflicting results in frictional pressure loss measurements obtained from lab studies and field investigations. Hemphill and Ravi (2005) reported significant increase in pressure loss with increasing rotation speed. On the other hand, Luo and Peden (1990) presented a study that reported the reduction of pressure loss due to drillstring rotation. It is however becoming more accepted that the frictional pressure drop may either increase or decrease with eccentricity and pipe rotation.

A number of studies (Marken et al., 1992; Cartalos and Dupuis, 1993; and Ooms et al, 1999) focused on determining the reasons for the conflicting observations. Marken et al. (1992) after studying isolated variables such as drillstring rotation, drillstring dynamics, vibrational energy, the fluid flow including centrifugal instabilities, irregular flow and rheology, and eccentricity, pointed out that most conditions work together in complex ways. A similar study (Cartalos and Dupuis, 1993) suggested considering the tooljoint diameter as a factor for developing a well plan. The critical Reynolds number (Re_c) corresponds to the onset of inertial flow and was found to depend on the Power Law index (n). Ooms et al. (1999) concluded that for large values of inertial forces the pressure loss strongly depends on the rotation speed.

Theoretically, stable laminar flows in concentric annulus do not show pressure increase with rotation. Figure III and Figure IV compare numerically predicted pressure loss with and without pipe rotation as the function of eccentricity for Newtonian fluids (Ooms et al., 1999). For concentric annulus, pressure loss remains constant regardless of pipe rotation speed. However, with increasing eccentricity, the pressure loss increases reaching its local maximum, and then decreases and finally increase sharply as the relative eccentricity approaches unity. The magnitude of the increase and the maximum value point depends on the gap width, eccentricity and Taylor number. In particular, for annuli with small clearance gap, high eccentricity and high Taylor number, the pressure loss is significant. At high Reynolds number, the pressure loss is less dependent on rotation speed.

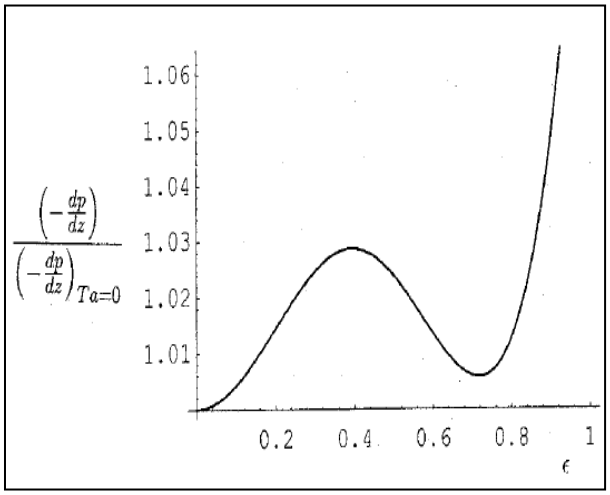

Figure III - Influence of inertia on the pressure drop, Ooms et al. (1999).

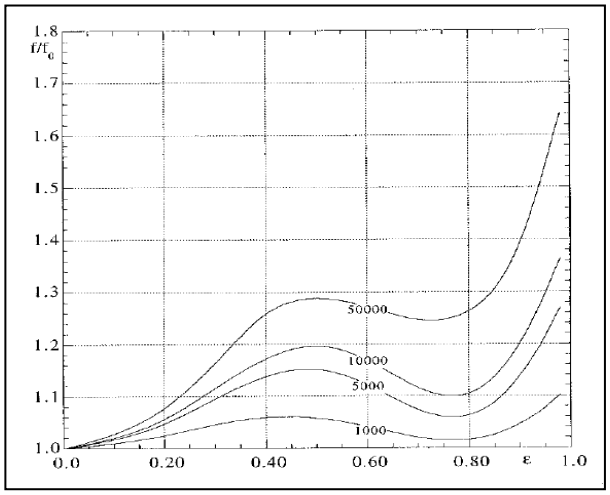

Figure IV - Ratio of friction factors as a function of eccentricity, Ooms et al. (1999).

A number of numerical studies (Haciislamoglu and Langlinais, 1990; Cui and Lui, 1995; Hussain and Sharif, 2000; Wan et al., 2000; Escudier et al., 2000; Fang and Manglik, 2002; Escudier et al. 2002) have been conducted to explain the flow of Newtonian and non-Newtonian flows in eccentric annulus with drillpipe rotation. A simulation study by Haciislamoglu and Langlinais (1990) on non-

Newtonian annular flow showed that annular pressure losses decrease (as much as 60 %) if eccentricity is increased, at constant flow rate. Another simulation study (Cui and Lui, 1995) compared predictions with measurements obtained with an aqueous solution of CMC, and found good agreements. In addition, comments were made on the formation of the secondary flow and the shear-thinning effect of the rotational flow.

An extensive numerical study on fully developed laminar flow of Newtonian and non-Newtonian fluid in eccentric annulus with combined axial flow and inner cylinder rotation was conducted by Escudier et al., (2000, 2002). For fully developed stable Newtonian flow, the radial velocity was found to be decoupled from the axial motion. Using the continuity and momentum equations for three-dimensional, incompressible Newtonian fluid flow as their basis, they calculated the frictional pressure loss for a range of diameter ratios (κ= 0.2, 0.5 and 0.8), Taylor numbers (Ta = 0, 100, 1000, 2 500, 5 000, 10 000, 50 000) and eccentricities (0 - 0.98). The results (Figure V) presented in terms of the hydraulic resistance (fRe) showed that the pressure loss substantially decreases with eccentricity.

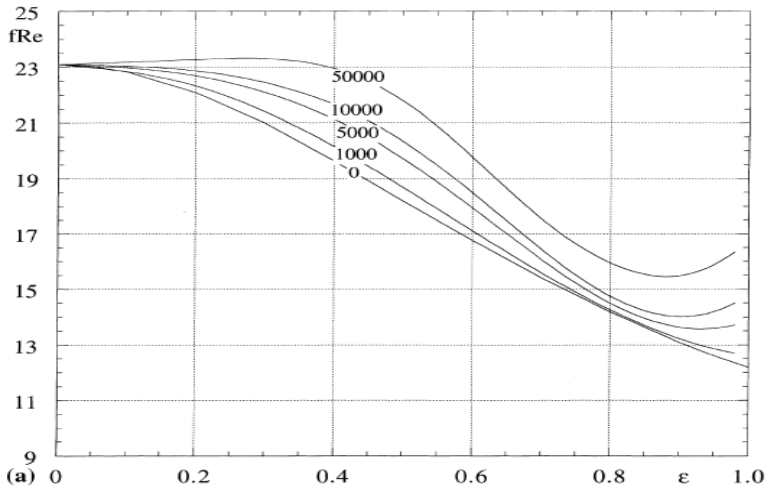

Figure V - Variation of frictional pressure loss as a function of eccentricity and Taylor number (κ=0.2), Escudier et al. (2000).

A similar study conducted by Fang and Manglik (2002) presented similar results. Their simulations showed that eccentricity and diameter ratio have significant effects on the flow patterns. For increasing eccentricity (Figure VI), the growth and onset of a kidney-shaped vortex in the wider gap of the annulus was observed. The center of this body seems to be moving counterclockwise (in the direction of rotation) with increasing rotation. The separation point moves upstream (clockwise) and the reattachment point moves downstream (counterclockwise). The separation point moves downstream with increasing diameter ratio (Figure VII), but the reattachment point seems unaffected.

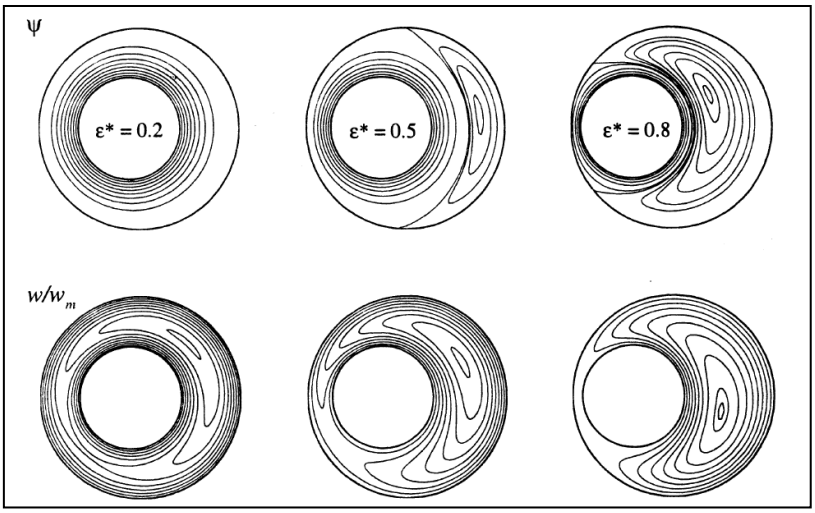

Figure VI- The effect of eccentricity on the stream function (ψ) and axial velocity (w/w_m) distribution for flow in an annulus with κ=0,506 and Re_r=56, Fang and Manglik (2002).

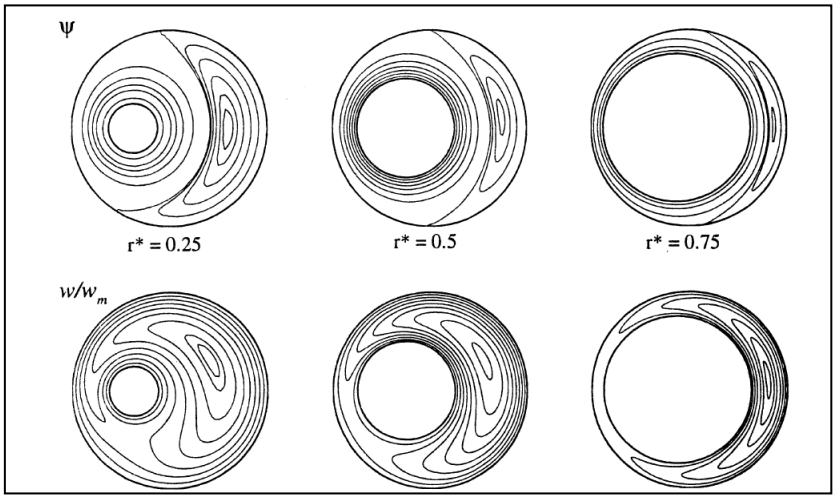

Figure VII-The effect of radius ratio on the stream function (ψ) and axial velocity (w/w_m) distribution for flow in an annulus with κ=0,5 and Re_r=40, Fang and Manglik (2002).

Furthermore, numerical studies (Hussain and Sharif, 2000; Adariani, 2005) were carried out to develop a general numerical model capable of predicting non-Newtonian flow through eccentric annuli. Ozbayoglu et al. (2008) proposed a neural network and evolutionary programming approach to model the behavior of non-Newtonian fluid flow in an eccentric annulus. An existing model developed by Hemphill et al. (2008) permits users to calculate pressure drop with simple formulas. The ECD prediction is a function of diameter ratio, length of a hydraulic section and number of revolutions per minute.

Based on analytical solution of Coleman and Noll (1959), a recent study (Ahmed and Miska, 2008) presented an analytical solution for YPL fluid together with experimental measurements. The study concluded that in a highly eccentric annulus, the inertial phenomena, which offset the effect of shear thinning, tends to dominate, causing increased pressure loss. In slightly eccentric annulus, the shear-thinning effects are dominant, reducing the pressure loss. At low flow rates (low Reynolds numbers), the inertial effects are nearly negligible. Flow regime was found to affect the relationship between

pipe rotation and friction factor. Under laminar flow conditions, pressure loss changes were substantial, whereas with increasing Reynolds number (transition flow) the variation in pressure loss reduced. At high flow velocities, the effect of pipe rotation is minimal. For non-Newtonian fluids, the change in apparent viscosity with respect to the tangential shear rate change diminishes as axial shear rate increases. The axial shear rate dominates over the rotational shear rate in this case. The evolvement of other flow phenomena was also indicated in addition to the shear thinning. For fully eccentric annulus, the inertial effects are dominant and the pressure loss is increased with increasing rotation speed. This is especially true at high Reynolds numbers, or high flow rates.

3. The Fundamentals in Annular Flow of Drilling Fluids

3.1. The Behaviour of Annular Flows Affected by Pipe Rotation

Simplified hydraulic models have been used for many years in the industry. The models directly relate the annular pressure loss with flow rate, annulus dimensions and fluid properties. When well pressures require a fluid density which is very close to the formation fracturing pressure, more accurate prediction is needed. It is then necessary to pay more attention to the other factors that affect pressure loss.

The behavior of annular flows is dependent on many factors including fluid properties (rheology and density), flow regime, diameter ratio, pipe rotation speed and eccentricity. In this chapter, important parameters and characteristics of annular flows with pipe rotation will be briefly discussed.

3.1.1. Drillstring Motion and Vibration

Marken et al. (1992) commented that lateral, rotational and axial vibration and motion of the drillstring disrupt fluid patterns, especially if these changes are rapid. An extreme form of rotational motion is torsional oscillation due to stick-slip motion. This happens when the bottom of the drillpipe ceases to rotate while the topdrive is still rotating. When the drillstring is finally winded up, there is a huge release in energy that may cause the bit to rotate at double speed for a moment. The lateral motion of the drillpipe is a complex motion affected by the rotation speed, and perhaps best described as a movement that gyrates around the borehole.

3.1.2. Secondary Flows and Taylor Vortices

A complicating factor that affects flow regime and annular pressure loss is drillstring rotation. The flow between two rotating cylinders is called a Couette flow (see Figure VIII). For low angular velocities the flow is steady and purely azimuthal.

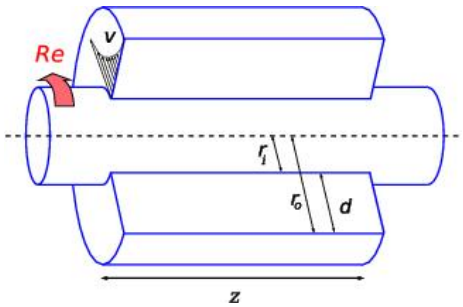

Figure VIII- Schematic of the Taylor-Couette system. The outer cylinder is not rotating, Avila (2012).

In oil well drilling, the flow of the drilling muds in the concentric annulus formed by the drillpipe and the casing or wellbore is helical flow (see Figure IX).

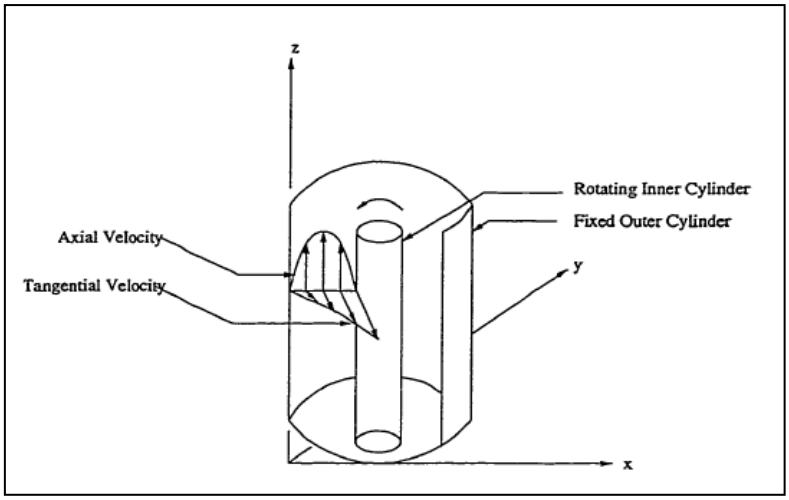

Figure IX -Flow with rotating inner cylinder, Hussain (1999).

In the case of flow between a stationary outer and rotating inner cylinder, secondary flows may form due to shear and centrifugal instabilities. When the rotating speed of the inner cylinder is raised over a threshold value ($Ta > Ta_c$), the flow becomes unstable. Ta is the Taylor number expressed as:

$$Ta = \left(\frac{\rho\omega}{\mu}\right)^2 \cdot R_I \cdot (R_o - R_I)^2 \quad \text{.....(1)}$$

The centripetal force on the fluid throws the fluid away from the rotating drillstring. The "void" left by this outward-bound fluid will be filled by fluid from the outer part of the annulus. This phenomenon creates a secondary flow of ring-like vortices, called Taylor vortices. These are large toroidal vortices stacked upon each other, see Figure X. It is a stable secondary flow until large Reynolds numbers are reached, and "wavy vortexes" start to form (see Figure XI).

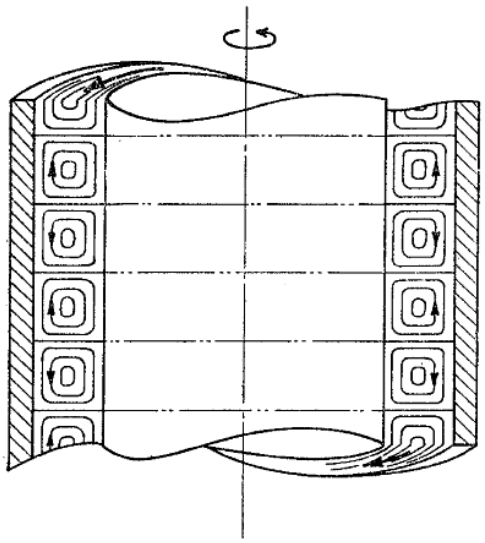

Figure X-Taylor vortices, Yamada (1962).

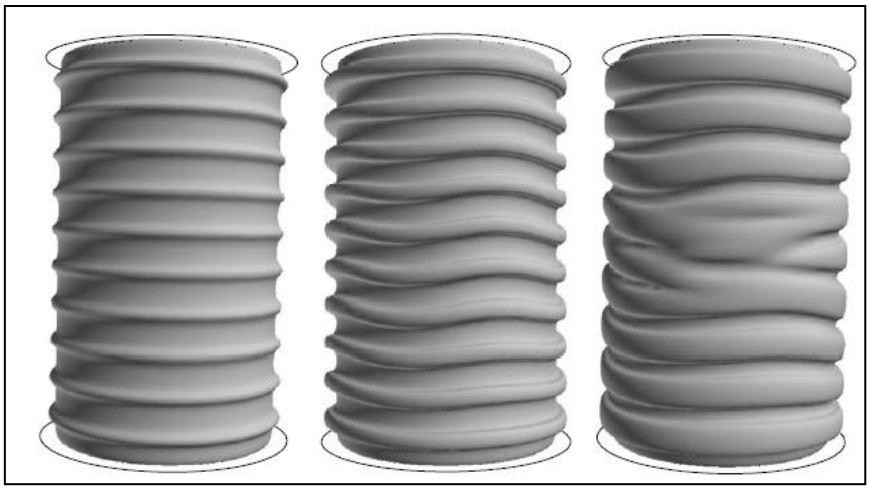

Figure XI- Axisymmetric Taylor vortices (left), wavy vortices (middle) and wavy vortices with a single dislocation (right), Serre et al. (2008).

The presence of secondary flows increases hydraulic resistance of the flow due to the more dissipative nature of the flow. Transversal, torsional and axial vibrations of the drillstring during drilling induce complicated flow structures. Additional difficulties may arise from the fact that the flow structure may influence drillstring motion. The eccentricity of the inner cylinder tends to delay the formation of Taylor vortices.

3.1.3. Shear-Thinning Effects

Newtonian fluids exhibit a linear relationship between shear rate and shear stress, non-Newtonian flows do not. Most drilling muds are non-Newtonian and their viscosity most often decrease with increased shear rate. This behavior is called shear-thinning, see Figure XII.

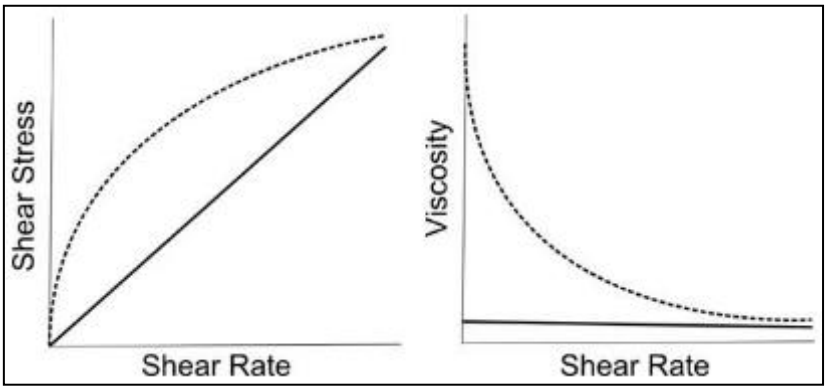

Figure XII- Shear-thinning Non-Newtonian flows (dotted line) and Newtonian flows (full line), White et al. (2010).

Inner pipe rotation adds a tangential shear rate to the overall shear rate. Thus, the relevant shear rate for concentric annulus may be approximated as:

$$\dot{\gamma} = \sqrt{\dot{\gamma}_{ax}^2 + \dot{\gamma}_{tan}^2} \quad \text{..... (2)}$$

Drillstring rotation may thus significantly increase the relevant shear rate. Therefore, for shear-thinning fluid, the effective viscosity reduces with the rotation and flow enhancement may occur for a constant pressure gradient condition. In other words, this leads to reduced friction pressure loss due to the coupling of axial and rotational flow at a constant flow rate. Figure XIII shows an example of viscosity distribution. The drillpipe is eccentric and laying on the lower side of the well. The viscosity is lower near the borehole wall and around the rotating drillstring (blue and green), than the area in-between (red). This is due to higher shear forces near the wall and around the drillpipe. The distribution varies with fluid properties, flow regime and wellbore geometry.

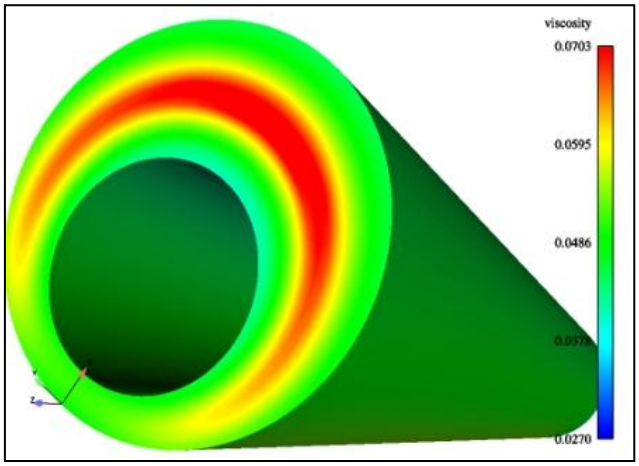

Figure XIII - Viscosity distribution in eccentric borehole (Power Law fluid, n=0,75), Elias (2004).

3.1.4. Geometric Irregularities and Inertial Effects

The annular geometry and time-dependent behavior of the fluid affect the annular pressure loss. In a concentric annulus, the drillstring is situated at the center of the borehole all the time. Hence, the flow pattern is expected to be perfectly helical and the velocity from a set distance from the inner pipe is constant. Many models and formulas are today assuming a concentric annulus, but it has been shown almost impossible to keep the drillstring in concentric condition. As a result, the drillpipe often settles in eccentric position. Eccentricity is defined by:

$$\varepsilon = \frac{e}{R_o - R_i} \qquad \text{..... (3)}$$

In this formula, e is the distance between the centers of the inner and outer pipes; and R_i and R_o the inner and outer radius, respectively. The parameter is dimensionless, equal to 0 for concentric annulus and equal to 1 for a fully eccentric annulus (see Figure XIV). During directional drilling, the weight of the pipe causes the drillstring to lie on the lower side of the borehole. It is difficult to predict eccentricity as it can vary throughout the hole, except for highly deviated wells where it is accepted to see the wellbore as fully eccentric. Accounting for eccentricity increases the accuracy of numerical models of the annular flow because of its impact on parameters that are commonly incorporated such as velocity profile of frictional pressure loss.

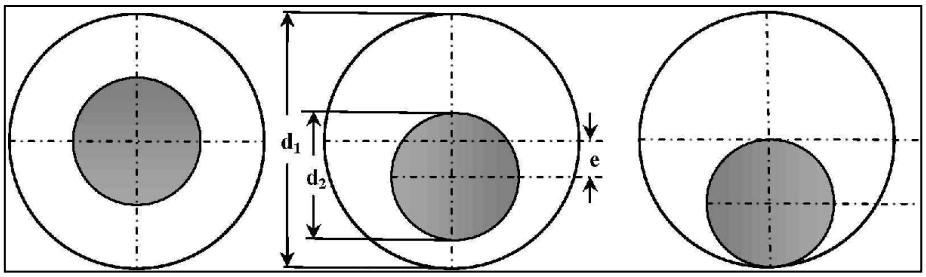

Figure XIV - From left to right: concentric borehole, partially eccentric borehole and fully eccentric borehole, Ogugbue (2009).

Studies show that the angular position of the pipe has a significant effect on the resulting pressure loss. The annuli with high diameter ratios are expected to have considerable discrepancies. Experiments showed that the pressure loss varies with time in a cyclic manner, in relation to the rotation of the pipe and subsequent change in eccentricity.

The inertial effects due to pipe eccentricity and/or geometric irregularities cause the flow to accelerate in a different pattern. The peak axial velocity is lowered and a higher friction factor is obtained. Figure XV shows example of streamline distribution in an eccentric borehole. The flow near the wall can be observed as straight, whereas the helical pattern is found around the cylinder (drillstring). Compared together with Figure XIII, we see that the viscosity is reduced around the drillstring, but that the flow pattern is complicated. It is therefore difficult to say if the pressure drop is reduced or increased. The distribution changes with fluid and eccentricity.

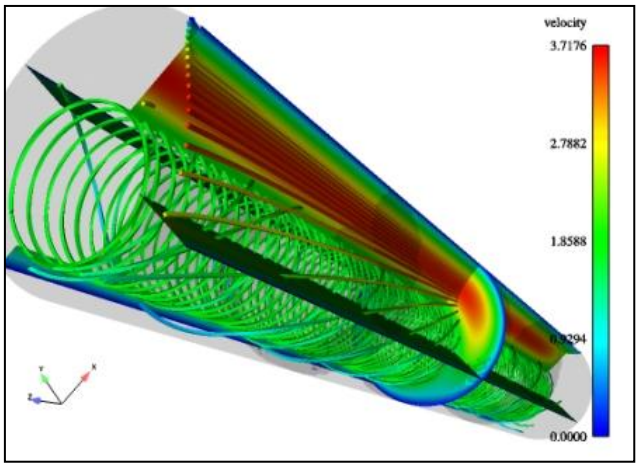

Figure XV - Streamline distribution in eccentric borehole (Power Law fluid, n=0,75), Elias (2004).

3.2. Theoretical Modeling of Annular Flows

During drilling, mud is circulated through the tubing and up the annulus for several reasons: maintaining hydrostatic pressure, transporting cuttings to the surface, lubricating and cooling the drillstring and transmitting hydraulic horsepower, among others. For most conventional drilling uses, water-based, oil-based or synthetic-base fluids are used. For unconventional drilling like UBD (Underbalanced Drilling), foam and aerated fluids are commonly used, and maintain a lower bottomhole pressure.

Newtonian fluids are the fluids where the shear stress is proportional to the shear rate:

$$\tau = \mu\dot{\gamma} \quad \text{..... (4)}$$

Most drilling muds are shear-thinning fluids and their viscosities reduce with increased shear. The most common rheological models for non-Newtonian fluids include the Bingham plastic (BP), the Power Law (PL) and the Herschel-Bulkley (Yield Power Law) models. The Yield Power Law (YPL) model includes both the characteristics of the Bingham plastic and Power Law models, and can thus be seen as the most preferable. The model is expressed as:

$$\tau = \tau_y + K\dot{\gamma}^m \quad \text{..... (5)}$$

For non-Newtonian fluids it is preferable to use the apparent viscosity function to represent the viscosity of the fluid:

$$\eta = \frac{\tau_y}{\dot{\gamma}} + K\dot{\gamma}^{m-1} \quad \text{..... (6)}$$

Fluid viscosity is a function of temperature and pressure. It should be noted that some drilling fluids may not be perfectly represented by the YPL model. For example bentonite muds and polymer based fluids at low shear rates, time-dependent fluids and fluids with both viscous and elastic properties are complex to model.

Rheological properties of drilling fluids are often measured using rotational viscometers. The narrow slot approximation, or the linear velocity distribution, may be used for viscometers with radius ratio ($\kappa = \frac{R_i}{R_o}$) greater than 0.99. For any κ value less than this, the approximation may not be accurate. Subsequently, the shear rate can be expressed as:

$$\dot{\gamma} = \frac{wR_i}{R_o - R_i} \quad \text{.....(7)}$$

For drilling applications, annular pressure loss prediction is critical in the well planning process. The drillpipe eccentricity and the ratio between the pipe diameter and the borehole diameter (diameter ratio, κ) have impacts on this characteristic. For conventional drilling the diameter ratio is around 0.4 to 0.6 (see Table B).

Table B- Typical drillpipe and hole sizes, Aadnoy et al. (2009).

Table of Typical Drillpipe and Hole Sizes		
Pipe Diameter (in.)	Hole Diameter (in.)	Diameter Ratio (κ)
5	12 1/4	0.4082
4 1/2	8 3/4	0.5143
3 1/2	6 3/4	0.5185
2 7/8	6 1/4	0.4600
2 3/8	5 1/2	0.4318

Dodge and Metzner (1959) presented a relationship between the pressure loss and the mean flow rate. They also proved that the mean velocity is relatively insensitive to any variations in near the center of the tube, while highly-dependent on the high shear rates near the wall. This can be explained by examining the contribution of the differential slice in Figure XVI.

The volumetric flow rate is given by:

$$\partial Q = \pi r^2 \partial u \qquad \text{.....(8)}$$

The fraction of the velocity which would not be accounted for if the velocity profile was cut flat from the radius to the center line is given by

$$\frac{\Delta Q}{Q} = \frac{\Delta V}{V} = \frac{\int_u^U r^2 \partial u}{\int_0^U r^2 \partial u} \qquad \text{.....(9)}$$

Figure XVI shows the fractional flow contribution as a function of the shear rate over the shear rate at the wall ($\frac{\tau}{\tau_w}$). The result shows that the mean velocity is highly dependent on the shear rates in the proximity of the wall and that the influence curves drastically in the area in the center of the pipe. 74 % of the mean flow contribution is attributable to the shear stresses between $\boldsymbol{\tau_w}$ and 0.96$\boldsymbol{\tau_w}$ and 93 % is between $\boldsymbol{\tau_w}$ and 0.8$\boldsymbol{\tau_w}$ (see Figure XVII). Based on this observation the wall shear rate is assumed as the average shear rate; an assumption used in the development of the new model.

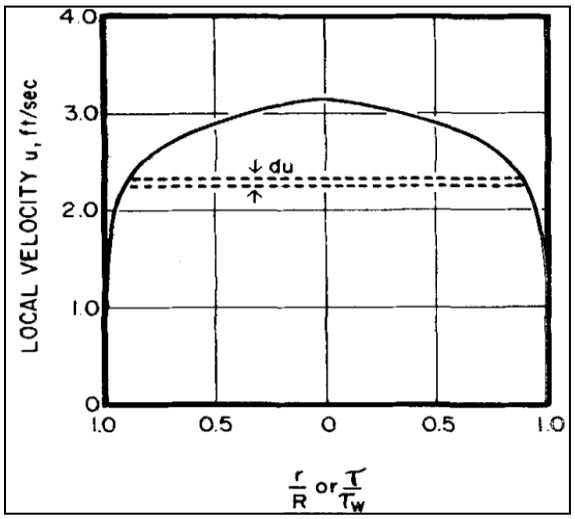

Figure XVI – Newtonian turbulent velocity distribution (N_{Re}=20 000, D=1 in., water at 20°C), Dodge and Metzner (1959).

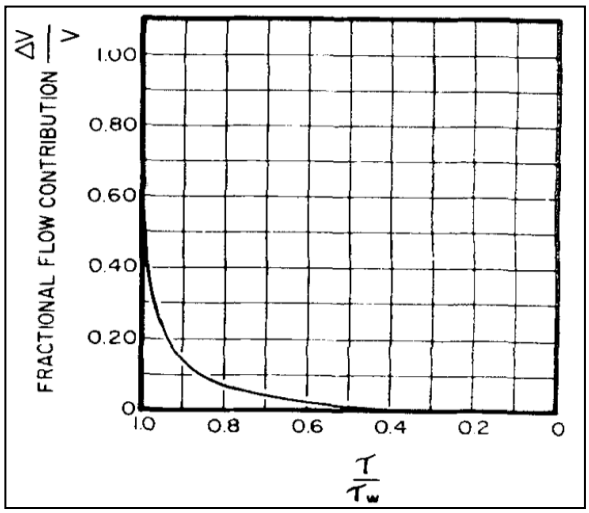

Figure XVII – Newtonian fractional flow contribution, Dodge and Metzner (1959).

To formulate a hydraulic model for Herschel-Bulkley fluids, the apparent viscosity is defined as (Ahmed and Miska, 2008):

$$\mu_{app} = \frac{\tau_y}{\dot{\gamma}_{\theta-z}} + K\dot{\gamma}_{\theta-z}^{m-1} \quad \text{.....(10)}$$

where the combined shear rate, $\dot{\gamma}_{\theta-z}$ is given by:

$$\dot{\gamma}_{\theta-z} = \sqrt{(\dot{\gamma}_z^2 + \dot{\gamma}_\theta^2)} \quad \text{.....(11)}$$

where $\dot{\gamma}_z$ and $\dot{\gamma}_\theta$ are the wall shear rates of axial and tangential flows, respectively. By applying the narrow slot approximation technique, the wall shear rate of axial flow at the wall can be estimated as:

$$\dot{\gamma}_z = \frac{1+2N}{3N}\frac{12U}{D_o - D_i} \quad \text{.....(12)}$$

The tangential shear at the pipe wall can be approximated as:

$$\dot{\gamma}_\theta = \frac{wD_i}{D_o - D_i} \quad \text{.....(13)}$$

The generalized flow behavior index N is computed using the following formula:

$$\frac{3N}{2N+1} = \frac{3m}{2m+1}\left[1 - \left(\frac{1}{m+1}\right)x - \left(\frac{m}{m+1}x^2\right)\right] \quad \text{.....(14)}$$

Where $x = \frac{\tau_y}{\widehat{\tau_w}}$.

The formulas and assumptions presented in this chapter were also used in the development of the new model.

4. Development of new model based on the direct numerical solution, the dividing of an eccentric annulus into several concentric annulus and a correlation for inertial effects

In this chapter, each step in the creation of the new model is explained in detail. Relevant equations and assumptions are also listed. See Figure XVIII for a chart explaining the different steps in the creation of the new model. In chapter 5, the model is validated against laboratory and field data published in the literature.

The new model was created by using the existing model for YPL fluid in concentric annulus with inner pipe rotation by Ahmed and Miska (2008). Eccentricity of the pipe was approximated with several sectors of concentric annuli of varying radii, an approach presented by Luo and Peden (1990). The final step was to add a correlation for inertial effects. Numerical results by Escudier et al. for Newtonian (2000) and Non-Newtonian (2002) flows were analyzed to develop this correlation.

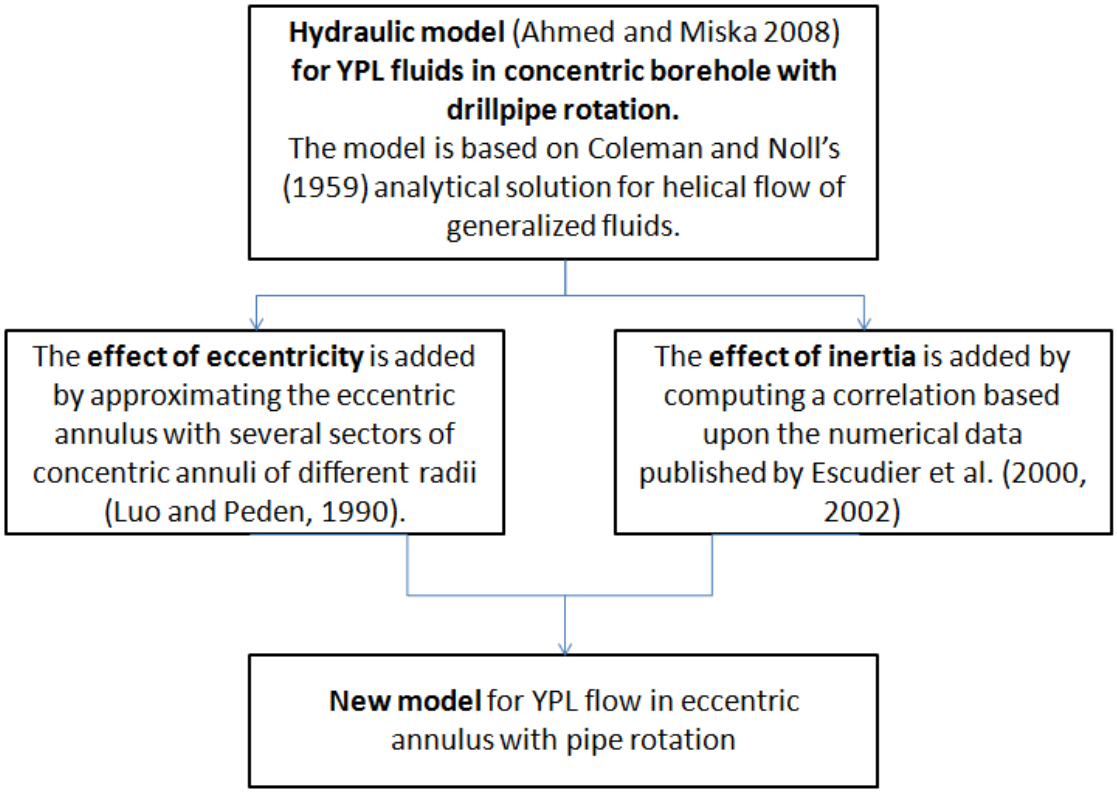

Figure XVIII- Chart of the development steps in the creation of the new model.

4.1. Concentric annuli with rotation

The direct numerical model was used to describe the flow through concentric annulus with pipe rotation. The basics of this method are described in this paper. The reader is directed to the papers by Ahmed and Miska (2008) and Coleman and Noll (1959) for a more detailed presentation of the solution.

For a typical YPL flow, there will be three main regions: the plug that moves at equal speed, a sheared region closer to the pipe and a sheared region closer to the wall (Figure XIX).

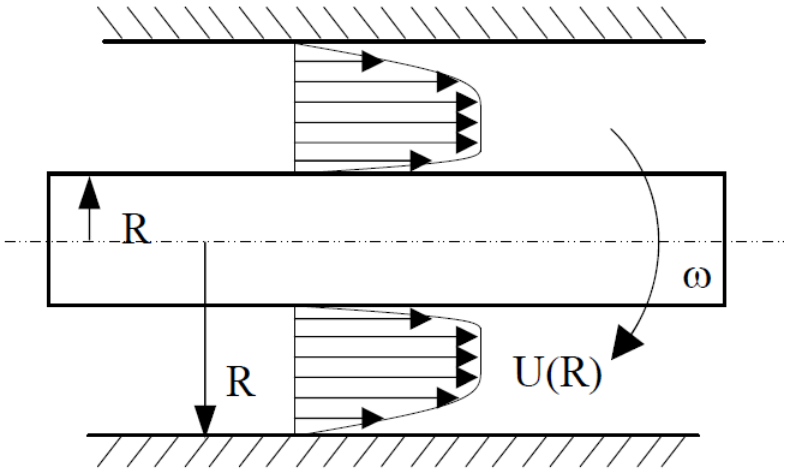

Figure XIX- YPL flow in concentric annulus, Ahmed and Miska (2008).

The momentum balance for any ring with outer radius r and inner radius R_i, can be written as:

$$\Delta p\pi\left(r^2 - R_i^2\right) = 2\pi\Delta L(\tau_{w,i}R_i - \tau r) \quad \text{.....(15)}$$

Assuming no-slip conditions at the wall it is possible to set the velocity profile for the sheared region near the pipe as:

$$v_I(r) = \int_{R_i}^{r}(c_{1,i}r + \frac{c_{2,i}}{r} - c_{3,i})^{\frac{1}{m}}dr \quad \text{.....(16)}$$

Where $c_{1,i} = \frac{-\Delta P}{2\Delta LK}$ $c_{2,i} = \frac{R_i}{K}(\tau_{w,i} + \frac{\Delta PR_i}{2\Delta L})$ $c_{3,i} = \frac{\tau_y}{K}$

A corresponding integral can be set up for the other sheared region. Knowing that the plug velocity is constant we can set the velocity at the endpoints of the sheared regions equal to this constant:

$$Up = v_I(a) = v_{II}(b) \quad \text{.....(17)}$$

a is the inner radius of the plug and b is the outer radius. This can be written as integrals:

$$\int_b^{R_o}(c_{1,o}r + \frac{c_{2,o}}{r} - c_{3,o})^{\frac{1}{m}}dr = \int_{Ri}^{a}(c_{1,i}r + \frac{c_{2,i}}{r} - c_{3,i})^{\frac{1}{m}}dr \quad \text{.....(18)}$$

Using these equations one can calculate the pressure drop of YPL flow in a concentric pipe with rotation.

4.2. Representing an eccentric borehole by several concentric boreholes

The next step is to include eccentricity. The eccentric annular flow of YPL fluid will be analyzed by using a method proposed by Luo and Peden (1990). The method consists of representing an eccentric annulus by an infinite number of concentric annuli with different variable outer radii (see Figure XX).

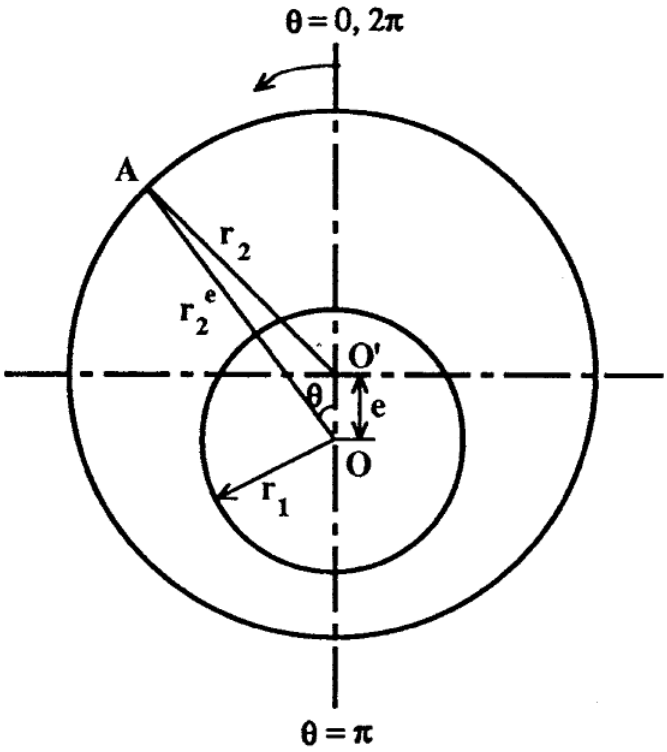

Figure XX- Eccentric Annuli, Luo and Peden (1990).

e is the eccentricity; point O is the center of the inner tube, taken as the center of the eccentric annulus and point O' is the center of the outer tube.

The formula for a circle gives:

$$R^2 = x^2 + (y - e)^2 \quad \text{.....(19)}$$

Where $y = x\tan(\theta - \frac{\pi}{2})$ for the coordinate system as shown above.

Substituting y yields:

$$R^2 = x^2 + (x\tan(\theta - \frac{\pi}{2}) - e)^2 \text{ or } Ax^2 + Bx + C = 0 \quad \text{.....(20)}$$

where

$$A = 1 + \tan(\theta - \frac{\pi}{2})^2,\ B = -2e\tan(\theta - \frac{\pi}{2}) \text{ and } C = e^2 - R^2 \quad \text{.....(21)}$$

A matching correlation successfully used by Guckes (1975) and Haciislamoglu and Langlinais (1990) is introduced to reduce discrepancies. The correlation is:

$$\left(\frac{dP}{dL}\right)_{corrected} = \frac{1}{\frac{R_i}{R_o}^{0,27e}} \times \left(\frac{dP}{dL}\right)_{model} \quad \text{.....(22)}$$

4.3. Empirical correlation for inertial effects

The final step was to incorporate the effect of inertia. Analysis of the numerical data provided by Escudier et al. (2000, 2002) was used to develop correlations. They published numerical solutions of frictional pressure drop of a Newtonian (2000) and Power Law (2002) fluid. Their results are presented as frictional pressure loss (fRe) as a function of Taylor number, eccentricity and radius ratio; see Appendix B and C. A correlation was developed by analyzing results found with curve fitting softwares DataFit and LabFit. The relationship between the frictional pressure drop at no rotation and at different rotations was computed:

$$\Delta fRe_{inertia} = A \cdot n^B \cdot \kappa^C \cdot Re^D \cdot e^E \cdot Ta^F + G \quad \text{.....(23)}$$

Where $A = 0.200, B = 0.403, C = -0.749, D = -0.268, E = 0.394, F = 0.363$ and $G = 0.232$.

$\Delta fRe_{inertia}$ is the change in frictional pressure loss due to pipe rotation in eccentric annulus, n is the fluid behavior index, κ is the radius ratio, Re is the Reynolds number, e the eccentricity and Ta is the Taylor number.

The radius ratio is defined as the ratio between the inner and outer radii:

$$\kappa = \frac{R_I}{R_O} \quad \text{.....(24)}$$

The Reynolds number is expressed as:

$$Re = (1 + \epsilon^2)^{\frac{1-n}{2}} \cdot Re_0 \quad \text{.....(25)}$$

Where $Re_0 = \frac{\rho U^{2-n} \cdot D_H^n}{K}$ .....(26)

Epsilon is defined as:

$$\epsilon = \frac{wR_I}{U} \quad \text{.....(27)}$$

The Taylor number is also dependent on epsilon:

$$Ta = (\frac{1}{\epsilon^2} + 1)^{1-n} \cdot Ta_0 \quad \text{.....(28)}$$

Where $Ta_0 = \frac{1}{8}(\rho \frac{\omega^{2-n}}{K})^2 \cdot D_H^{2n+1} \cdot R_I^{3-2n}$ .....(29)

The programming software would conclude that the pressure loss due to inertia is most dependent on the Taylor number; then eccentricity.

4.4. The code procedure

The procedure of the code can be simplified as follows:

1. The inputs are inserted: Inner and outer diameter, rheological parameters (yield stress, consistency index and fluid behavior index), eccentricity, density, rotation speed and flowrate.
2. The maximum pressure loss is approximated to be more than the calculated pressure loss for concentric annulus with rotation.
3. The minimum pressure loss is approximated to be less than the calculated pressure loss using the narrow slot approximation for concentric annulus without rotation.
4. The minimum flowrate (Qmin) is calculated from the minimum pressure loss with the matching torque found through iteration.
5. The maximum flowrate (Qmax) is calculated from the maximum pressure loss with the matching torque found through iteration.
6. The desired flowrate (Q) is found by an iteration procedure between Qmin and Qmax, where each approximation is called Qmid. Qmid goes through iterations to find the associated torque and pressure loss.
7. In the case of an eccentric annulus, Qmid is approximated by several sectors of concentric annuli with a calculated torque and pressure loss.
8. When the desired flowrate is found, the effect of inertia is added by using the computed correlations to change the pressure loss adequately.
9. The outputs are given as frictional pressure loss (the output parameters can be altered if desired).

The code is available in Appendix D – Program code of the new model.

5. Validation of the model

5.1. Comparison to numerical models

The code was first validated against numerical solutions presented by Walker and Al-Rawi (1970), Escudier et al. (2000) for Newtonian flows and Escudier et al. (2002) for Non-Newtonian flows. Irregularities and imperfections appear in experimental results, often due to the near impossibility of keeping a rotating pipe concentric. Therefore numerical solutions were chosen as the best basis on which to make a first comparison.

5.1.1. Comparison to Escudier et al. (2000) for Newtonian fluid

Escudier et al. (2000) conducted a computational and experimental study of fully developed laminar flow off a Newtonian liquid through an eccentric annulus with combined bulk axial flow and inner cylinder rotation. They computed the variation of frictional pressure loss (fRe) as a function of the radius ratio κ, the Taylor number Ta and eccentricity e.

Simulations were run to compare the new model's results with the available data. The results were shown as a plot of the frictional pressure drop from the model (Calculated) and the frictional pressure drop computed by Escudier et al. This means that if all the results were a perfect match, all the points would be on the red line (Perfect fit), see Figure XXI.

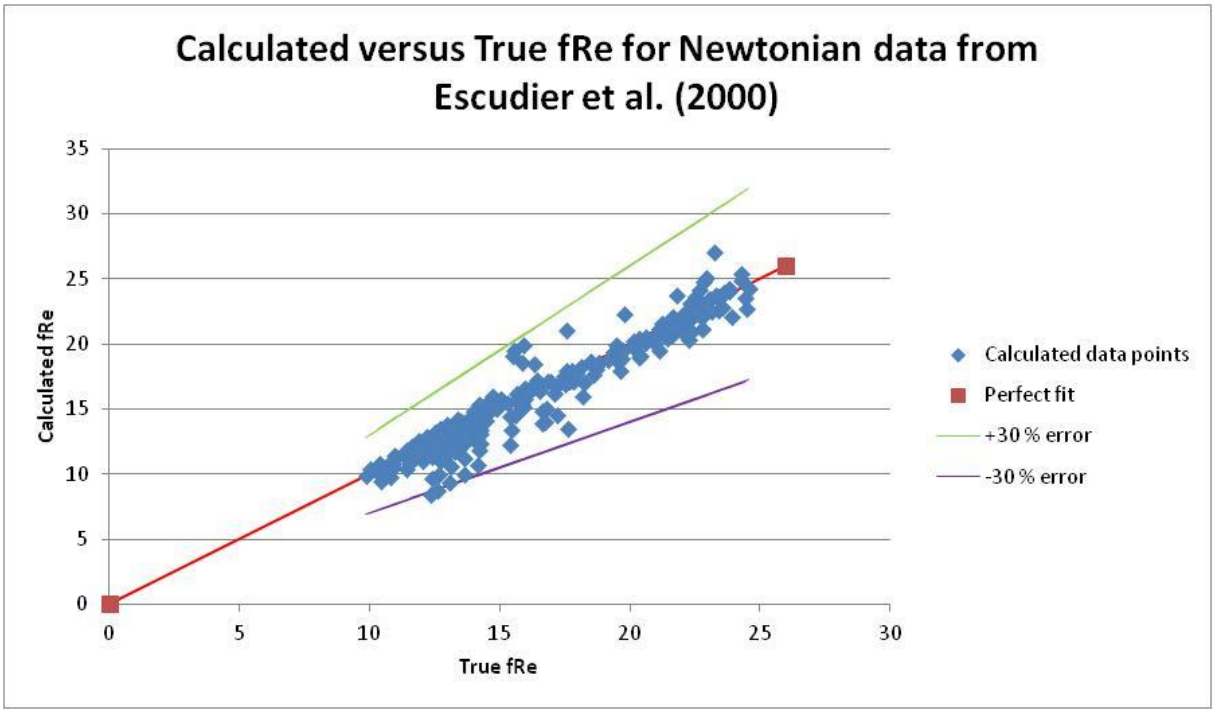

Figure XXI- Calculated fRe against true fRe for Newtonian flow.

The model is shown to be accurate for these data. The maximum error is 32 % and the average error is 6%, see Table C. The model predicts frictional pressured loss for Newtonian fluids well.

Table C- Error table for calculated fRe against true fRe for Newtonian flow.

Error Table	
Minimum Deviance	-32 %
Maximum Deviance	25 %
Average Error	-2 %
Average Absolute Error	6 %

5.1.2. Comparison to Escudier et al. (2002) for Power Law fluid

Escudier et al. (2002) conducted a similar computational and experimental study of fully developed laminar flow off a Non-Newtonian liquid through an eccentric annulus with combined bulk axial flow and inner cylinder rotation. Simulations were run to compare the new model's results with the available data (see Figure XXII).

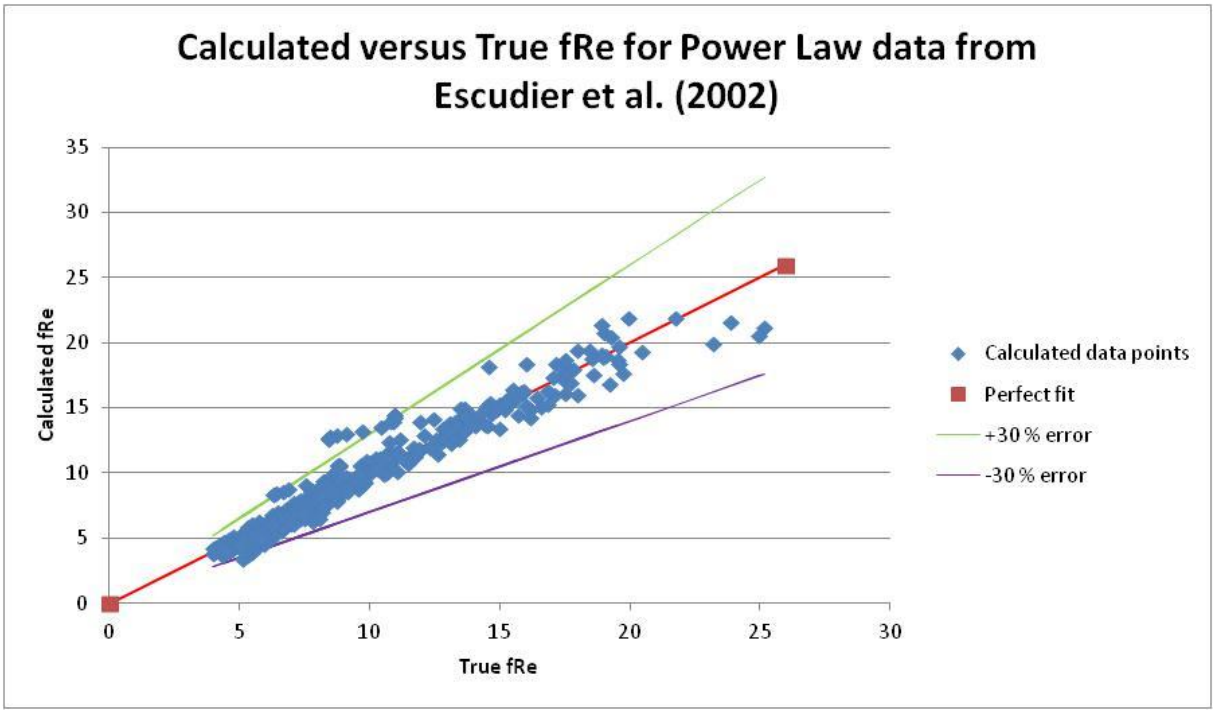

Figure XXII- Calculated fRe against true fRe for Power Law flow.

The accuracy is lower than for Newtonian fluids, but the results are still satisfying, see Table D. The highest error is 51 % and the average error is 7 %.

Table D- Error table for calculated fRe against true fRe for Power Law flow.

Error Table	
Minimum Deviance	-33 %
Maximum Deviance	51 %
Average Error	0 %
Average Absolute Error	7 %

The results for both Newtonian and Power Law fluids were added together (see Figure XXIII).

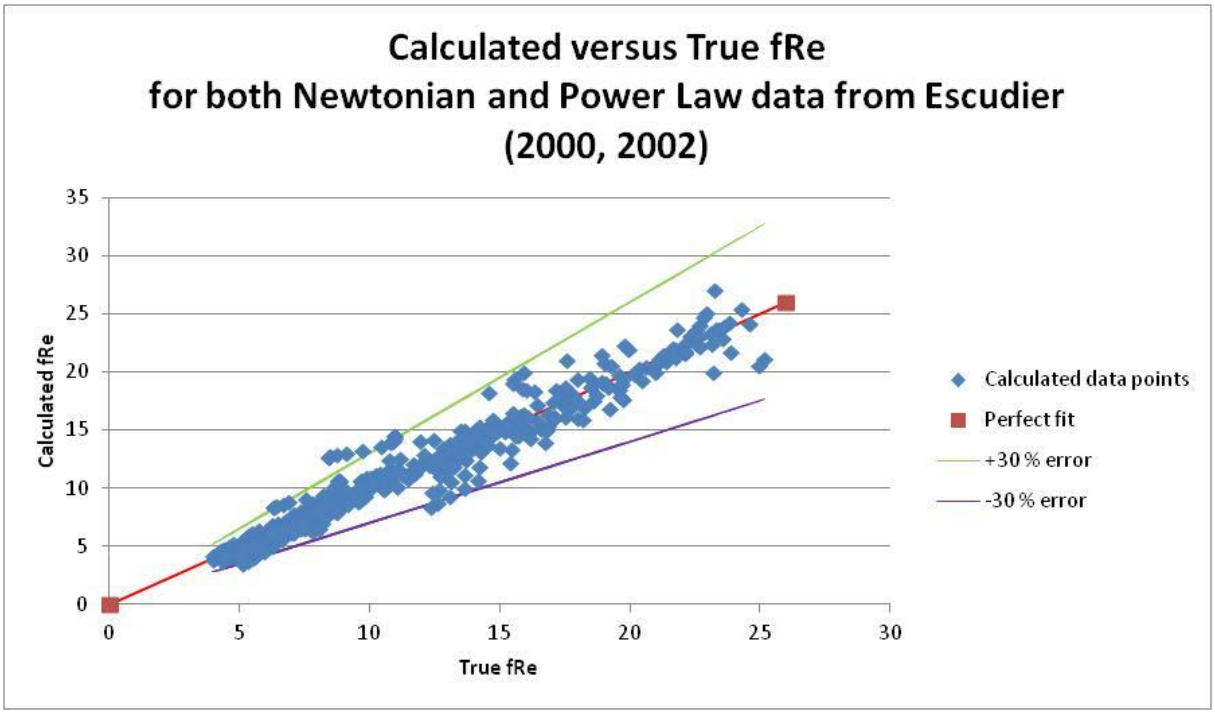

Figure XXIII- Calculated fRe against true fRe for both Newtonian and Power Law flow.

The error table (Table E) shows that for all the data presented by Escudier et al. (2000, 2002) the new model has an average absolute error of 12%.

Error Table	
Minimum Deviance	-48 %
Maximum Deviance	51 %
Average Error	-8 %
Average Absolute Error	12 %

Table E- Error table for calculated fRe against true fRe for both Newtonian and Power Law flow.

5.2. Comparison to laboratory measurements

Pressure loss prediction values from the new model were compared with published laboratory experiments and model predictions by Walker and Al-Rawi (1970) and Ahmed and Miska (2008).

5.2.1. Comparison to Walker and Al-Rawi

Walker and Al-Rawi (1970) conducted laboratory experiments with four bentonite-water mixtures. A method for calculation for laminar flows was used to predict the results. Simulations with the new model were run to compare with both their measured and model-predicted data. The measured values by Walker and Al-Rawi (1970) are represented by a thin blue line (Observed), the computed values by the authors are shown as red squares (Computed) and the results from the simulations are shown as green triangles (Calculated).

Table 2

Table 2 data is taken from Table 2 in the paper by Walker and Al-Rawi (1970) which includes experimental and computed pressured drops for nominal 10 lb/bbl sodium bentonite. The calculations showed good results compared to the computed values as expected. Compared to the measured values, the pressure drop is overpredicted. For 11.2 ft/min the maximum error was 30 % for measured values and 11% for calculated values; the average error was 18 % to measured values and 5 % to the computed values (see Figure XXIV).

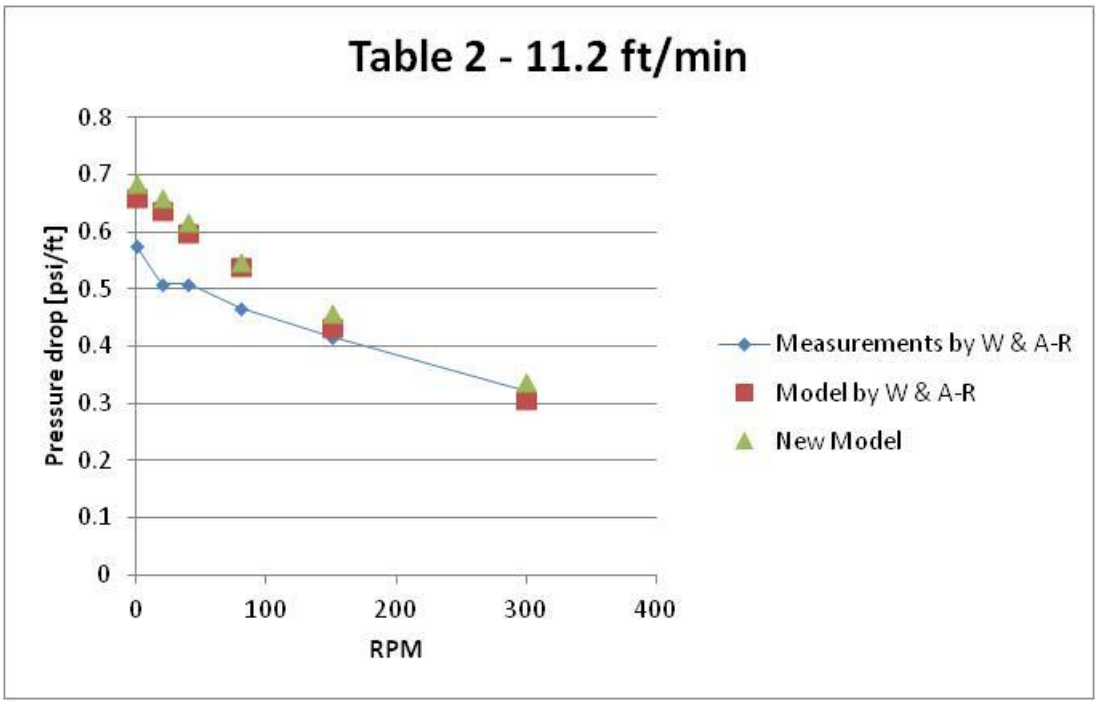

Figure XXIV- Comparison to data from Table 2 by Walker and Al-Rawi for velocity equal to 11.2 ft/min

For 6.8 ft/min the maximum error was 15 % for measured values and 8% for calculated values; the average error was 11 % to measured values and 6 % to computed values (see Figure XXV).

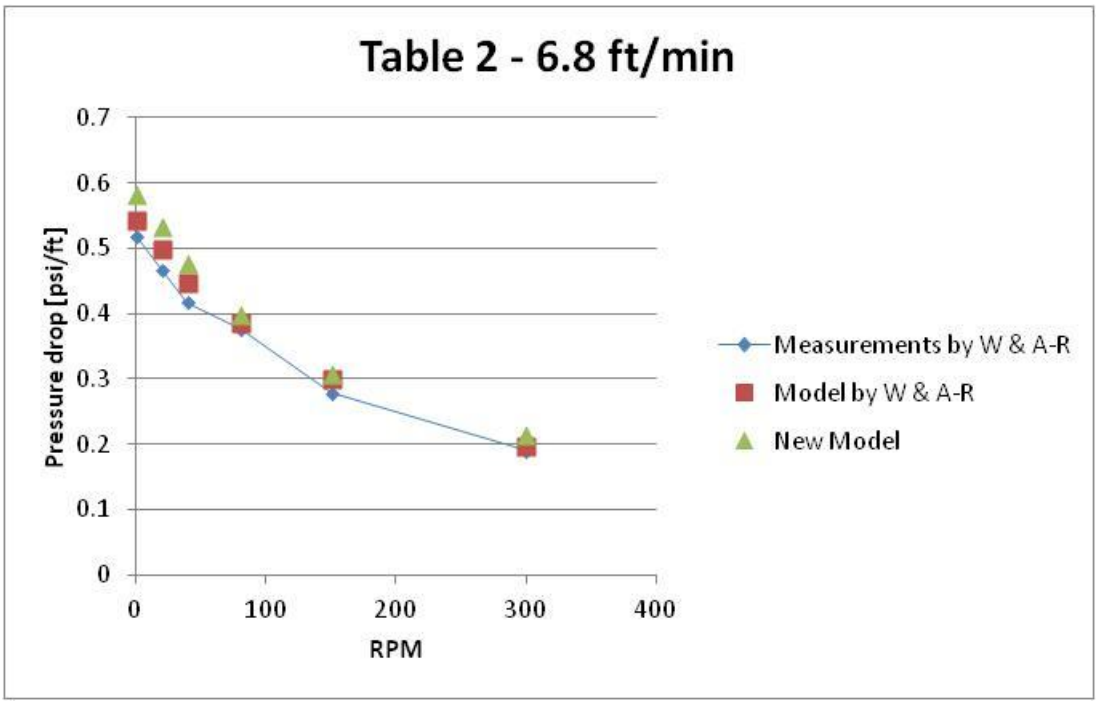

Figure XXV- Comparison to data from Table 2 by Walker and Al-Rawi for velocity equal to 6.8 ft/min

For the low flowrates of 4.8 ft/min and 3.6 ft/min, the program gives no convergence for high rotation speeds. The calculations at lower speeds are as accurate as the other data points above. These errors will be discussed in 6.1.1. Limitations of the model and in detail in Appendix E – Error source for no convergence of low flowrates.

Table 3

Table 3 data is taken from Table 3 in the paper by Walker and Al-Rawi (1970) which includes experimental and computed pressured drops for nominal 16 lb/bbl common bentonite. The calculations showed good results compared to the computed values as expected. Compared to the measured values, the pressure drop is overpredicted. For 17.7 ft/min the maximum error was 28% for measured values and 1% for calculated values; the average error was 20% to measured values and 3% to computed values (see Figure XXVI).

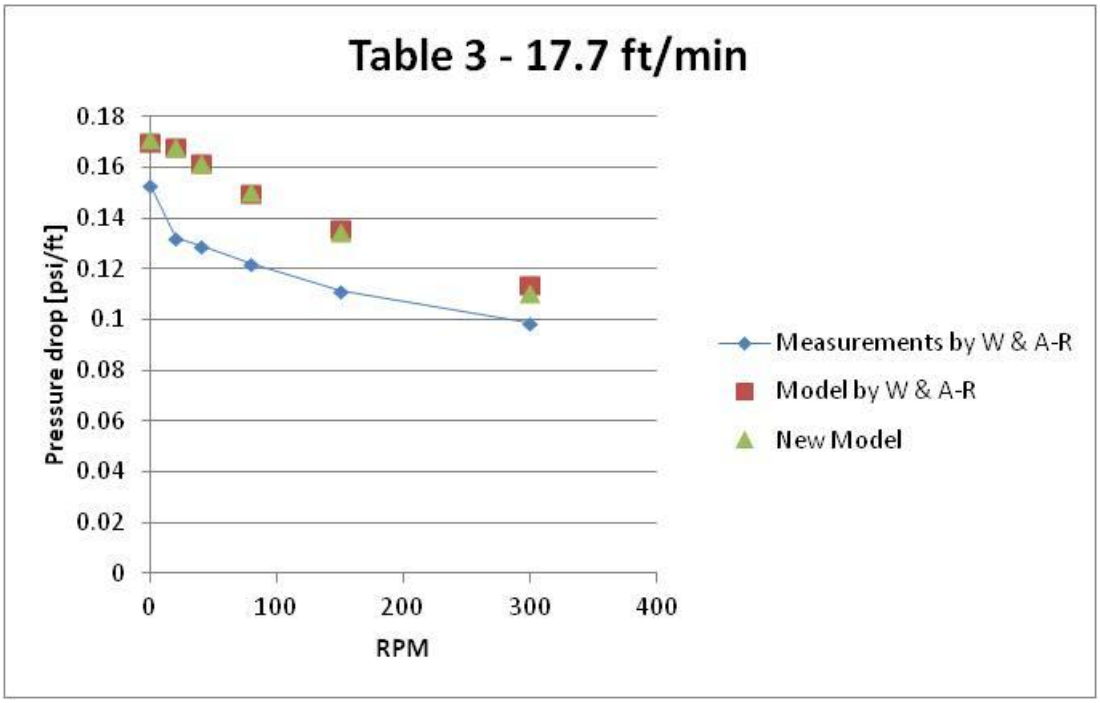

Figure XXVI- Comparison to data from Table 3 by Walker and Al-Rawi for velocity equal to 17.7 ft/min

For 14.2 ft/min the maximum error was 31 % for measured values and 2 % for calculated values; the average error was 19 % to measured values and 2 % to computed values (see Figure XXVII).

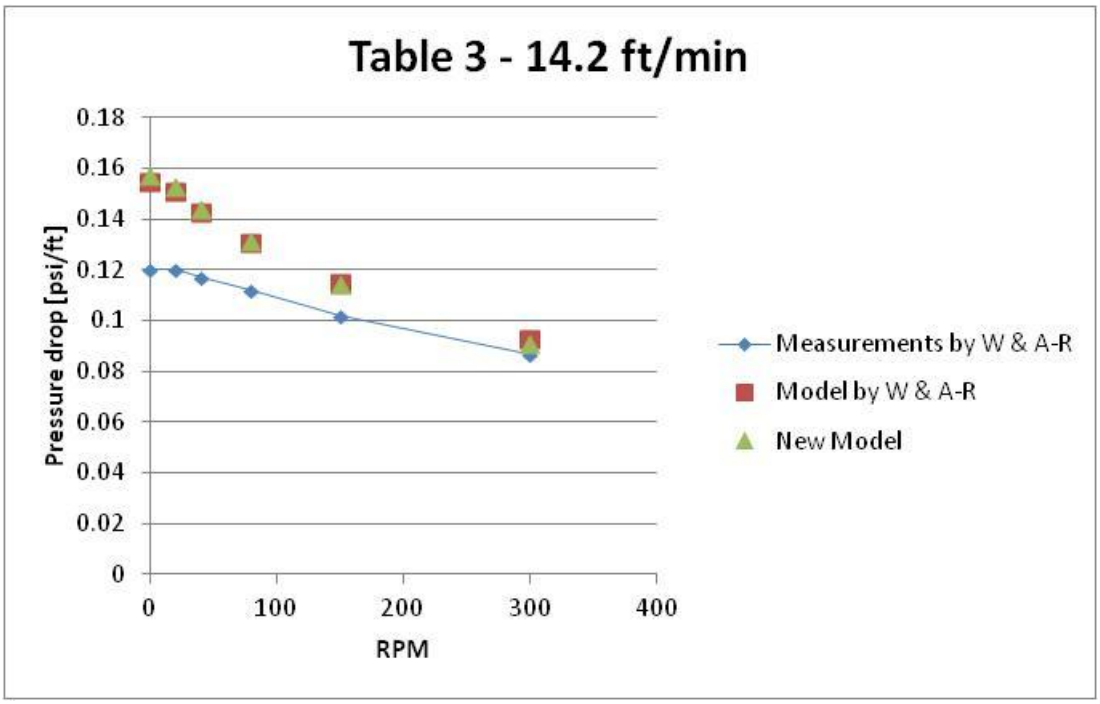

Figure XXVII- Comparison to data from Table 3 by Walker and Al-Rawi for velocity equal to 14.2 ft/min

For 10.7 ft/min the maximum error was 28 % for measured values and 2 % for calculated values; the average error was 16 % to measured values and 1 % to computed values (see Figure XXVIII).

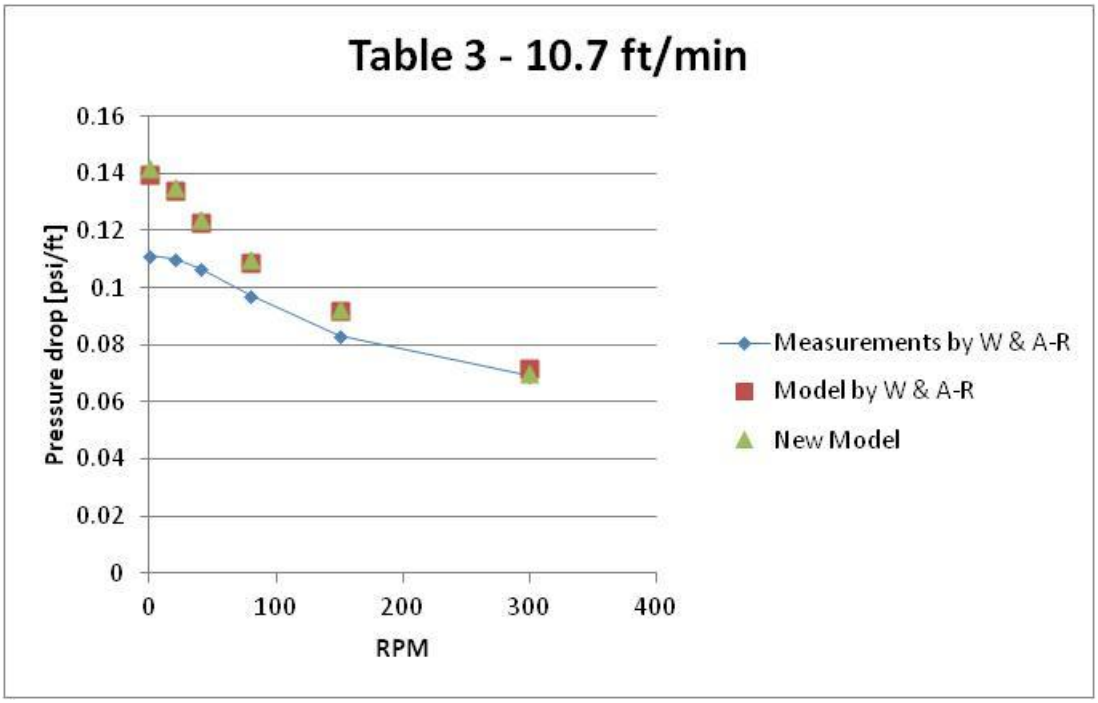

Figure XXVIII- Comparison to data from Table 3 by Walker and Al-Rawi for velocity equal to 10.7 ft/min

For the low flowrates of 7.3 ft/min and 4.6 ft/min the program gives no convergence for high rotation speeds. The calculations at lower speeds are as accurate as the other data points above. For the very low flowrate of 2.1 ft/min, only the simulation at 0 RPM yielded a good result. These errors will be discussed later.

Table 4

Table 4 data is taken from Table 4 in the paper by Walker and Al-Rawi (1970) which includes experimental and computed pressured drops for nominal 23 lb/bbl common bentonite. The calculations showed good results compared to the computed values as expected. Compared to the measured values, the pressure drop is underpredicted. For 18.0 ft/min the maximum error was 14 % for measured values and 3 % for calculated values; the average error was 14 % to measured values and 3 % to computed values (see Figure XXIX).

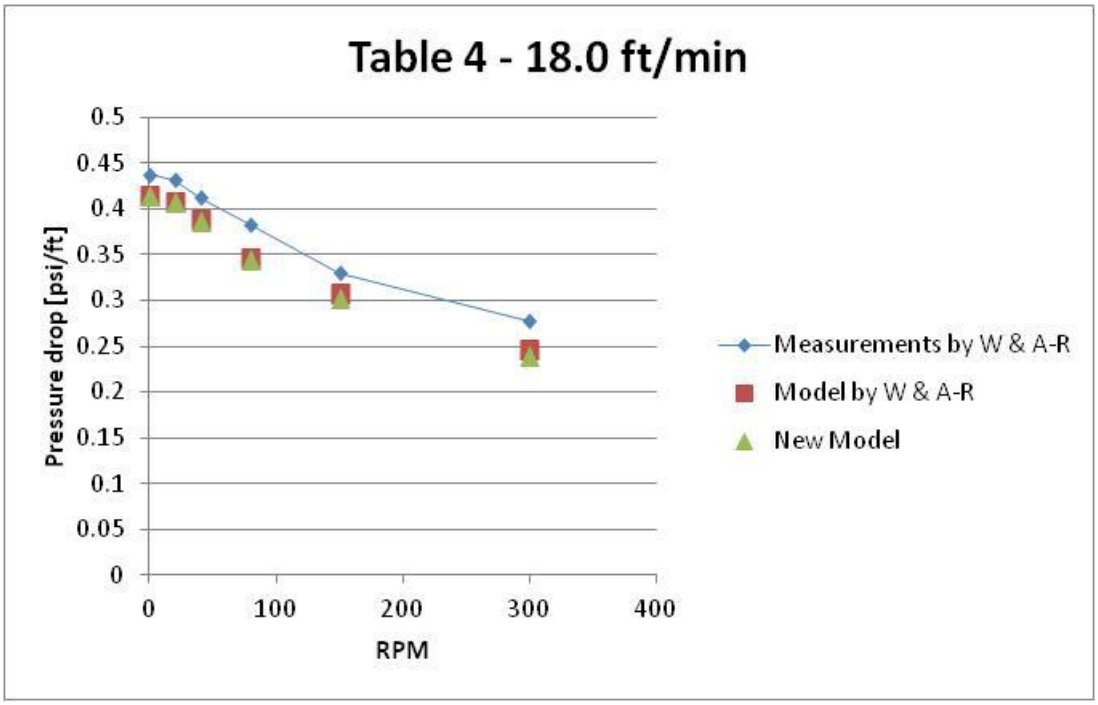

Figure XXIX- Comparison to data from Table 4 by Walker and Al-Rawi for velocity equal to 18.0 ft/min

For 14.6 ft/min the maximum error was 9 % for measured values and 10 % for calculated values; the average error was 6 % to measured values and 2 % to computed values (see Figure XXX).

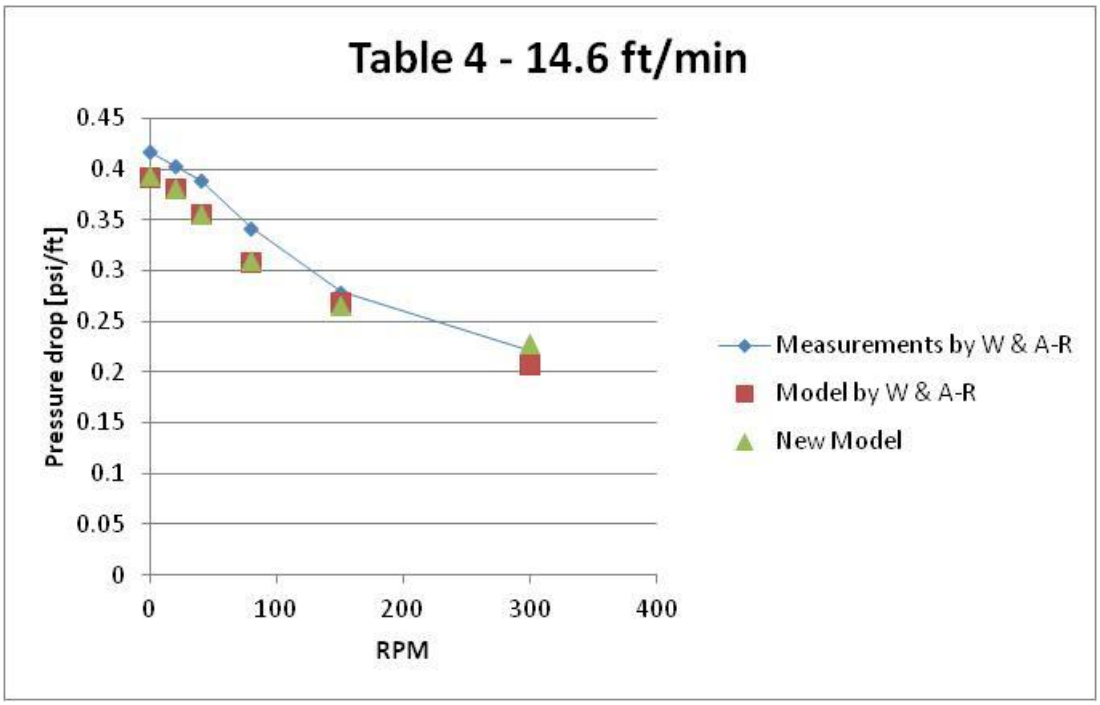

Figure XXX- Comparison to data from Table 4 by Walker and Al-Rawi for velocity equal to 14.6 ft/min

For the low flowrates of 8.0 ft/min and 5.0 ft/min the program gives no convergence for high rotation speeds. The calculations at lower speeds are as accurate as the other data points above. For the very low flowrate of 2.6 ft/min, only the simulation at 0 RPM yielded a good result.

Summary

It was found that for low flowrates the program is unsuccessful in finding a meaningful solution. This is especially true for high rotation speeds. See Appendix D for more information on this error. In Figure XXXI, the calculated value for the highest rotation speed (300 RPM) is off by a high error. This was common for low flowrates and accentuated for high rotation speeds. Nevertheless these complications were overlooked as these flowrates were deemed too small for drilling applications and therefore it was not needed for these to yield a correct result.

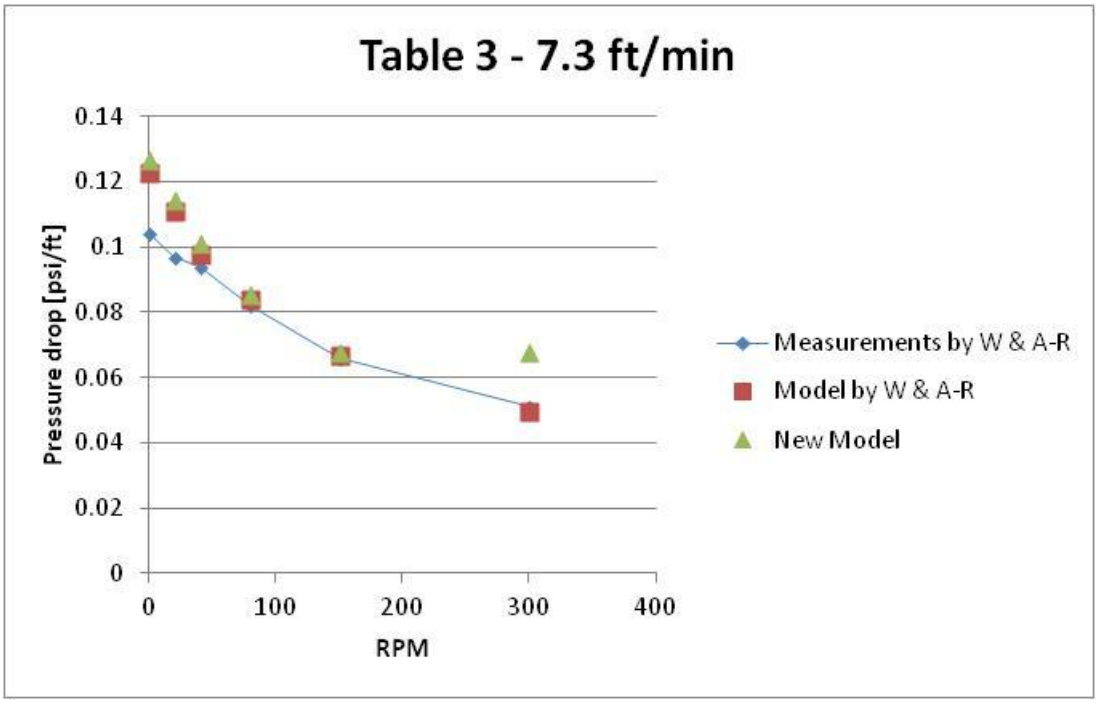

Figure XXXI- Comparison to data from Table 4 by Walker and Al-Rawi for velocity equal to 7.3 ft/min

Omitting the results for low flowrates, the calculated values fit very well with the computed values by Walker and Al-Rawi; and are comparable to their measured data.

5.2.2. Measurements by Ahmed and Miska (2008)

The model was validated against laboratory measurements by Ahmed and Miska (2008). They carried an experimental investigation with five polymer-based fluids in a testing facility. Four different annular geometries were considered, where two of them were fully eccentric, while the two other were fully concentric. The flowrate and the rotational speed off the pipe were varied. Five test fluids were tested for each annular geometry.

The results will be presented as follows: points for the new model calculations (denoted “calculated” or “C”), full lines for measured experimental data by named author (denoted “measured”) and dotted lines for model predictions by named author (denoted “predicted” or “P”).

Concentric annulus without pipe rotation

Ahmed and Miska (2008) compared their predicted and measured pressure loss values for a concentric annulus without rotation for different flowrates. This Power Law test fluid showed measured (blue) pressure losses that were approximately 30 % less than the predicted (green) ones. The simulations from the program (red) gave the same predicted values.

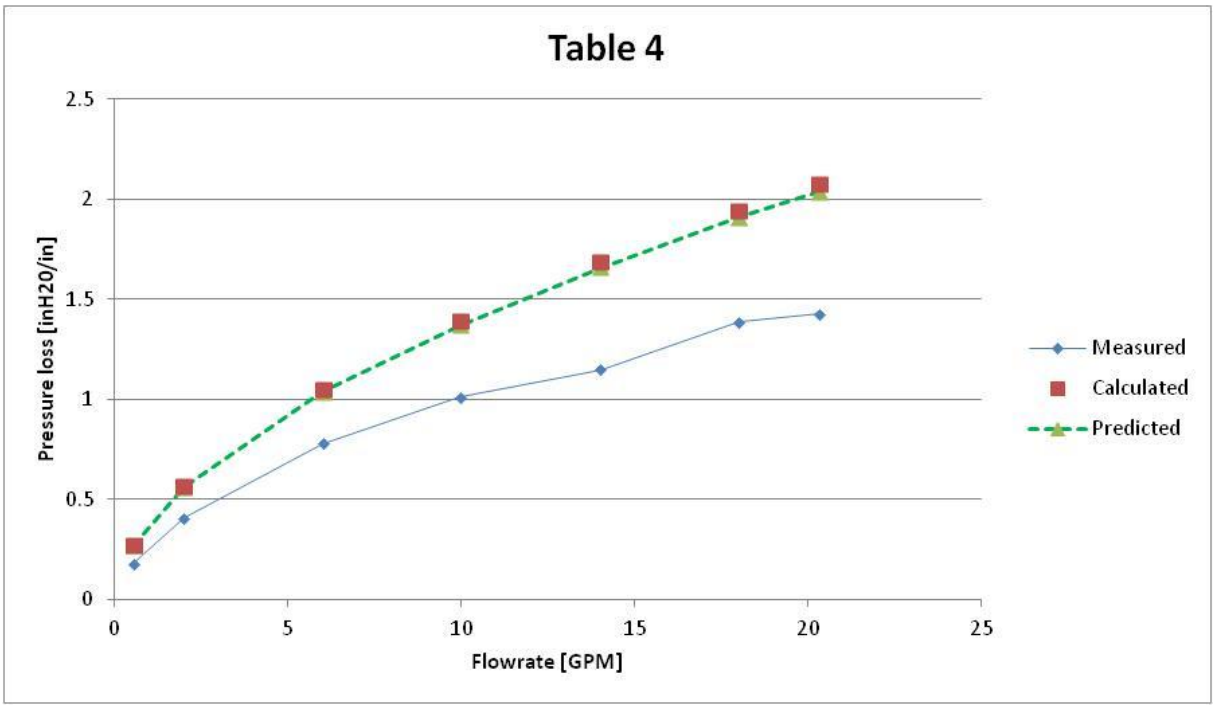

Figure XXXII- Comparison to Table 4 from Ahmed and Miska (2008).

Concentric annulus with pipe rotation

Power Law fluids

In Figure XXXII, measured data by Ahmed and Miska (2008) for a Power Law fluid in a concentric annulus with pipe rotation (lines) is compared to simulations by the new model (points). The fluids consistency index is K=2.10 Pas^m and the fluid behavior index is m=0.38.

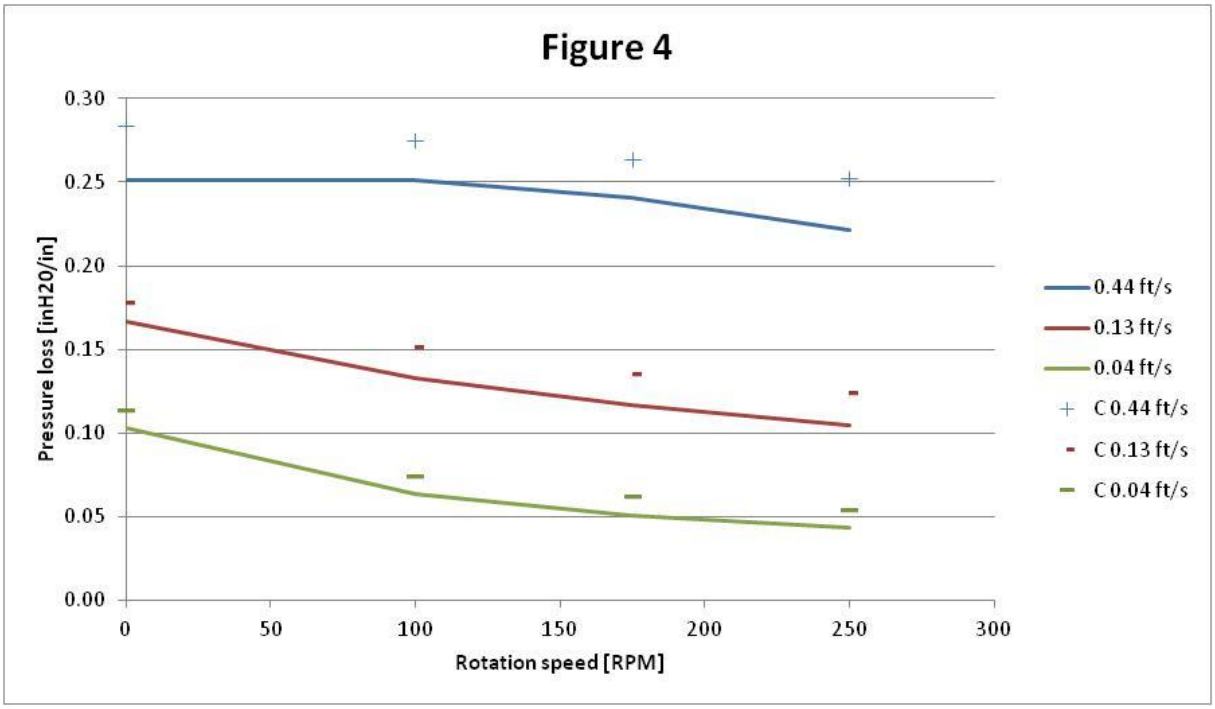

Figure XXXIII- Comparison to Figure 4 from Ahmed and Miska (2008).

The new models results show a higher pressure loss than measured, but are still satisfying. The decreasing trend is well captured by the program as well. The maximum deviance is 25 %, the average difference is 15 %.

In Figure XXXIV, the fluid's rheological parameters are K=0.83$Pas^m$and m=0.56. The annulus is 1 ½ x 1" concentric annulus. The computational results are shown in Figure XXXIV.

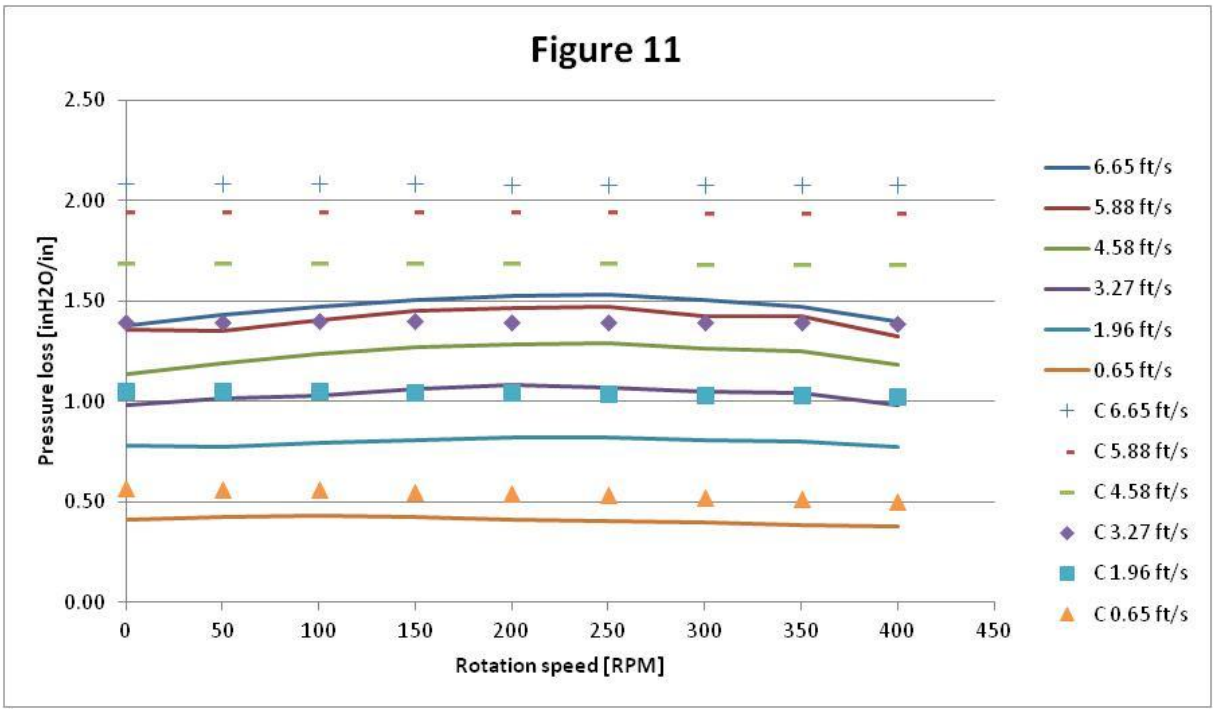

Figure XXXIV-Comparison to Figure 11 from Ahmed and Miska (2008).

The program overpredicts the pressure loss for all the flowrates, the difference increases with flowrate. The average error is 36 % and the maximum error is 51 %.

Yield-Power Law fluids

Yield-Power Law fluids have a yield stress (τ_y) in addition to the consistency index and fluid behavior index. The fluid in use in Figure 5 has τ_y= 9.00Pa, K=3.83 Pas^n and n= 0.35. The program was run for these data, see Figure XXXV.

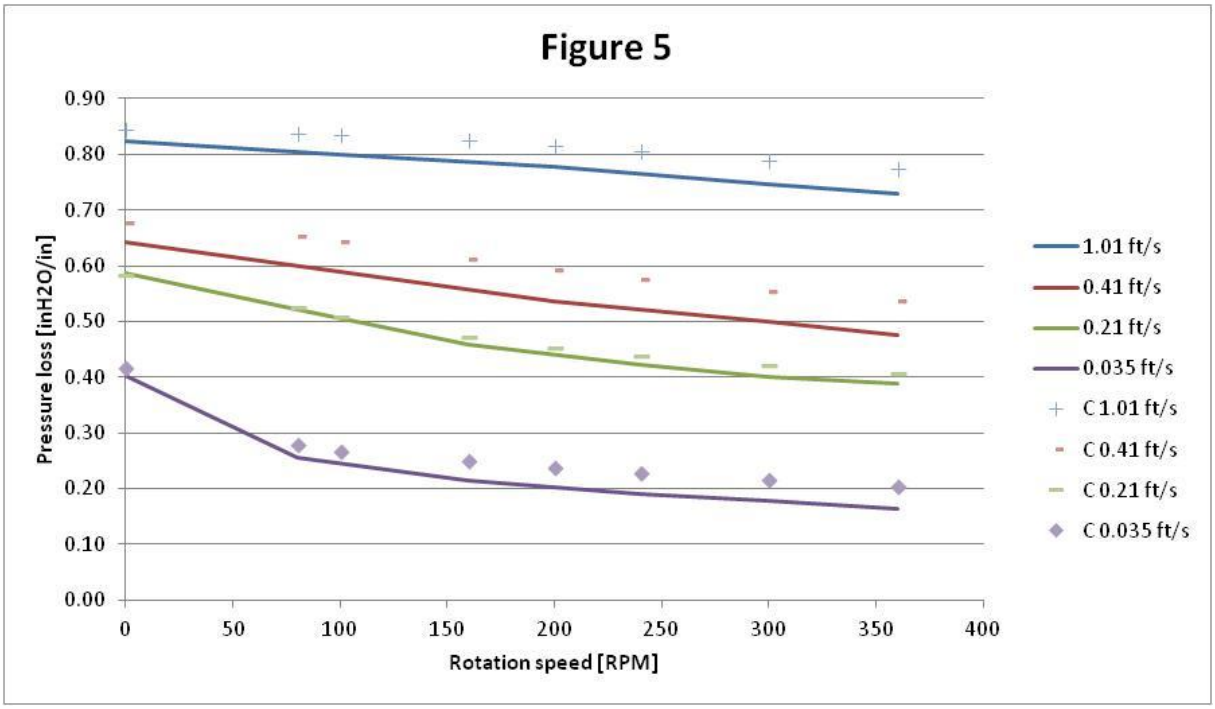

Figure XXXV- Comparison to Figure 5 from Ahmed and Miska (2008).

The pressure loss and its decreasing trend is captured very well for this fluid. The maximum error is 26 % and the average error is 8 %.

Figure 7 used another YPL fluid with the following rheological data: τ_y=6.20Pa, K=1.36 Pas^n and n= 0.43. The computed values for pressure loss showed accurate results for this fluid (see Figure XXXVI). The predicted values from Ahmed and Miska (2008) are also presented (dotted lines or "P").

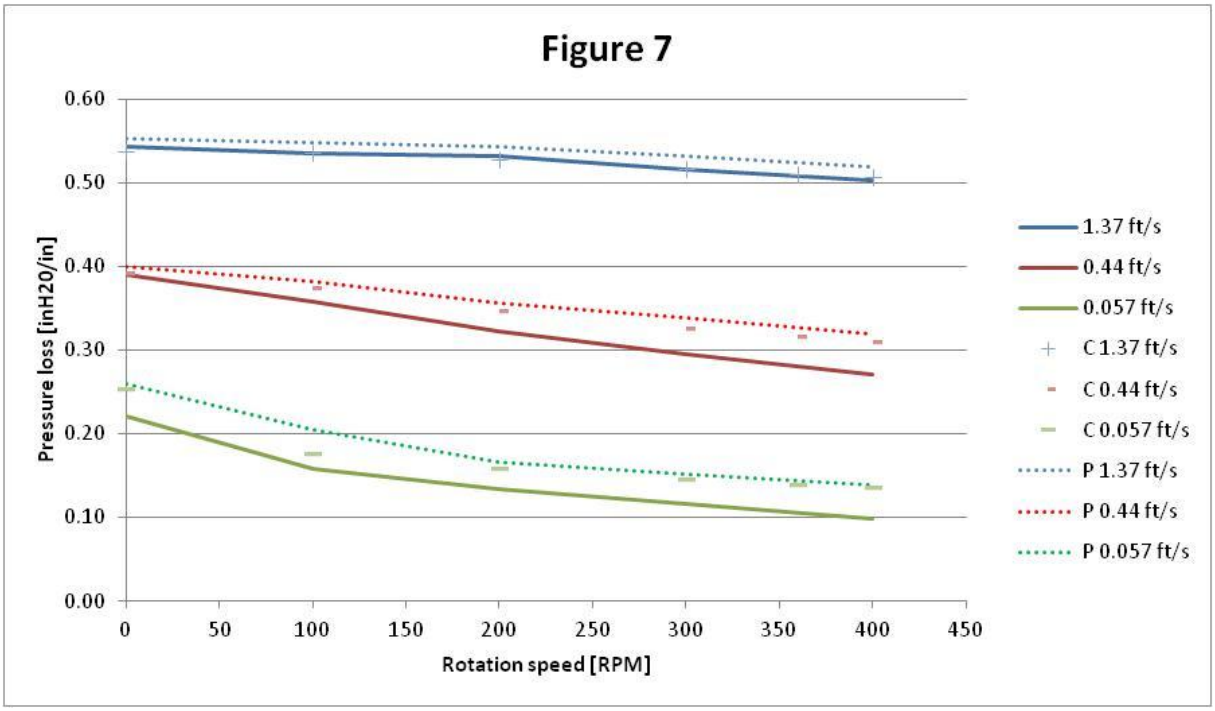

Figure XXXVI- Comparison to Figure 7 from Ahmed and Miska (2008).

The computed data follow the measured data tightly, but the maximum error is 55 % for the lowest flowrate at 400 RPM. The average pressure loss calculation error is 13 %.

Figure XXXVII shows the calculations done for Figure 8 where the applied fluid had a yield stress of 0.40, K=0.84 Pas^n and n= 0.47.

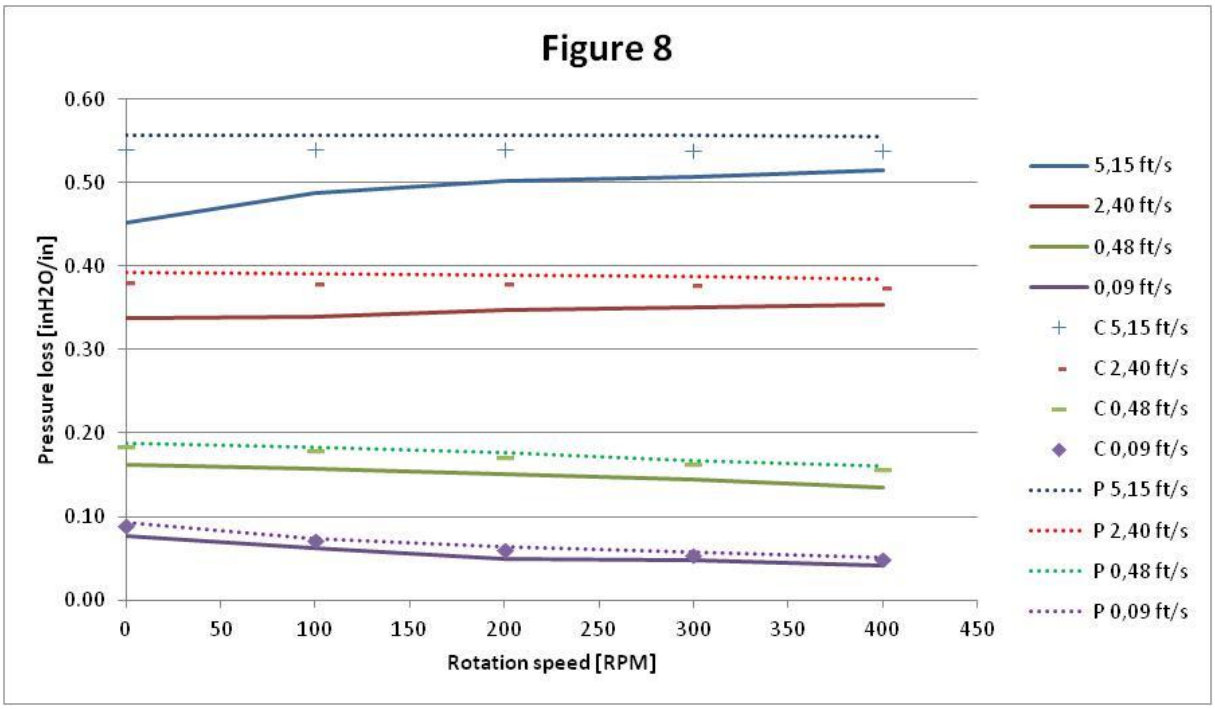

Figure XXXVII-Comparison to Figure 8 from Ahmed and Miska (2008).

Compared to the measured data, the computed data follows the same trends. The values have an average deviance to the measured values by 13 % and the maximum error is 26 %. One point that seems not to have been captured correctly is the pressure loss at 0 RPM for the highest flowrate.

Figure XXXVIII displays the results for the fluid with τ_y= 11.00Pa, K=1.05 Pas^n and n= 0.52 in a 1 ½" x 1" concentric annulus.

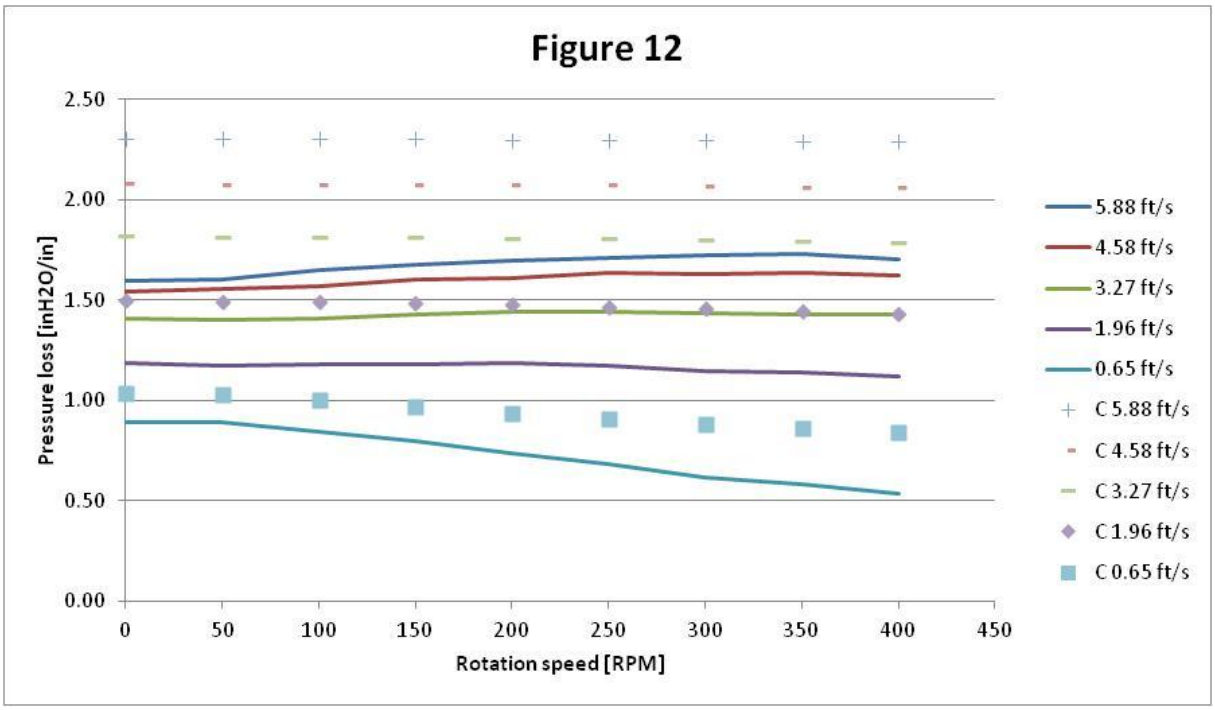

Figure XXXVIII-Comparison to Figure 12 from Ahmed and Miska (2008).

The simulations overpredict the pressure loss for all flowrates. The linear trends of the higher flowrates are comparable. The lowest flowrate data should decrease faster than the simulated data. The average error for thee computations is 30 % and the maximum error exists for the lowest flowrate at 400 RPM (56 %).

Eccentric annulus with pipe rotation

Power Law fluids

The following measurements by Ahmed and Miska (2008) were made for different fluids at varying flowrate and rotation speed in two different sized fully eccentric annuli. The first is a 1 ½" x ¾" annulus and the second is a 1 ½" x 1" annulus.

A fluid with K=0.25 Pas^n and n= 0.61 was tested in the 1 ½" x ¾" annulus. The results are shown in Figure XXXIX.

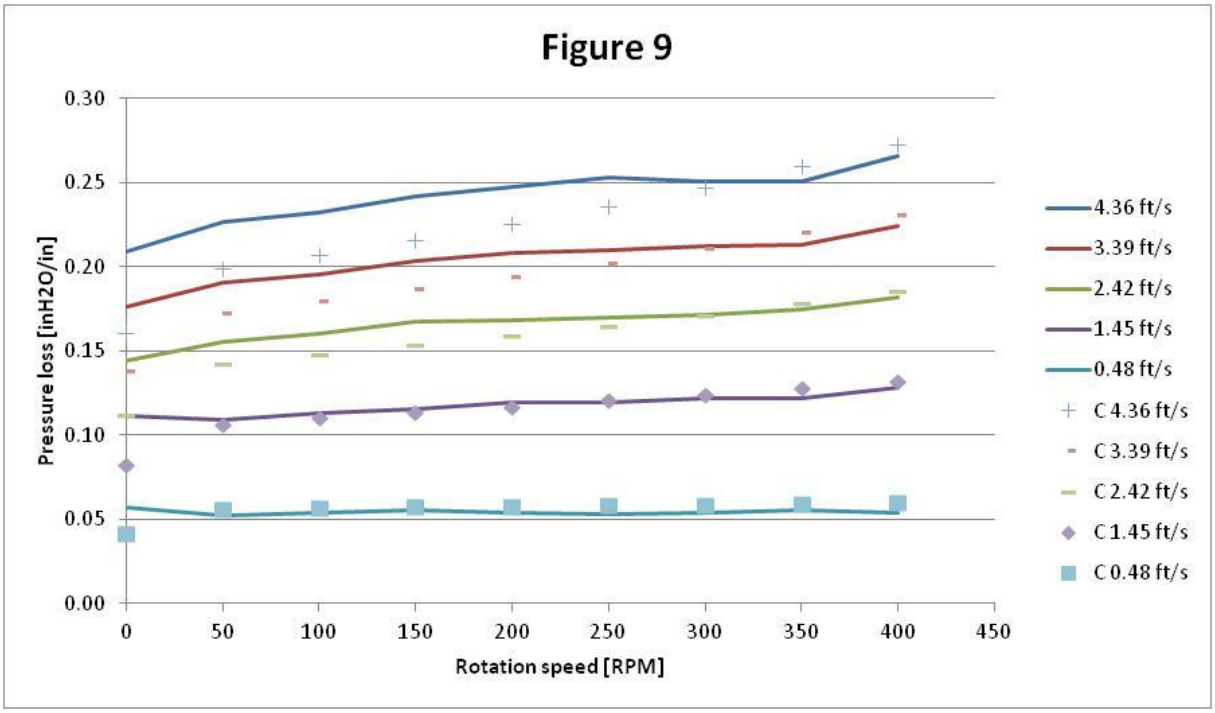

Figure XXXIX- Comparison to Figure 9 from Ahmed and Miska (2008).

The average error was found to be 8 % and the maximum error of 27 % was found for the highest flowrate at 0 RPM. It is also observable that for all predictions at 0 RPM (no rotation) the program underpredicts the pressure loss. For higher flowrates, the program underpredicts for low rotation speeds, and overpredicts for high speeds (350 and 400 RPM). The increasing trend of the curves is captured by the program.

Figure XL shows the results for the Power Law fluid with rheological parameters K=0.93 Pas^n and n= 0.52.

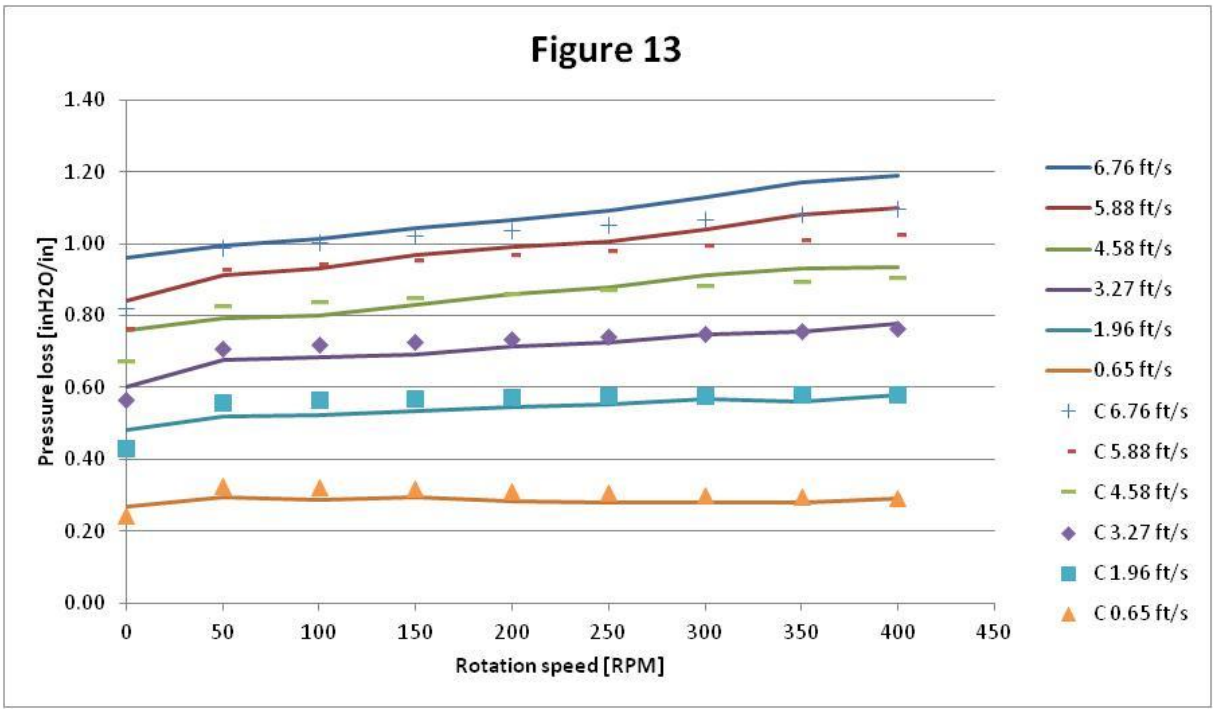

Figure XL- Comparison to Figure 13 from Ahmed and Miska (2008).

The average error is 5 % and the maximum error is 15 %, which indicates that the results match well the measured values. The highest errors can be observed for 0 RPM and for the highest flowrates at the highest rotation speeds.

Yield-Power Law fluids

Figure 10 used an YPL fluid with the following rheological data: τ_y=10.50Pa, K=0.97 Pas^n and n= 0.53 (fluid C_2). The computed values for pressure loss showed comparable results for this fluid at high flowrates (see Figure XLI).

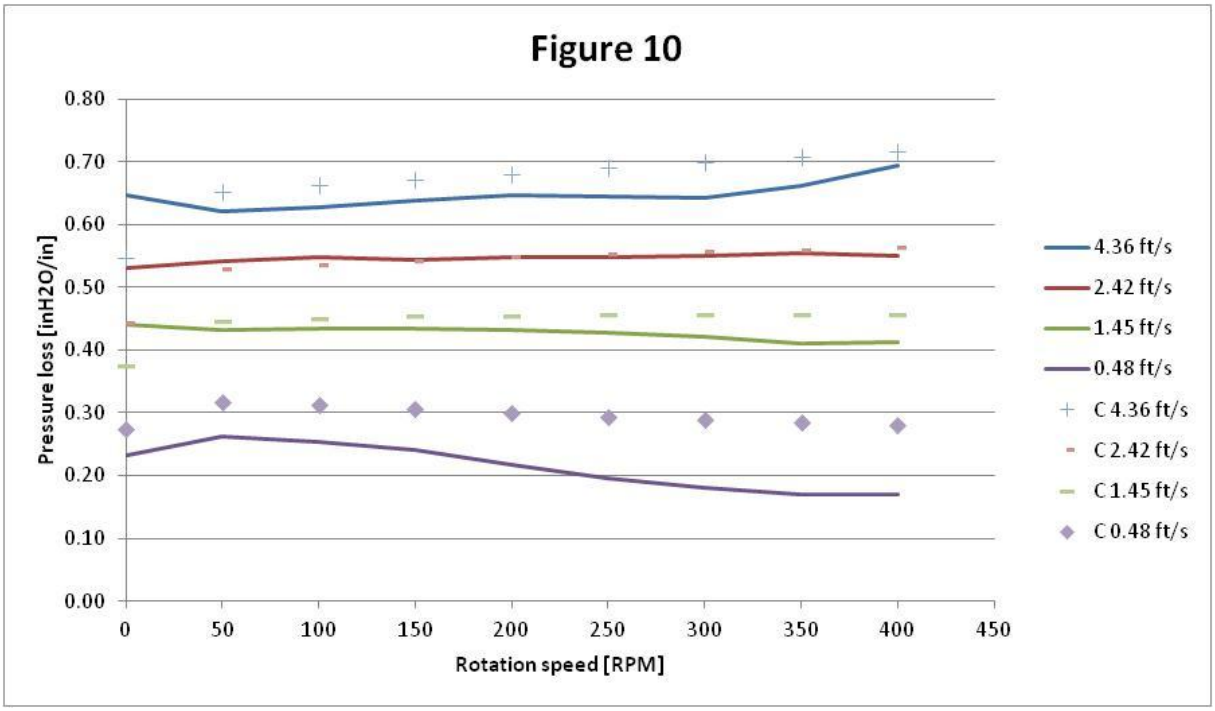

Figure XLI- Comparison to Figure 10 from Ahmed and Miska (2008).

The highest deviances fro Figure 10 are observed for the lowest flowrate (67 %), the simulation results do not decrease as rapidly as the measured values. The program seems to overpredict the pressure loss, and overall the results are within 15 % average error compared to the measured values.

Comparison with Figure 14 which uses fluid D4 (τ_y=3.10Pa, K=0.74 Pas^n and n= 0.48) is shown in Figure XLII.

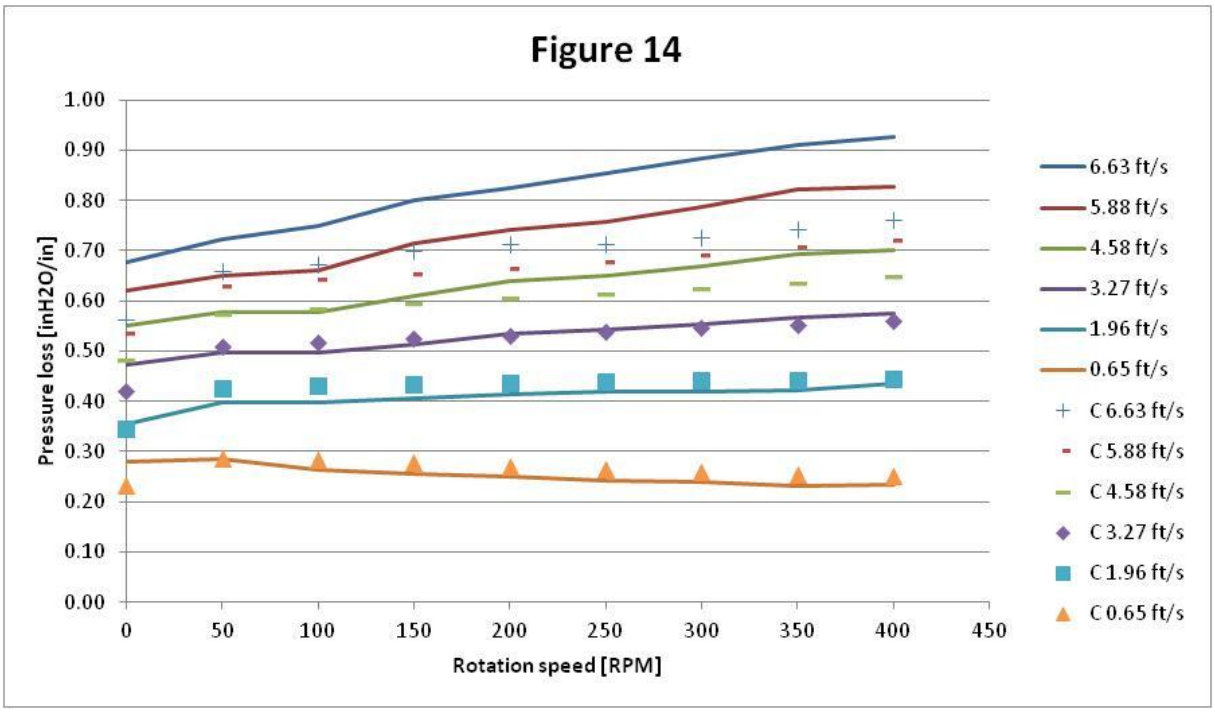

Figure XLII-Comparison to Figure 14 from Ahmed and Miska (2008).

It is observed that for the higher flowrates (4,58 ft/s and above) the program underpredicts the pressure loss. For the flowrates underneath, the results are similar. The average discrepancy is 8 % and the maximum is 18 %.

Figure XLIII displays the results for the fluid with τ_y=1.50Pa, K=0.30 Pas^n and n= 0.52 (fluid E4) in a 1 ½" x 1" fully eccentric annulus.

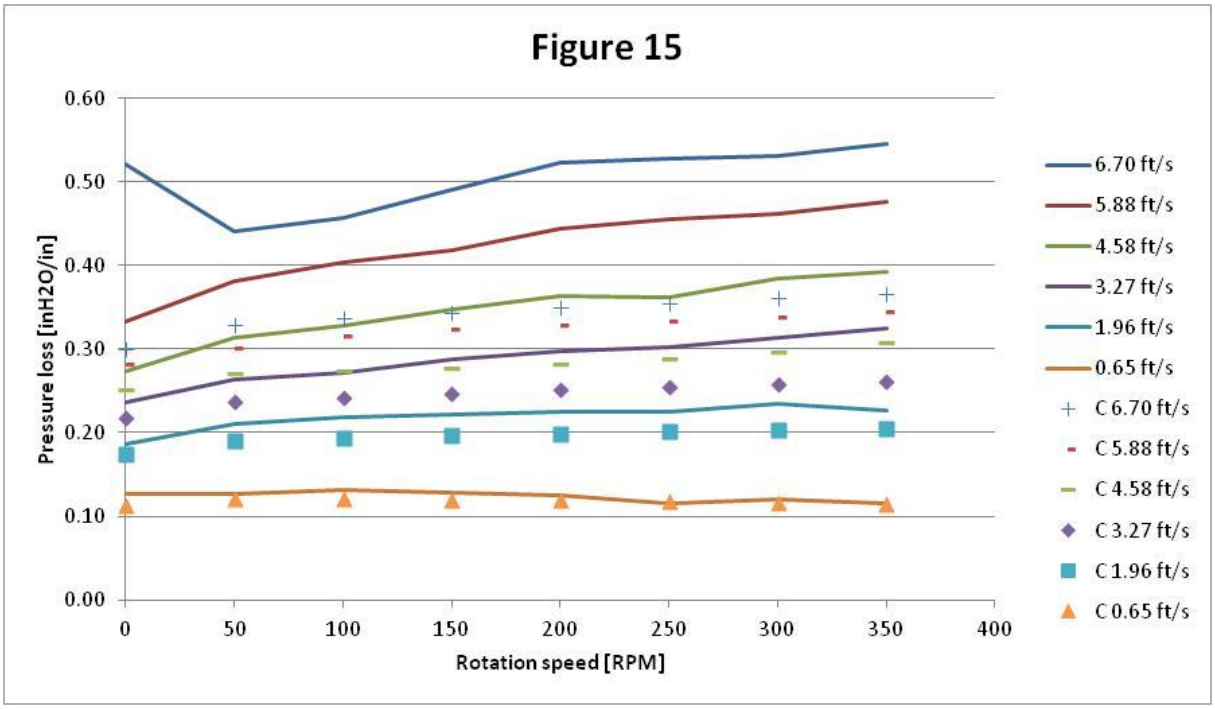

Figure XLIII-Comparison to Figure 15 from Ahmed and Miska (2008).

The average difference between the measured and the computed values is 42 % and it is the calculation for 0 RPM for 6.70 ft/s velocity. Contrary to the other data points the follow the same trend as the measurements, the prediction at 0 RPM starts lower than the prediction at 50RPM. For the measured data, the pressure loss decreases from 0 RPM to 50 RPM. Overall, the simulated values are underpredicting the pressure loss, especially at higher flowrates. The average discrepancy is 16 %.

5.3. Test Runs-Study

A test runs-study was conducted by the author to validate the program. Sensitivity analysis will be conducted to examine the effects of each important parameter and will be studied in detail. A Power Law and Yield-Power Law fluid was chosen for the test runs. Comparison between these two fluids will show the effect of shear-thinning and inertial effects more clearly. Table F shows the standard input data for the test runs, which have been varied depending on the desired sensitivity analysis conducted.

Table F- Inputs for the Power Law and Yield-Power Law fluid

Input Table		
Pipe Inner Diameter [m]	0.1270	
Pipe Outer Diameter [m]	0.2159	
Flow Behaviour Index (m)	0.52	
Eccentricity (ε)	1	
Density (ρ) [kg(m^3]	1000	
Flowrate (Q) [m^3/s]	9.71E-03	
Pipe Rotation Speed (RPM)	100	
	Power Law	*Yield-Power Law*
Consistency Index (K) [Pas^m]	0.93	1.05
Yield Stress (τ_y) [Pa]	0.0	11.0

Simulations were run for the specified scenario with a PL fluid in an eccentric annulus with pipe rotation. At 0 eccentricity (concentric annulus) the highest pressure loss is observed for the case of no rotation and subsequently lowers with increasing rotation. This is due to the shear-thinning effects due to rotation, see Figure XLIV. In the case of no rotation (blue line) the pressure loss decreases more rapidly than for the cases with rotation; which proves the existence of a secondary effect. For eccentricity higher than 0.7, the pressure loss is higher for higher rotation speeds. The explanation for this behavior is that the inertial forces are stronger than the shear-thinning effect after 0.7 eccentricity for his case.

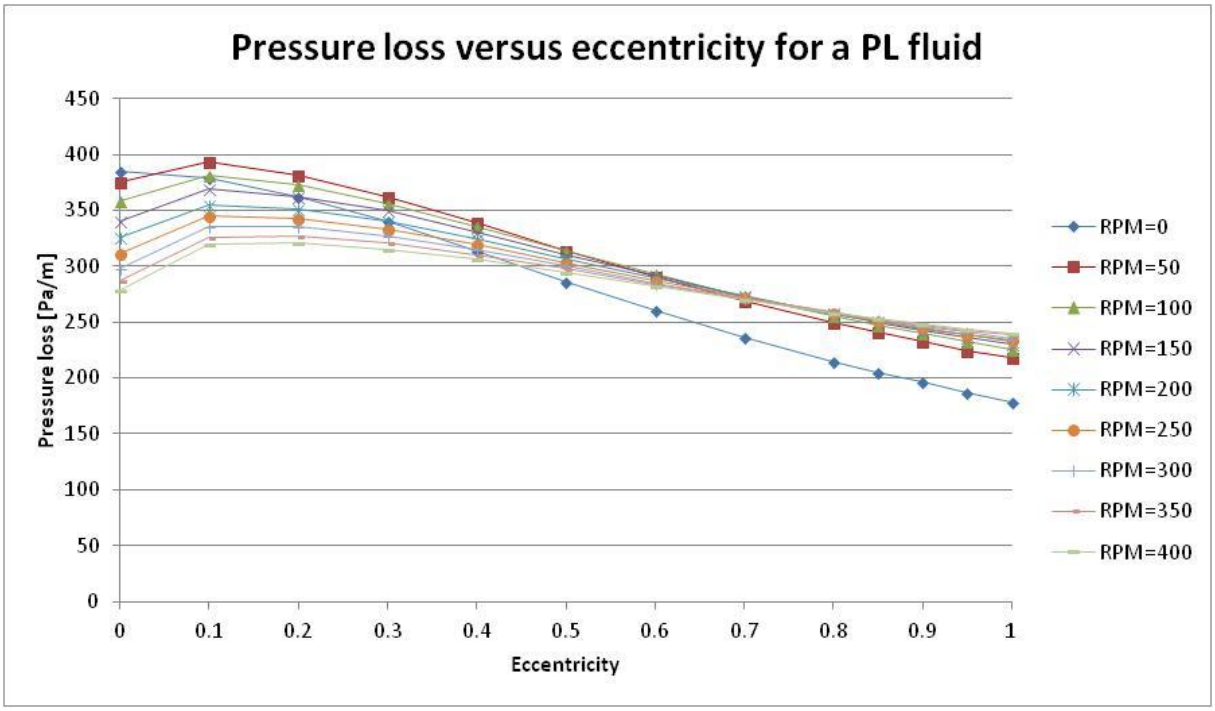

Figure XLIV- Pressure loss versus eccentricity for a PL fluid

The pressure loss for the same PL fluid was plotted against rotation speed for a simulated concentric (*e*=0) and a fully eccentric annulus (*e*=1) (Figure XLV).

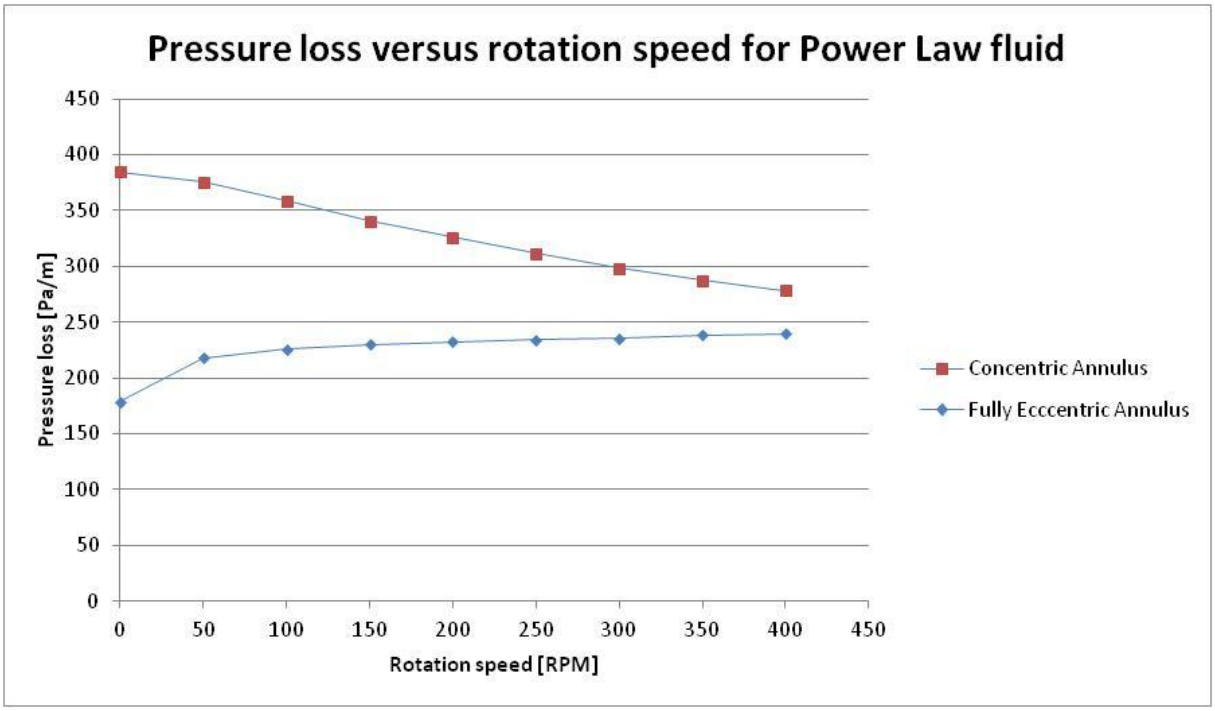

Figure XLV-Pressure loss versus rotation speed for PL fluid

In the case of a concentric annulus, the flow will be purely helical. As such, no inertial effects will exist. The decrease in pressure loss for concentric annuls is therefore a result of pure shear-thinning. In the case of the fully eccentric annulus, acceleration of the flow will counteract the effect of shear-thinning. In this example case study, the Power Law fluid is subjected to higher inertial effects than

shear-thinning effects, and the pressure loss is therefore increasing with rotation speed. The rate of change of pressure loss seems to decrease with rotation speed.

The effect of eccentricity and rotation on pressure loss was computed for the YPL fluid (see Figure XLVI).

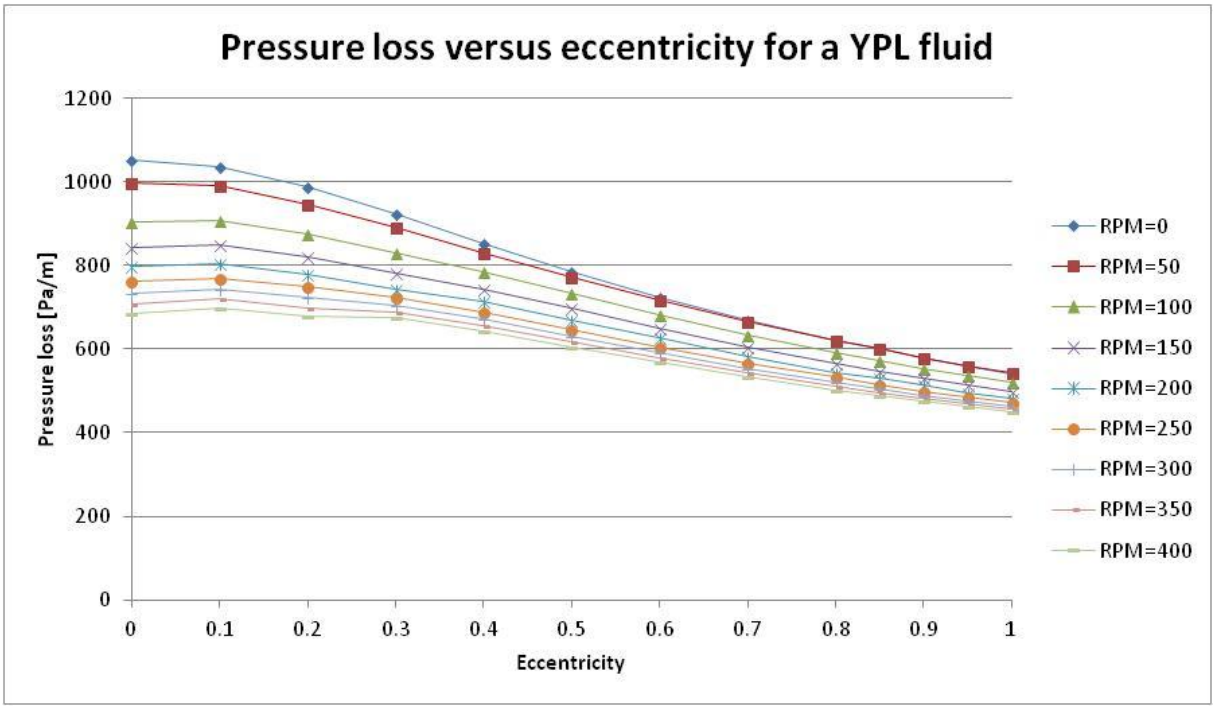

Figure XLVI- Pressure loss versus eccentricity for a YPL fluid

The pressure loss decreases with both eccentricity and rotation speed. It is observed that the effect of rotation is diminished with increasing numbers of eccentricity. Yield-Power Law fluids have a yield stress and are therefore highly prone to shear-thinning which reduces the pressure loss. In this specific case, the shear-thinning effect outbeats the inertial effects. The effect of rotation seems to decrease after 150 RPM. For each increment after this rotation speed, the pressure loss change is decreasing.

The pressure loss versus rotation speed for the YPL fluid was plotted for a concentric annulus and a fully eccentric annulus (see Figure XLVII).

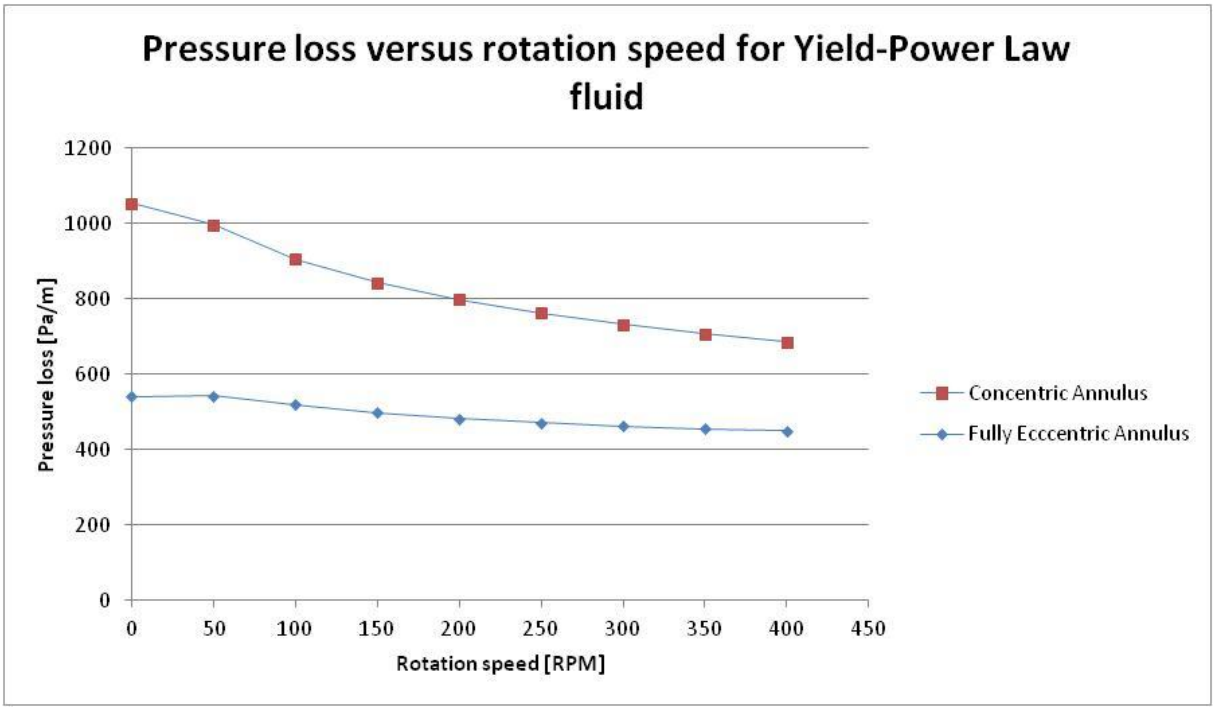

Figure XLVII- Pressure loss versus rotation speed for Yield-Power Law fluid

The above figure shows that the shear-thinning effects are dominant over the inertial effects for this case. This is a confirmation of the observations above.

To determine the effect the fluid behavior index has on the pressure loss, simulations with different values were run (see Figure XLVIII). It should be noted that the consistency index was not changed accordingly with n, but was maintained constant. The consequence is that we will get quite different fluids for each n.

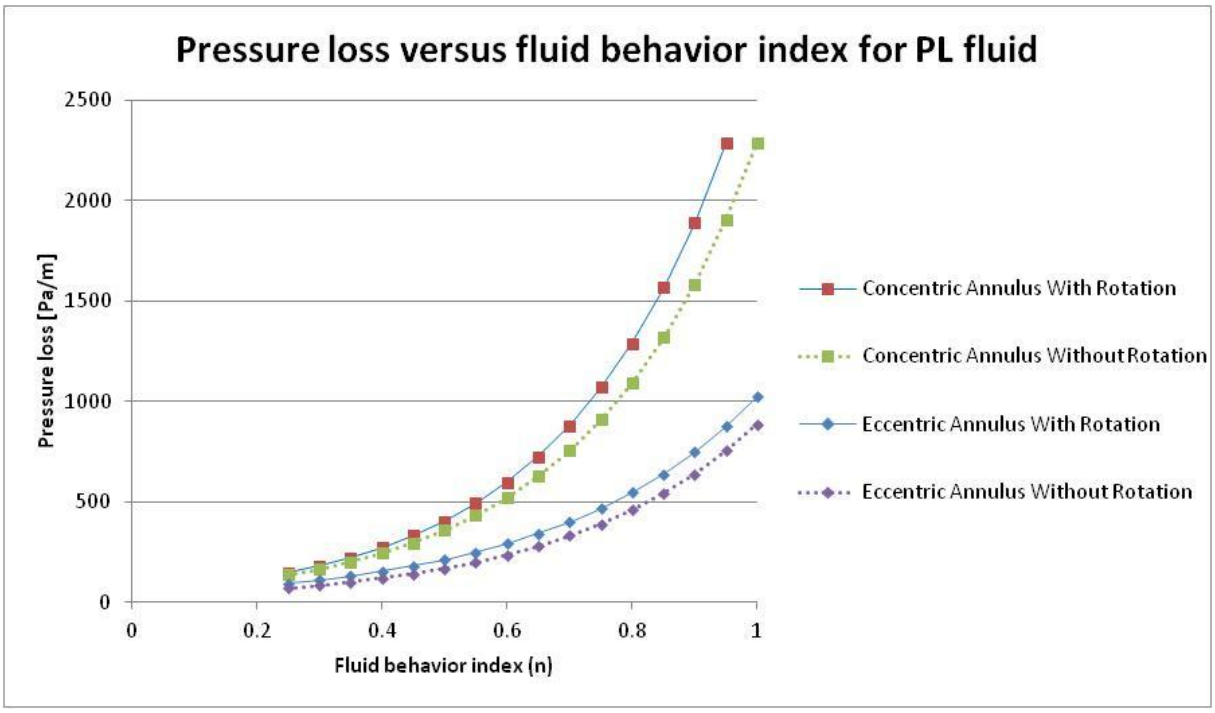

Figure XLVIII-Pressure loss versus fluid behavior index for PL fluid

The pressure loss is significantly dependent on the fluid behavior index (rheological parameters). The rate of change in pressure loss is different from the concentric to the eccentric annulus, since the maximum value for pressure loss for fully eccentric annulus is under half of the same value for concentric annulus. The maximum pressure loss is observed for n=1, which is for Newtonian fluid which is not affected by shear-thinning. The same simulations were done for the YPL fluid, see Figure XLIX.

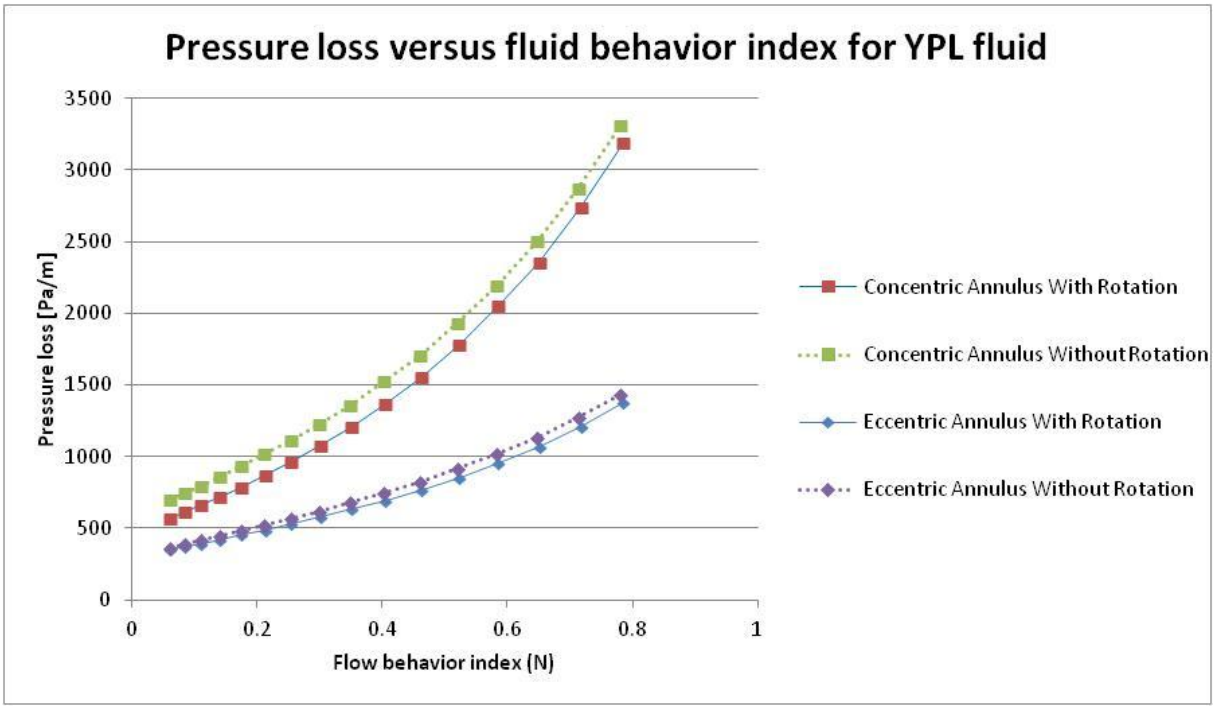

Figure XLIX - Pressure loss versus flow behavior index for YPL fluid

The pressure loss was plotted against flow behavior index (N). The pressure loss is smaller in the eccentric annulus than concentric. The higher the flow behavior index, the higher the pressure loss. YPL fluids are highly shear-thinning; as such the pressure loss is higher without rotation for both cases.

6. Discussions

6.1. Limitations

6.1.1. Limitations of the model

The limitations for the model are sorted into six categories: the correlation for inertial effects, diameter ratio, fluid behavior index, low flowrates, the range of available data and the program code.

The correlation for inertial effects

The new correlation is not based on theory other than being a function of important parameters (Reynolds number, Taylor number, eccentricity, radius ratio and flow behavior index) related to published data in the literature. Therefore, the correlation is only as good as the results it gives. With a closer look on the constants used in the correlation for inertia, it is observed that the constants in the power of the Reynolds number and radius ratio are negative. This supports that the correlation may not be accurate enough.

It is in the author's belief that a more accurate correlation can be found using extensive curve fitting techniques. However the combined simplicity and acceptable accuracy of the model goes hand in hand with the goal of creating a field-friendly model.

Diameter ratio

While attempting to find a correlation for the effect of inertia, an alternative approach was considered. The function of $\frac{fRe_w}{fRe_0}$ against eccentricity for different Taylor numbers was normalized for the given three radius ratios in the published data (κ=0.2, 0.5 and 0.8); see Figure L, Figure LI and Figure LII. fRe_w is the frictional pressure loss with pipe rotation; and $fRe_0$is the frictional pressure loss without rotation.

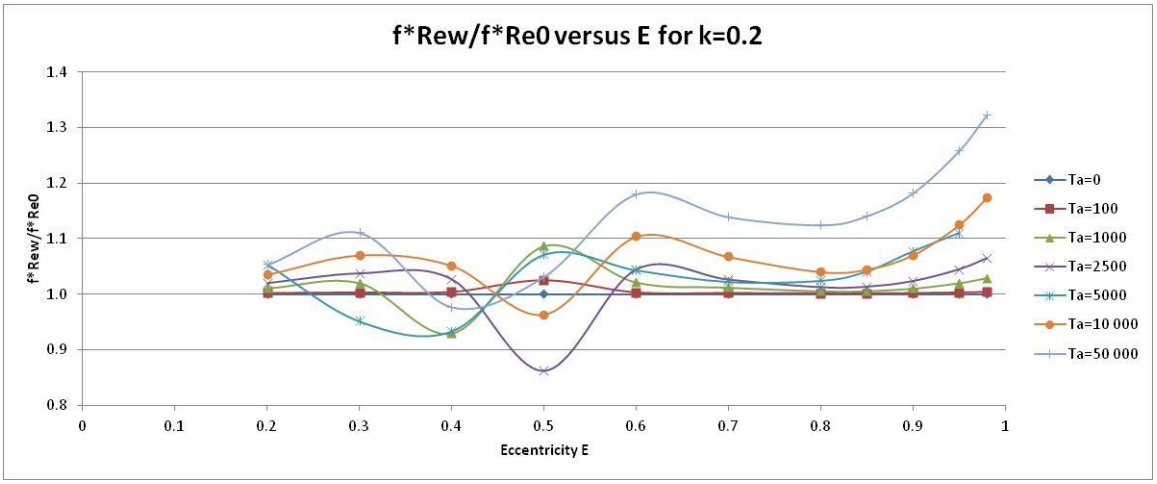

Figure L- The function of fRe_w/fRe_0 against eccentricity for different Taylor numbers for radius ratio κ=0.2.

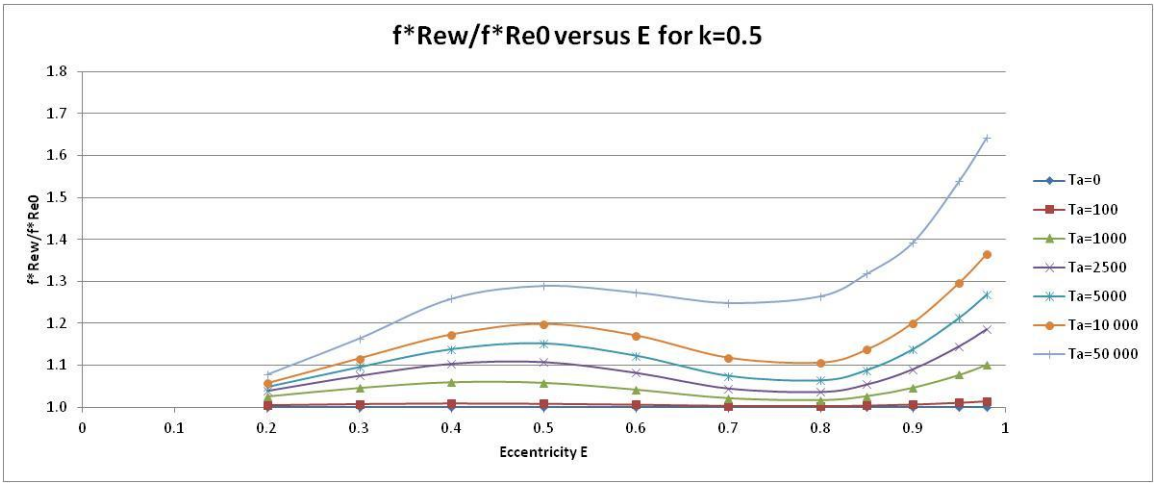

Figure LI- The function offRe_w/fRe_0 against eccentricity for different Taylor numbers for radius ratio κ=0.5.

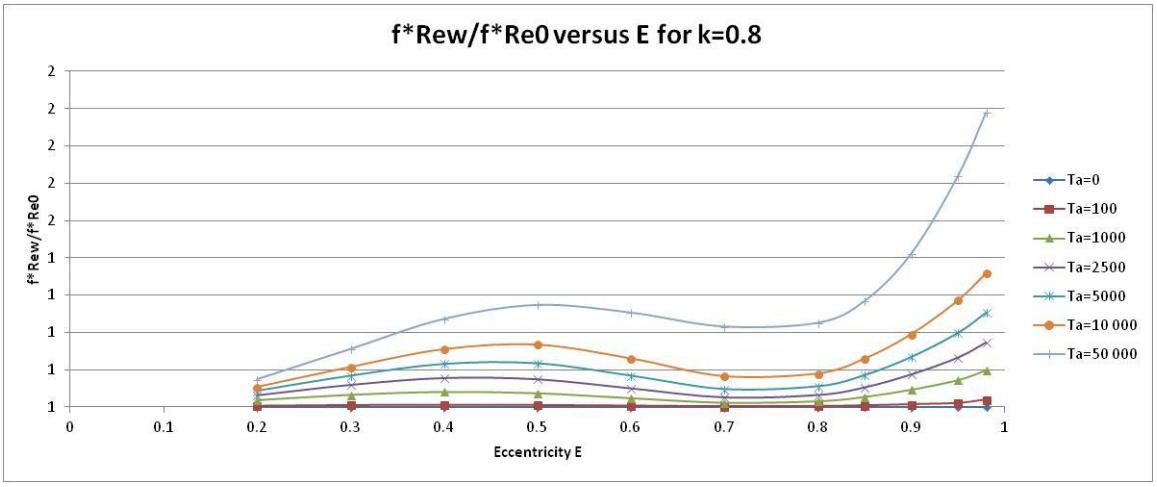

Figure LII- The function of fRe_w/fRe_0against eccentricity for different Taylor numbers for radius ratio κ=0.8.

The resulting correlation was found to be less accurate than the equation proposed by LabFit, so the LabFit equation was chosen instead. From the graphs, it was however possible to observe that the $\frac{fRe_w}{fRe_0}$ ratio showed clear trends for κ=0.5 and 0.8. The three areas of increasing frictional pressure drop from approximately 0<e<0.5, decreasing from 0.5<e<0.75 and increasing sharply from 0.75<e<1, as commented by Escudier et al. (2000), appear on these graphs.

The trends were irregular for a diameter ratio of 0.2, and it was therefore decided not to pursue to include this diameter ratio in the model. The new model is therefore only applicable for diameter ratios of 0.5 and 0.8, but approximate values can be expected for diameter ratios between 0.5-0.8, where a similar relationship is assumed.

Fluid behavior index

The program was unsuccessful in yielding any meaningful results for low values of the fluid behavior index, m. The reason for this limitation is assumed to be caused by mathematical errors associated with dealing with numbers in the power of a function of m. Problems were observed only in the low range, at approximately up to 0.2. Most drilling muds used in the field however have a higher fluid behavior index value. The fluid behavior index for the drilling muds used in Ahmed and Miska's experiments (2008) range from 0.35 to 0.61.

Low flowrates

For some scenarios, low flowrates caused the program not to converge for any values of pressure loss. Flowrates of less than 3 $\mathrm{ft/min}$ commonly has problems, but non-convergence was also experienced at 4 $\mathrm{ft/min}$ in combination with rotation speeds of 300 RPM. These flowrates are very low and not regularly associated with field conditions. It was decided to take extra precautions for flowrates of less than 6ft $/\mathrm{min}$. In any case, the program is not in danger of yielding wrong results for this problem, since non-convergence returns no values. All flowrates above 6 $\mathrm{ft/min}$ were considered good annular speeds. More on this problem is discussed in Appendix E – Error source for no convergence of low flowrates.

The range of the available data

The available data by Escudier et al. (2000, 2002) range from Taylor numbers 0 to 50 000. Higher Taylor numbers may be experienced in the field; hence results from the new model for these numbers may be less accurate. A similar relationship was assumed between Taylor number and pressure loss in the new model for Taylor numbers higher than 50 000.

Nonetheless, a wide range of rheological parameters have been used. The fluid behavior index has ranged from 0.35-0.61, the consistency index from 0.25-3.83 and yield stress from 0.00-11.00. A

huge number of frictional pressure loss values (660 in total) have been related to their corresponding parameters including a wide range of Reynolds and Taylor numbers in the laminar region. The applicability area is therefore quite significant.

The program code

Plausible explanations for the discrepancies between the new model and the numerical results include the fact that the model goes through several iterations, and the tolerance limits for the errors in these calculations were set for the purpose of finding a good fit between the computation time and the desired error. By setting a very low tolerance, the computations will show precisely the same results for each simulation, but will run for a longer time. Minor differences may be observed for equal simulations due to the desire to have a program that runs fast at the expense of extensive precision.

It is shown by the computational results that there are discrepancies even without rotation, but these are negligible. However for some simulations for concentric annulus, the resulting frictional pressure loss is less than the value for 0.1 eccentricities. This is contradicting the trend of decreasing frictional pressure drop with eccentricity. The differences are very small, and do not impose any significant problems. The discrepancies are mainly observed at high Taylor numbers for specific correlations.

Additional changes in laminar flow patterns that result from tooljoints, BHA (Bottomhole Assembly) and washouts have not been accounted for in the model. These effects have showed to have a significant effect on pressure loss, as commented by Marken et. al (1992). Discrepancies between results from the new model and published field data may dependent on these factors. Cartalos and Dupuis (1993) commented that the altered flow by rotation again has an effect on drillstring placement in borehole. Any further changes of fluctuations in downhole pressure can be caused by other factors such as cuttings bed buildup, barite sag occurrence, pump rate changes, etc…(Hemphill et al., 2008).

The limitations of the new model pose some questions as to the usability of the model. As discussed in above, the new model is only applicable for diameter ratios of 0.5 and 0.8, but approximate values can be expected for diameter ratios between 0.5-0.8. For low flowrates the model did not always reach convergence, especially at high flowrates. The program based on the new model was unsuccessful in yielding any meaningful results for low values of the fluid behavior index (m). The reason for this limitation is assumed to be caused by mathematical errors associated with dealing with numbers in the power of a function of m. The scenarios discussed above are either very rare or never applicable to field conditions. As such, the problems associated with these assumptions are insignificant. It should also be noted that in case one of the above scenarios are chosen as input for the program, the program will stop; certifying that no false values are outputted.

6.1.2. Limitations of the data

Compared to the numerical data of Walker and Al-Rawi (1970), the simulated results by the program based on the new model are predicting the pressure loss well. In the case of a concentric annulus with rotation, the simulated data matched the numerically predicted data almost perfectly. Compared to the measurements, the program was overpredicting for the 10 lb/bbl sodium bentonite and the 16 lb/bbl common bentonite. For the nominal 23 lb/bbl common bentonite, there was a slight underprediction. Walker and al-Rawi (1970) state that errors of plus or minus 10 % and an occasional error over 10 % are normal for experimental measurements like the ones they conducted. They also assumed that for a given shear stress, there is only one related shear rate. In actuality, there may be a range of shear stresses that can yield different shear rates.

Walker and Al-Rawi (1970) pointed out the fact that the rheological parameters were taken at steady-state conditions, which was assumed to be when the shear stress no longer changed with time during pipe rotation; a time that was different for each fluid. The rheological parameters were presented in figures, and as such, small differences may have occurred when these were extracted for use in this paper. During the experiments, the rheological conditions were dynamic rather than steady-state and the flow was exposed to varying degrees of shear, dependent on the location in the flow loop. Another comment is that their measurement tools do not work well when approaching the lowest they can measure; the value will go towards zero. It can be assumed that the discrepancies between predicted and measured pressure loss is caused by eccentricity of the pipe. Keeping a wellbore concentric is extremely difficult even in laboratory settings with short pipe sections. In reality, there will always be a small eccentricity, especially with pipe rotation.

In comparison with the measurements by Ahmed and Miska (2008) the results by the new model were interchangeable. An average discrepancy of 30 % or above was only found for three of the twelve data sets (Table 4, Figure 11 and Figure 12). The common denominator for these three measurements is that they are the only measurements for the 1 ½" x 1" concentric annulus. Drillpipe eccentricity could be one of the possible causes for low pressure loss measurements during the experiments. Even though efforts were put into keeping the pipe in perfect concentricity, it is extremely difficult to manage because of the dynamic movement of the pipe during rotation. Discrepancies are relatively high at lower flow rates because measurements were extremely small for the measuring system. It should be noted that the error given by the new model is a combination of the uncertainty of the measurements combined with the new model's own error.

Based on the observations by Dodge and Metzner (1959), the wall shear rate is assumed to be equal the average shear rate in the creation of the new model. This is discussed in detail in chapter 3.2, and should be a valid assumption.

Eccentricity is not constant throughout borehole. This change in annular geometry is not perfectly portrayed by the approximated average eccentricity assumed at the beginning of each simulation run.

6.2. Recommendations for future work on the new model

- A correlation for the change in pressure loss due to inertial effects for YPL fluids should be developed once numerical data for this type of flow is available. The measured trends for YPL fluids in the experiments were not captured perfectly by the new model. Hence it would be purposeful to see if a more suited correlation would yield better results, or if the discrepancies are due to an unidentified effect.
- It would be advisable to extend the model to be based upon and yield accurate results for an extended range of parameters, including very high Taylor numbers and small diameter ratios. It would be favorable to make it predict pressure loss for turbulent flow.
- The program should be compared against more published field data from various sources to further validate its use.
- A sensitivity analysis of the tolerance for convergence of the iterations in the program should be made to confirm that the resulting discrepancies always are negligible.

7. Conclusions

- A new model for prediction of pressure loss was developed on the basis of an existing model for concentric boreholes with drill string rotation; to which the effects of eccentricity and acceleration of the flow due to pipe rotation was incorporated systematically. Eccentricity of the annulus was approximated by several sectors of concentric annuli with varying radii. For the inertial effects, a correlation was developed between published numerical data with and without the named effect.
- Pressure loss predictions of the new model are in agreement with existing simulation and laboratory results. The corresponding program can yield a pressure loss result within seconds for a specific set of input data. The new model is therefore simple to use and ideal for field conditions. The use of a safety factor is recommended for added safety during operations.
- For concentric annulus, the new model provides accurate predictions when compared with experimental measurements. The model captures the trends of the pressure loss curves as the pipe rotation increases.
- For eccentric annulus, the average discrepancy between reported measurements and model predictions is 12 %. In some cases, the predicted trend is not as good as the predictions for a concentric annulus.
- Possible reasons for discrepancies in the reported measurements can be mainly attributed to pipe eccentricity. Other explanations include the assumptions when steady-state is reached, when rheological measurements should be done, the assumption that there is only one shear rate corresponding to a set shear stress and low measurements.
- Some limitations of the new model include the range of parameters, that no convergence is achieved for simulations with fluid behavior index of approximately 0.2 and problems with calculations for some specific conditions with low flowrates.
- Analysis of published numerical data on the inertial effects on pressure loss yielded a correlation dependent on the Taylor number, Reynolds number, radius ratio, eccentricity and fluid behavior index. The regression results of these data showed that the Taylor number (that incorporates rotation speed) and eccentricity have substantial impact on the pressure loss resulting from the inertial effects.
- The results of the bullet point above were supported by the test runs-study that showed significant changes in pressure loss due to these parameters. It was deducted that dependent on the specific scenario, the fluid is more or less shear-thinning and the pressure loss may increase/decrease if the inertial effects are dominant/inferior. The effects seemed to nullify each other with increasing rotation speed.

Nomenclature

Abbreviations

AIME	American Institute of Mining, Metallurgical and Petroleum Engineers
ASME	American Society of Mechanical Engineers
BHA	BottomHole Assembly
BHP	BottomHole Pressure
BP	Bingham Plastic
CFD	Computational Fluid Dynamics
CMC	CarboxyMethylCellulose
ECD	Equivalent Circulating Density
HEC	Hydroxyethyl-Cellulose
HPHT	High Pressure High Temperature
IADC	International Association of Drilling Contractors
IPT	Department of Petroleum Engineering and Applied Geophysics (Institutt for Petroleumsteknologi og Anvendt Geofysikk)
JSME	Japan Society Mechanical Engineering
MMH	Mixed-Metal Hydroxide
MPGE	Mewbourne School of Petroleum & Geological Engineering
NTNU	Norwegian University of Science and Technology (Norges Teknisk-Naturvitenskapelige Universitet)
OBM	Oil-Based Mud
OU	University of Oklahoma
PAC	PolyAnionic Cellulose
PL	Power Law
PWD	Pressure While Drilling
RPM	Revelations Per Minute
SPE	Society of Petroleum Engineers
UBD	UnderBalanced Drilling
WBM	Water-Based Mud
XG	Xanthan Gum
YPL	Yield-Power Law

Units

bbl	barrels
ft	feet
gal	gallons
gpm	gallons per minutes

inH20	inches of water
lb	pounds
psi	pounds per square inch
rev/min	revelations per minute

Latin letters

A, B, C	Arbitrary constants
a	the inner radius of the plug
b	the outer radius of the plug
C	Celsius (degrees)
D	Diameter
dp/dz	Pressure loss
e	The distance between the centers of the inner and outer pipes
f	Friction factor
h	Slot height/local annular clearance
fRe	Frictional pressure loss
K	Consistency index
L	Lenght
m	Fluid behavior index
N	Flow behavior index
$\mathrm{N_{Re}}$	conventional Reynolds number(dimensionless), $\frac{DV\rho}{\mu}$
O	the center of the inner tube
O'	the center of the outer tube
p	Pressure
Q	Flowrate
r	Radius
Re	Reynolds number
n	Flow behaviour index
Ta	Taylor number
U	Velocity
Up	Plug velocity
V	Volume
v	Velocity

Non-latin letters

κ	Diameter ratio
π	Pi
ρ	Density

ω	Angular velocity
μ	Viscosity
$\dot{\gamma}$	Shear rate
ψ	Stream
ε	Eccentricity
τ	Shear stress
τ_y	Yield stress
η	Apparent viscosity function
μ_{app}	Apparent viscosity $[Pa \cdot s]$
θ	Characteristic angle [rad]

Subscripts

ax	axial
C	calculated
c	critical
i	inner
o	outer
0	in the case of no rotation (RPM= 0)
Pl	Power Law
r	rotational
tan	tangential
w	in the case of pipe rotation
w	wall
z	axial
θ	tangential
I	Sheared region I
II	Sheared region II

References

Aadnoy, B.S., Cooper, I., Miska, S.Z., Mitchell, R.F. and Payne, M.L. 2009. *Advanced Drilling and Well Technology*. Richardson, Texas, SPE.

Adriani, Y.H. 2005. Numerical Simulation of Laminar Flow of Non-Newtonian Fluids in Eccentric Annuli. M.Sc. Thesis, University of Tulsa, Tulsa, Oklahoma, USA (2005).

Ahmed, R. and Miska, S. 2008. Experimental Study and Modeling of Yield Power-Law Fluid Flow in Annuli with Drillpipe Rotation. Paper SPE 112604 presented at the IADC/SPE Drilling Conference, Orlando, 4-6 March. http://dx.doi.org/10.2118/135587-MS.

Ahmed, R., Enfis, M., Miftah-El-Kheir, H., Laget, M. and Saasen, A. 2010. The Effect of Drillstring Rotation on Equivalent Circulating Density: Modeling and Analysis of Field Measurements. Paper SPE 135587 presented at the SPE Annual Technical Conference and Exhibition held in Florence, Italy, 19-22 September. http://dx.doi.org/10.2118/135587-MS.

Avila, M. 2012. Taylor-Couette flow, http://www-fa.upc.es/websfa/fluids/marc/tc.php?lang=eng (accessed 19th January 2012).

Bailey, W.J., Peden, J.M. 1997. A Generalised and Consistent Pressure Drop and Flow Regime Transition Model for Drilling Hydraulics Suitable for Slimhole, Underbalanced and Horizontal Wells. Paper SPE 39281 presented at the SPE/IADC Middle East Drilling Technology Conference in Bahrain, 23-25 November. http://dx.doi.org/10.2118/39281-MS.

Ballal, B.Y. and Rivlin, R.S. 1976. Flow of a Newtonian fluid between eccentric rotating cylinders: Inertial effects. *Arch. Rational Mech. Anal.* **62**: 237-294.

Batra, R.L. and Eissa, M. 1994. Helical Flow of a Sutterby Model Fluid. *Polym.-Plast. Technol. Eng.* **33** (4) : 489-501.

Bird, R.B. 1965. Experimental Tests of Generalized Newtonian Models Containing a Zero-Shear Viscosity and a Characteristic Time. *Can. J. Chem. Eng.* **75** (August): 161-168.

Bode, D.J., Noffke, R.B. and Nickens, H.V. 1991. Well-Control Methods and Practices in Small-Diameter Wellbores. *J. Pet Tech* **43** (11): 1380-1386. SPE-19526.http://dx.doi.org/10.2118/19526-PA.

Cartalos, D., Lecourtier, J., and Marsot, J. 1992. Hydraulique de Forage en Diametre Reduit. Formulation des fluides et Calcul de Pertes de Charge a l'Aide des Lois Rheologiques Simples. IFP Report W 39814, June 1992.

Cartalos, U. and Dupuis, D. 1993. An Analysis Accounting for the Combined Effect of Drillstring Rotation and Eccentricity on Pressure Losses in Slimhole Drilling. Paper SPE 25769 presented at the IADC/SPE Drilling Conference, Amsterdam, 23-25 February. http://dx.doi.org/10.2118/25769-MS.

Castle, P. and Mobbs, F.R. 1968. Hydrodynamic stability of the flow between eccentric rotating cylinders: Visual observations and torque measurements. *In: Proc. IMechE 182 Part 3N*. Tribology Convention.

Charlez, P., Easton, M., Morrice, G. and Tardy,P. 1998. Validation of Advanced Hydraulic Modeling using PWD Data. Paper OTC 8804 presented at the Offshore Technology Conference, Houston, Texas, 4 May-7 May. http://dx.doi.org/10.4043/8804-MS.

Chin, W.C. 1992. Borehole Flow Modeling in Horizontal, Deviated and Vertical Wells. Gulf Publishing Co, Houston, Texas.

Cole, J.A. 1968. Taylor vortices with eccentric rotating cylinders. *Trans. ASME J. Lub. Technol.*: 285-296.

Coleman, B.D. and Noll, W. 1959. Helical Flow of General Fluids. *J. Appl. Phys.* 30, 1508. Published by the American Institute of Physics.

Cui, H.-Q. and Liu, X.-S. 1995. Research on Helical Flow of Non-Newtonian Fluids in Eccentric Annuli. Paper SPE 29940 presented at the International Meeting on Petroleum Engineering held in Bejing, PR China, 14-17 November. http://dx.doi.org/10.2118/29940-MS.

Diaz, H.J. 2002. Field Experimental Study and Modeling of ECD in Casing Drilling Operations. MSc. Thesis, University of Tulsa, Tulsa (2002).

Diaz, H., Miska, S., Takach,N. and Yu,M. 2004. Modeling of ECD in Casing Drilling Operations and Comparison with Experimental and Field Data. Paper SPE 87149 presented at the IADC/SPE Drilling Conference, Dallas, Texas 2-4 March. http://dx.doi.org/10.2118/87149-MS.

Delwiche, R.A., Lejeune, M.W.D., Mawet, P.F.B.N. and Vighetto, R. 1992. Slimhole Drilling Hydraulics. Paper SPE 24596 presented at the SPE Annual Technical Conference and Exhibition, Washington, D.C., 4-7 October. http://dx.doi.org/10.2118/24596-MS.

Dodge, D.W. and Metzner, A.B. 1959. Turbulent Flow of Non-Newtonian Systems. *A.I.Ch.E. Journal* Vol. 5 (2): 189-204.

Elias, R. N. 2004. Non-Newtonian Eccentric Annulus Flow, http://www.nacad.ufrj.br/~rnelias/gallery/anecc.html (accessed 19th January 2012).

Escudier, M.P. and Gouldson, I.W. 1995. Concentric Annular Flow With Centerbody Rotation of a Newtonian and a Shear-Thinning Liquid. *International Journal of Heat and Fluid Flow* **16**: 156-162.

Escudier, M.P. and Gouldson, I.W. 1997. Effects of Centerbody Rotation on Laminar Flow Through an Eccentric Annulus. *In: Developments in Laser Techniques and Applications to Fluid Mechanics*, Proc. 7th International Symposium, Lisbon, Springer-Verlag, Berlin.

Escudier, M.P., Gouldson, I.W., Oliveira, P.J. and Pinho, F.T. 2000. Effects of inner cylinder rotation on laminar flow of a Newtonian fluid through an eccentric annulus. *Int. J. Heat Fluid Flow* 21, pages 92-103.

Escudier, M.P., Oliveira, P.J. and Pinho, F.T. 2002. Fully developed laminar flow of purely viscous Non-Newtonian liquids through annuli, including the effects of eccentricity and inner-cylinder rotation. *Int. J. Heat Fluid Flow* 23, pages 52-73.

Fang, P. and Manglik, R.M. 2002. The Influence of Inner Cylinder Rotation on Laminar Axial Flows in Eccentric Annuli of Drilling Bore Wells. *I. J. Trans. Phenomena*, Vol.4, pp. 257-274.

Fordham, E.J. Bittleston, S.H. and Tehrani, M.A. 1991. Viscoplastic Flow in Centred Annuli, pipes and Slots. *Ind. Eng. Chem. Res.* **30** (3): 517-524.

Fredrickson, A.G. and Bird, R.B. 1958. Non-Newtonian Flow in Annuli. *Ind. Eng. Chem.* **50** (3): 347-352.

Green, M.D., Thomesen, C.R., Wolfson, L. and Bern, P.A. 1999. An Integrated Solution of Extended-Reach Drilling Problems in the Niakuk Field, Alaska: Part II- Hydraulics, Cuttings Transport and PWD. Paper SPE 56564 presented at the SPE Annual Technical Conference and Exhibition, Houston, Texas, 3-6 October. http://dx.doi.org/10.2118/56564-MS.

Guckes, T.L. 1975. Laminar Flow of Non-Newtonian Fluids in an Eccentric Annulus. *J. Eng. Ind.* (May) : 498-506.

Haciislamoglu, M. and Langlinais, J. 1990. Non-Newtonian Fluid Flow in Eccentric Annuli. *J. Energy Res. Technol.* **112**: 163-169.

Hanks, R.W. 1979. The Axial Laminar Flow of Yield-Psuedoplastic Fluids in a Concentric Annulus. *Ind. Eng. Chem. Process Des. Dev.* **18** (3): 488-493.

Hansen, S.A. and Sterri, N. 1995. Drill Pipe Rotation Effects on Frictional Pressure Losses in Slim Annuli. Paper SPE 30488 presented at the SPE Annual Technical Conference and Exhibition, Dallas, Texas, 22-25 October. http://dx.doi.org/10.2118/30488-MS.

Hansen, S.A., Rommetveit, R., Sterri, N. and Aas, B. 1999. A New Hydraulics Model for Slim Hole Drilling Applications. Paper SPE 57579 presented at the SPE/IADC Middle East Drilling Technology Conference, Abu Dhabi, United Arab Emirates, 8-10 November. http://dx.doi.org/10.2118/57579-MS.

Hemphill, T. and Ravi, K. 2005. Calculation of drillpipe Rotation Effects on Axial Flow : An Engineering Approach. Paper SPE 97158 presented at the SPE Annual Technical Conference and Exhibition, Dallas, Texas, 9-12 October.

Hemphill, T., Bern, P. and Rojas, J.C. 2007. Field Validation of Drillpipe Rotation Effects on Equivalent Circulating Density. Paper 110470 presented at the SPE Annual Technical Conference and Exhibition, Anaheim, California, U.S.A., 11-14 November. http://dx.doi.org/10.2118/110470-MS.

Hemphill, T., Ravi, K., Bern, P. and Rojas, J.C. 2008. A Simplified Method for Prediction of ECD Increase with Drillpipe Rotation. Paper SPE 115378 presented at the 2008 SPE Annual Technical Conference and Exhibition held in Denver, Colorado, USA, 21-24 September. http://dx.doi.org/10.2118/25768-MS.

Ho Tung, J.N., Kleis, S.J. and VanArsdale, W.E. 1993. The effect of polymer on azimuthal velocity profiles in an eccentric cylinder apparatus. *In: Developments in Non-Newtonian Flow*s **AMD-175**: 65-70.

Hussain, Q.E. 1999. Numerical Investigation of Viscoplastic Fluid Flow in Irregular Eccentric Annuli. Dissertation, University of Alabama, Alabama(1999).

Hussain, Q.E. and Sharif, M.A.R. 2000. Numerical Modeling of Helical Flow of Viscoelastic Fluids in Eccentric Annuli. *AIChE J.* **46** (10): 1937-1946.

Isambourg, P., Bertin, D.L. and Brangetto, M. 1999. Field Hydraulic Tests Improve HPHT Drilling Safety and Performance. *SPE Drill & Compl* **14**(4): 219-227. SPE-59527-PA. http://dx.doi.org/10.2118/59527-PA.

Iyoho, A.W. and Azar, J.J. 1981. An Accurate Slot Flow Model for Non-Newtonian Fluid Flow Through Eccentric Annuli. *Soc. Pet. Eng. J*: 565-572.

Kamal, M.M. 1966. Separation in the flow between eccentric cylinders. *ASME J. Basic Eng.*,717-724.

Kozicki, W., Chou, C.H. and Tiu, C. 1966. Non-Newtonian Flow in Ducts of Arbitrary Cross-Sectional Shape. *Chem.. Eng. Sci.* **21**: 665-679.

Laird, W.M. 1957. Slurry and Suspension Transport. Basic Flow Studies on Bingham Plastic Fluids. *Ind. Eng. Chem.* **49** (1): 138-141.

Lockett, T.J.. 1992. Numerical simulation of inelastic non-Newtonian fluid flows in annuli. Ph.D. Thesis. Imperial College of Science, technology and Medecine, London, United Kingdom.

Lockett, T.J., Richardson, S.M. and Worraker, W.J. 1993.The Importance of Rotation Effects for Efficient Cuttings Removal During Drilling. Paper SPE/IADC 25768 presented at the 1993 SPE/IADC Drilling Conference held in Amsterdam 23-25 February. http://dx.doi.org/10.2118/25768-MS.

Luo, Y., Peden, J.M. 1990. Flow of Non-Newtonian Fluids Through Eccentric Annuli. *SPE Prod Eng* **5** (1): 91-96. SPE-16692-PA. http://dx.doi.org/10.2118/16692-PA.

Manglik, R.M. and Fang, P.P. 1995. Effects of Eccentricity and Thermal Boundary Conditions on Laminar and Fully Developed Flow in Annular Ducts. *Int. J. Heat Fluid Flow* **16** (4): 298-306.

Marken, C.D., He, X. and Saasen, A. 1992. The influence of drilling conditions on annular pressure losses. Paper 24598 presented at the 67th Annual Technical Conference and Exhibition of The Society of Petroleum Engineers held in Washington, DC, October 4-7. http://dx.doi.org/10.2118/24598-MS.

McCann, R.C., Quigley, M.S., Zamora, M. and Slater, K.S. 1995. Effects of High-Speed Pipe Rotation on Pressures in Narrow Annuli. *SPE Drill & Compl* **10** (2): 96-103. SPE-26343. http://dx.doi.org/10.2118/26343-PA.

Meuric, O.F.J., Wakeman, R.J., Chin. T.W. and Fischer, K.A. 1998. Numerical Flow Simulation of Viscoplastic Fluids in Annuli. *Can. J. Chem. Eng.* **76** (February): 27-39.

Mitsuishi, N., and Aoyagi, Y. 1973. Non-Newtonian fluid flow in an eccentric Annulus. *J. Chem. Eng. Japan* **6** (5): 402-408.

Nebrenský,J. and Ulbrecht, J. 1968. Non-Newtonian Flow in Annular Ducts. *Collect. Czech Chem. Commun.* **33** : 363-375.

Nebrenský, J.,Wein, O. and Ulbrecht, J. 1970. Non-Newtonian Flow in Channels of Annular Corss Section II, Ree-Eyring Fluid. *Collect. Czech Chem. Commun.* **35** : 1964-1971.

Nouri, J.M. and Whitelaw, J.H. 1994. Flow of Newtonian and Non-Newtonian Fluids in a Concentric Annulus with Rotation of the **Inner** Cylinder. *ASME J. Fluids Eng.* **116** : 821-827.

Nouri, J.M. and Whitelaw, J.H. 1997. Flow of Newtonian and Non-Newtonian Fluids in an Eccentric Annulus with Rotation of the Inner Cylinder. *International Journal of Heat and Fluid Flow* **18**: 236-246.

Ogugbue, C. C. E. 2009. Non-Newtonian power-law fluid flow in eccentric annuli: CFD simulation and experimental study. Doctoral Thesis / Dissertation, University of Oklahoma, Oklahoma (2009).

Ooms, G., Burgerscentrum, J.M. and Kampman-Reinhartz, B.E. 1999. Influence of Drillpipe Rotation and Eccentricity on Pressure Drop over Borehole during Drilling. Paper SPE 56638 presented at the SPE Annual Technical Conference and Exhibition, Houston, 3-6 October. http://dx.doi.org/10.2118/56638-MS.

Ozbayoglu, A.M., Aydiner, Z. Kasnakoglu, C. and Ozbayoglu, M.E. 2008. Neural Network and Genetic Programming in Pressure Loss Estimation in Eccentric Pipe Flow. *Intelligent Engineering Systems Through Artificial Neural Networks* **18** : 163-170. New York : ASME Press.

Pattison, M.J. 2011. Secondary Flows, http://www.thermopedia.com/content/1113/?tid=104&sn=1420 (accessed 19th January 2012).

Pham, T.V. and Mitsoulis, E. 1998. Viscoplastic Flow in Ducts. *Can. J. Chem. Eng.* **76** :120-125.

Piercy, N. A.V., Hooper, M. S. and Winny, H. F. 1933. Viscous flow through pipes with cores. *Phil. Mag. J. Sci.* **15**: 647-676. London, Edinburgh, Dublin.

Rayleigh, L. 1880. On the Stability, or Instability, of Certain Fluid Motions. *Proc. Royal Soc.* **11**: 57-70.

Rigbi, Z. and Galili, N. 1971. Helical Flow of Some Non-Newtonian Liquids. *Israeli J. Tech.* **9** (5) : 447-452.

Rivlin, R.S. 1956. Solution of Some Problems in the Exact Theory of Visco-Elasticity. *J. Rat. Mech. Anal.* **5** (1): 123-188.

Rotem, Z. 1962. Non-Newtonian Flow in Annuli. *Trans. ASME J. Appl. Mech.* (June): 421-424.

Russell, C.P and Christiansen, E.B. 1974. Axial, Laminar, Non-Newtonian Flow in Annuli. *Ind. Eng. Chem. Process Des. Dev.* **13** (4): 391-396.

San Andres, A. and Szeri, A.Z. 1984. Flow between eccentric rotating cylinders. *ASME J. Appl. Mech.* **51** : 869-878.

Savins, J.G. and Wallick, G.C. 1966. Viscosity Profiles, Discharge Rates, Pressures, and Torques for a Rheologically Complex Fluid in a Helical Flow. *AIChE Journal* **12** (2) : 357-363.

Serre, E., Sprague, M.A. and Lueptow, R.M. 2008. Stability of Taylor–Couette flow in a finite-length cavity with radial throughflow. *Physics of Fluids* 20, 034106. http://dx.doi.org/10.2118/59265-MS.

Schul'man,Z.P. 1970. Calculation of a Laminar axial Flow of a Nonlinear Viscoplastic Medium in an Annular Channel. *Inzherno-Fizicheskii Zhurnal* **19** (4) : 689-697 (in Russian).

Siginer, D.A. and Bakhtiyarov, S.I. 1998. Flow of Drilling Fluids in Eccentric Annuli, *Journal of Non-Newtonian Fluid Mechanics* 78: 119-131.

Skalland, A.H.P. 1967. Non-Newtonian Flow and Heat Transfer. John Wiley & Sons, New York.

Sorgun,M. 2012. Helical Flow of Non-Newtonian Fluids in a Concentric and Fully Eccentric Annulus. *Energy Sources, Part A*, 24: 404-412.

Sterri, N., Saasen, A., Aas, B. and Hansen, S.A. 2000. Frictional Pressure Losses During Drilling: Drill String Rotation Effects on Axial Flow of Shear Thinning Fluids in Eccentric Annulus. *Oil Gas European Magazine* **26** (3): 30-33.

Subramanian, R. and Azar, J.J. 2000. Experimental Study on Friction Pressure Drop for NonNewtonian drilling fluids in pipe and Annular Flow. Paper 64647 presented at the SPE International Oil & gas Conference and Exhibition in China held in Beijing, China, 7-10 November. http://dx.doi.org/10.2118/64647-MS.

Takeuchi, D.I. and Jankowski, D.F. 1982. A numerical and experimental investigation of the stability of spiral Poiseuille flow. *J. Fluid Mech.* **102**: 101-126.

Tiedt, W., 1966. Berechnung des Laminaren und Turbulenten Reibungswiederstandes Konzentrischer und Exzentrischer Ringspalte. Part I. *Chem-Ztg, Chem. Appar.* **90** : 813-821.

Tiedt, W., 1967. Berechnung des Laminaren und Turbulenten Reibungswiederstandes Konzentrischer und Exzentrischer Ringspalte. Part II. *Chem-Ztg, Chem. Appar.* **91** : 17-25.

Vaughn, R.D. 1965. Axial Laminar Flow of Non-Newtonian Fluids in Narrow Eccentric Annuli. *Soc. Pet. Eng. J.* (December): 277-280.

Vohr, J.H. 1968. An experimental study of Taylor vortices and turbulence in flow between eccentric rotating cylinders. *Trans. ASME J. Lub. Technol.*: 185-296.

Volarovich, M.P. and Gutkin, A.M. 1946. Flow of Plastic-Viscoplastic Material Between Two Parallel Flat-Walls and in Annular Space Between Two Coaxial Tubes. *J. Tech. Phys.* **XVI** (3): 321-328.

Walker, R.E. and Al-Rawi, O. 1970. Helical Flow of Bentonite Slurries. Paper SPE 3108 prepared for the 45th Annual Fall Meeting of the Society of Petroleum Engineers of AIME, Houston, 4-7 October. http://dx.doi.org/10.2118/3108-MS.

Walton, I.C. and Bittleston, S.H. 1991. The Flow of a Bingham Plastic Fluid in a Narrow Eccentric Annulus. *J. Fluid Mech.* 222: 39-60.

Wan, S., Morrison, D. and Bryden, I.G. 2000. The Flow of Newtonian and Inelastic Non-Newtonian Fluids in Eccentric Annuli with Inner-Cylinder Rotation. *Theoret. Comput. Fluid Dynamics* **13** : 349-359.

Wang, H.,Su Y.,Bai Y., Gao Z. and Zhang F.2000. Experimental Study of Slimhole Annular Pressure Loss and Its Field Applications. Paper IADC/SPE 59265 presented at the 2000 IADC/SPE Drilling Conference held in New Orleans, Louisiana, 23-25 February. http://dx.doi.org/10.2118/59265-MS.

Ward,C. and Andreassen, E. 1998. Pressure-While-Drilling Data Improve Reservoir Drilling Performance. *SPE Drill Eng* **13** (1): 19-24. SPE-37588-PA. http://dx.doi.org/10.2118/37588-PA.

Wei, X. 1997. Effects of Drillpipe Rotation on Annular Frictional Pressure Loss in Laminar, Helical flow of Power-Law Fluids in Concentric and Eccentric Annuli. MSc. Thesis, the University of Tulsa, Tulsa (1997).

White, K., Liu,P. and Kalindindi,S. 2010. Rheological Methods, http://plastics.tamu.edu/node/270 (accessed 31st March 2012).

Wikipedia. 2012. *Generalized Newtonian fluid* (23rd January 2012 revision), http://en.wikipedia.org/wiki/Taylor%E2%80%93Couette_flow (accessed 23rd January 2012).

Wikipedia. 2012. *Taylor-Couette flow* (19th January 2012 revision), http://en.wikipedia.org/wiki/Taylor%E2%80%93Couette_flow (accessed 19th January 2012).

Woo, N., Seo, B. and Hwang, Y. 2005. Flow of Newtonian and Non-Newtonian Fluids in Annuli with Rotating Inner Cylinder. 6th World Conference on Experimental Heat Transfer, Fluid Mechanics, and Thermodynamics, Matsushima, Miyagi, Japan, April 17-21.

Yamada, Y. 1962. Resistance of a flow through an annulus with an inner rotating cylinder. *Bulletin of JSME* 5(18), 302-310.

Appendix A – Data from Walker and Al-Rawi (1970)

Table 2 - Experimental and calculated pressure drops for nominal 10 lb/bbl sodium bentonite

Flowrate	11.2	[ft/min]		Flowrate	6.8	[ft/min]	
	0.249	[gal/min]			0.152	[gal/min]	
Rotation	Flowing Pressure [psi/ft]			Rotation	Flowing Pressure [psi/ft]		
[rev/min]	Observed	Computed	% Error	[rev/min]	Observed	Computed	% Error
0	0.575	0.660	14.9	0	0.519	0.544	4.7
20	0.508	0.638	25.6	20	0.468	0.499	6.6
40	0.508	0.600	18	40	0.417	0.448	7.4
80	0.466	0.541	16.1	80	0.376	0.386	2.6
150	0.417	0.434	4	150	0.278	0.300	8
300	0.32	0.307	-4	300	0.191	0.198	3.5

Flowrate	4.8	[ft/min]		Flowrate	3.6	[ft/min]	
	0.108	[gal/min]			0.081	[gal/min]	
Rotation	Flowing Pressure [psi/ft]			Rotation	Flowing Pressure [psi/ft]		
[rev/min]	Observed	Computed	% Error	[rev/min]	Observed	Computed	% Error
0	0.466	0.484	3.9	0	0.466	0.445	-4.5
20	0.366	0.371	1.5	20	0.327	0.358	9.4
40	0.278	0.331	19.2	40	0.303	0.298	-1.6
80	0.322	0.296	-8.1	80	0.226	0.226	0
150	0.212	0.222	4.5	150	0.160	0.169	5.5
300	0.139	0.143	3	300	0.104	0.108	3.8

Table 3- Experimental and calculated pressure drops for nominal 16 lb/bbl common bentonite

Flowrate	17.7	[ft/min]		Flowrate	14.2	[ft/min]	
	0.396	[gal/min]			0.316	[gal/min]	
Rotation	Flowing Pressure [psi/ft]			Rotation	Flowing Pressure [psi/ft]		
[rev/min]	Observed	Computed	% Error	[rev/min]	Observed	Computed	% Error
0	0.153	0.170	11.4	0	0.12	0.155	29.5
20	0.132	0.168	27.1	20	0.12	0.151	26.5
40	0.129	0.162	25.9	40	0.117	0.143	22
80	0.122	0.150	23.7	80	0.112	0.131	16.6
150	0.111	0.136	22.2	150	0.102	0.115	12
300	0.099	0.114	15	300	0.087	0.093	6.9

Flowrate	10.7	[ft/min]		Flowrate	7.3	[ft/min]	
	0.24	[gal/min]			0.162	[gal/min]	
Rotation	Flowing Pressure [psi/ft]			Rotation	Flowing Pressure [psi/ft]		
[rev/min]	Observed	Computed	% Error	[rev/min]	Observed	Computed	% Error
0	0.111	0.140	25.7	0	0.104	0.123	18.2
20	0.11	0.134	21.4	20	0.097	0.111	14.6
40	0.107	0.123	15	40	0.094	0.098	5
80	0.097	0.109	12.5	80	0.082	0.084	3.1
150	0.083	0.092	10.9	150	0.066	0.067	1.2
300	0.069	0.072	3.6	300	0.051	0.05	-1.9

Flowrate	4.6	[ft/min]		Flowrate	2.1	[ft/min]	
	0.103	[gal/min]			0.046	[gal/min]	
Rotation	Flowing Pressure [psi/ft]			Rotation	Flowing Pressure [psi/ft]		
[rev/min]	Observed	Computed	% Error	[rev/min]	Observed	Computed	% Error
0	0.097	0.109	12.1	0	0.086	0.093	8.6
20	0.086	0.089	3.1	20	0.064	0.057	-9.9
40	0.075	0.076	1.6	40	0.051	0.045	-10.7
80	0.059	0.06	2.3	80	0.037	0.031	-16.7
150	0.046	0.045	-2.7	150	0.027	0.021	-23.4
300	0.033	0.032	-4.6	300	0.019	0.014	-25.8

Table 4- Experimental and calculated pressure drops for nominal 23 lb/bbl common bentonite

Flowrate	18	[ft/min]		Flowrate	14.6	[ft/min]	
	0.402	[gal/min]			0.327	[gal/min]	
Rotation	Flowing Pressure [psi/ft]			Rotation	Flowing Pressure [psi/ft]		
[rev/min]	Observed	Computed	% Error	[rev/min]	Observed	Computed	% Error
0	0.438	0.415	-5.1	0	0.417	0.392	-5.9
20	0.431	0.408	-5.4	20	0.403	0.381	-5.5
40	0.413	0.388	-6	40	0.389	0.355	-8.6
80	0.382	0.346	-9.4	80	0.342	0.309	-9.7
150	0.33	0.307	-6.8	150	0.279	0.269	-3.7
300	0.278	0.246	-11.6	300	0.221	0.207	-6.3

Flowrate	8	[ft/min]	
	0.179	[gal/min]	
Rotation	Flowing Pressure [psi/ft]		
[rev/min]	Observed	Computed	% Error
0	0.337	0.341	1.2
20	0.309	0.308	-0.2
40	0.274	0.264	-3.9
80	0.236	0.223	-5.8
150	0.153	0.176	14.9
300	0.132	0.121	-8.2

Flowrate	5	[ft/min]	
	0.112	[gal/min]	
Rotation	Flowing Pressure [psi/ft]		
[rev/min]	Observed	Computed	% Error
0	0.330	0.312	-5.3
20	0.267	0.252	-5.6
40	0.222	0.201	-9.5
80	0.184	0.165	-10.2
150	0.135	0.12	-11
300	0.089	0.078	-12.5

Flowrate	2.6	[ft/min]	
	0.058	[gal/min]	
Rotation	Flowing Pressure [psi/ft]		
[rev/min]	Observed	Computed	% Error
0	-	-	-
20	0.316	0.175	-44.6
40	0.188	0.144	-23.4
80	-	-	-
150	0.076	0.066	-14
300	0.054	0.041	-24.2

Appendix B – Data from Escudier et al. (2000)

Table 2 -Computed variation of frictional pressure loss fRe with radius ratio k, Taylor Number Ta and eccentricity e (values Ta=0,k=0.2 and 0.8,e!=0.98, from Tiedt, 1967)							
k=0.2	e						
Ta	0.2	0.3	0.4	0.5	0.6	0.7	
-	22.093	20.985	19.641	18.197	16.760	15.407	
100	22.125	21.039	19.709	18.256	16.803	15.431	
1 000	22.327	21.397	20.151	18.682	17.111	15.587	
2 500	22.518	21.758	20.638	19.181	17.498	15.800	
5 000	22.688	22.096	21.124	19.717	17.945	16.068	
10 000	22.860	22.449	21.655	20.332	18.491	16.438	
50 000	23.267	23.303	22.943	21.788	19.775	17.547	
	0.8	0.85	0.9	0.95	0.98		
	14.181	13.625	13.105	12.625	12.356		
	14.194	13.636	13.124	12.657	12.400		
	14.255	13.699	13.235	12.874	12.712		
	14.350	13.799	13.407	13.184	13.148		
	14.493	13.952	13.640	13.598	13.714		
	14.741	14.222	14.019	14.195	14.497		
	15.944	15.540	15.486	15.879	16.335		
k=0.5							
Ta	e=0.2	0.3	0.4	0.5	0.6	0.7	
-	22.517	21.117	19.439	17.655	15.895	14.244	
100	22.629	21.282	19.619	17.804	15.993	14.292	
1 000	23.088	22.091	20.605	18.686	16.560	14.545	
2 500	23.396	22.703	21.454	19.555	17.196	14.879	
5 000	23.600	23.140	22.137	20.344	17.849	15.308	
10 000	23.800	23.568	22.804	21.149	18.603	15.917	
50 000	24.277	24.585	24.470	22.758	20.236	17.782	
	0.8	0.85	0.9	0.95	0.98		
	12.745	12.059	11.414	10.811	10.468		
	12.780	12.106	11.489	10.929	10.618		
	12.956	12.375	11.944	11.649	11.539		
	13.207	12.713	12.449	12.383	12.416		
	13.558	13.126	12.994	13.119	13.287		
	14.093	13.709	13.703	14.005	14.275		
	16.115	15.893	15.893	16.631	17.188		

k=0.8							
Ta	e=0.2	0.3	0.4	0.5	0.6	0.7	
-	22.631	21.146	19.367	17.480	15.622	13.882	
100	22.687	21.238	19.468	17.559	15.667	13.901	
1 000	23.041	21.834	20.149	18.121	15.989	14.038	
2 500	23.344	22.405	20.878	18.786	16.408	14.243	
5 000	23.597	22.912	21.602	19.527	16.933	14.540	
10 000	23.824	23.400	22.361	20.396	17.650	15.018	
50 000	24.298	24.425	23.936	22.258	19.573	16.872	
	0.8	0.85	0.9	0.95	0.98		
	12.304	11.581	10.903	10.277	9.859		
	12.328	11.623	10.975	10.381	10.049		
	12.489	11.892	11.405	11.016	10.823		
	12.701	12.192	11.858	11.645	11.567		
	12.981	12.566	12.364	12.325	12.360		
	13.403	13.073	13.028	13.216	13.396		
	15.078	14.865	15.383	16.642	17.644		

Appendix C – Data from Escudier et al. (2002)

Table 1 -Results of power-law calculations : dependence of f*Re on npl,k,e,Ta and Re

(a) npl=0.8, k=0.5 and Re=100

e	Ta					
	0	10	100	1 000	10 000	50 000
0.00	15.4380	15.4430	15.4890	15.8740	17.4510	18.8900
0.10	15.2360	15.2450	15.3250	15.8130	17.4710	18.9950
0.20	14.6630	14.6830	14.8420	15.6060	17.5070	19.2730
0.30	13.8110	13.8400	14.0720	15.1760	17.4620	19.5720
0.40	12.7940	12.8250	13.0780	14.4130	17.1310	19.5150
0.50	11.7190	11.7450	11.9580	13.2390	16.1980	18.6000
0.60	10.6590	10.6750	10.8150	11.7600	14.5130	16.8520
0.70	9.6656	9.6735	9.7461	10.3080	12.5770	15.0010
0.80	8.7619	8.7664	8.8100	9.1881	11.0550	13.5530
0.85	8.3463	8.3517	8.4022	8.8102	10.6250	13.0550
0.90	7.9549	7.9633	8.0376	8.5662	10.5230	12.8080
0.95	7.5872	7.6008	7.7169	8.4532	10.7820	12.9770
0.98	7.3776	7.3955	7.5453	8.4440	11.0650	13.3220

(b) npl=0.5, k=0.5 and Re=100

e	Ta						
	0	10	100	1 000	5 000	10 000	50 000
0.00	7.9468	7.9531	8.0094	8.4973	9.8219	10.7510	13.4370
0.10	7.8572	7.8726	7.9662	8.4905	9.8279	10.7660	13.4980
0.20	7.5955	7.6336	7.8291	8.4646	9.8406	10.8020	13.6630
0.30	7.2048	7.2624	7.5757	8.3994	9.8414	10.8340	13.8700
0.40	6.7428	6.8040	7.1792	8.2445	9.7836	10.7980	13.9560
0.50	6.2605	6.3101	6.6457	7.8793	9.5496	10.5490	13.6960
0.60	5.7895	5.8211	6.0510	7.1207	8.8597	9.8113	12.8500
0.70	5.3510	5.3670	5.4960	6.2032	7.7354	8.6860	11.6860
0.80	4.9518	4.9595	5.0276	5.5095	6.7902	7.7067	10.6410
0.85	4.7675	4.7742	4.8342	5.2743	6.4521	7.3312	10.2200
0.90	4.5932	4.6014	4.6722	5.1341	6.2533	7.0800	9.8687
0.95	4.4286	4.4416	4.5448	5.1127	6.3022	7.1148	9.6785
0.98	4.3342	4.3520	4.4864	5.1673	6.5099	7.3828	9.6959

(c) npl=0.2, k=0.5 and Re=100

e	Ta					
	0	10	100	1 000	10 000	50 000
0.00	3.8874	3.8921	3.9338	4.2988	6.2320	9.5576
0.10	3.8699	3.8792	3.9288	4.2991	6.2323	9.5689
0.20	3.7776	3.8216	3.9110	4.2977	6.2461	9.6019
0.30	3.6160	3.7095	3.8750	4.2926	6.2597	9.6520
0.40	3.4223	3.5366	3.8071	4.2801	6.2721	9.7043
0.50	3.2261	3.3205	3.6699	4.2511	6.2731	9.7170
0.60	3.0403	3.1013	3.3738	4.1749	6.2242	9.5879
0.70	2.8740	2.9049	3.0553	3.8560	5.9405	9.1365
0.80	2.7160	2.7336	2.8198	3.2385	5.2300	8.4145
0.85	2.6446	2.6571	2.7252	3.0914	4.9526	8.0801
0.90	2.5768	2.5865	2.6475	2.9833	4.7420	7.8048
0.95	2.5123	2.5230	2.5933	2.9324	4.6019	7.5755
0.98	2.4752	2.5064	2.5775	2.9649	4.6353	7.4563

(d) npl=0.5, k=0.8 and Re=100

e	Ta					
	0	10	100	1 000	10 000	50 000
0.00	7.9994	8.0264	8.2550	9.7343	13.2470	15.2940
0.10	7.8860	7.9248	8.1993	9.7166	13.2730	15.4960
0.20	7.5704	7.6333	8.0190	9.6523	13.3270	15.9260
0.30	7.1154	7.1938	7.6815	9.5021	13.3320	16.4270
0.40	6.5915	6.6668	7.1711	9.1790	13.1520	16.6150
0.50	6.0548	6.1131	6.5439	8.5441	12.5910	16.1630
0.60	5.5399	5.5781	5.8491	7.5656	11.4950	14.9930
0.70	5.0646	5.0865	5.2917	6.5262	10.0420	13.4390
0.80	4.6345	4.6486	4.7924	5.7392	8.6649	11.8710
0.85	4.4366	4.4512	4.5938	5.4900	8.1261	11.1220
0.90	4.2497	4.2268	4.4295	5.3436	7.7828	10.4170
0.95	4.0733	4.0994	4.2968	5.2904	7.7240	10.0490
0.98	3.9723	4.0048	4.2309	5.2966	7.8444	10.3260

(e) npl=0.5, k=0.2 and Re=100

e	Ta					
	0	10	100	1 000	10 000	50 000
0.00	7.7196	7.7212	7.7345	7.8633	8.8298	10.931
0.10	7.6770	7.6791	7.6958	7.8396	8.8249	10.937
0.20	7.5346	7.5346	7.5693	7.7655	8.8087	10.952
0.30	7.2975	7.3040	7.3573	7.6363	8.7751	10.964
0.40	6.9879	6.9977	7.0724	7.4386	8.7062	10.948
0.50	6.6397	6.6505	6.7328	7.1487	8.5556	10.835
0.60	6.2816	6.2909	6.3626	6.7487	8.2091	10.468
0.70	5.9349	5.9410	5.9883	6.2652	7.5587	9.7483
0.80	5.6169	5.6653	5.6427	5.7400	6.9058	9.0967
0.85	5.4707	5.5023	5.4945	5.5569	6.6612	8.7504
0.90	5.3330	5.3662	5.3684	5.4378	6.4429	8.5006
0.95	5.2064	5.2349	5.2500	5.3349	6.3290	8.4326
0.98	5.1344	5.1675	5.1988	5.2820	6.3098	8.4130

(f) npl=0.5, k=0.5 and Re=10

e	Ta						
	0	10	100	1 000	5 000	10 000	50 000
0.00	7.9468	8.4973	10.7510	14.6600	17.0780	17.8500	18.5530
0.10	7.8572	8.4065	10.6620	14.6210	17.1560	18.0050	18.8910
0.20	7.5955	8.1404	10.3940	14.4910	17.3610	18.4440	19.9500
0.30	7.2048	7.7320	9.9544	14.2360	17.6010	19.0550	21.7580
0.40	6.7428	7.2358	9.3750	13.8070	17.7200	19.5920	23.8490
0.50	6.2605	6.7094	8.7124	13.1630	17.5280	19.7330	25.1640
0.60	5.7895	6.1925	8.0238	12.2960	16.8690	19.2210	24.9370
0.70	5.3510	5.7115	7.3608	11.2660	15.6990	17.9800	23.2200
0.80	4.9518	5.2727	6.7567	10.1750	14.0600	16.0240	20.4750
0.85	4.7675	5.0759	6.4837	9.6384	13.0970	14.8800	18.9820
0.90	4.5932	4.8880	6.2309	9.1234	12.0890	13.6350	17.5130
0.95	4.4286	4.7113	5.9983	8.6640	11.1620	12.4410	16.0000
0.98	4.3342	4.6105	5.8706	8.4348	10.7700	11.9390	14.5910

(g) npl=0.5, k=0.5 and Re=1000							
e	Ta						
	0	10	100	1 000	5 000	10 000	50 000
0.00	7.9468	7.9469	7.8573	7.9531	7.9784	8.0094	8.2417
0.10	7.8572	7.8664	7.9051	7.9490	7.9857	8.0209	8.2717
0.20	7.5955	7.6278	7.7712	7.9334	8.0062	8.0536	8.3670
0.30	7.2048	7.2571	7.5237	7.8909	8.0346	8.1026	8.5214
0.40	6.7428	6.7994	7.1345	7.7820	8.0573	8.1568	8.6649
0.50	6.2605	6.3061	6.6061	7.4993	8.0355	8.1877	8.7291
0.60	5.7895	5.8175	6.0082	6.7911	7.8048	8.0712	8.2287
0.70	5.3510	5.3635	5.4513	5.8328	6.6172	7.1070	7.4490
0.80	4.9518	4.9570	4.9956	5.2166	5.6626	5.9587	6.7673
0.85	4.7675	4.7721	4.8088	5.0290	5.4402	5.7107	6.5268
0.90	4.5932	4.5998	4.6505	4.9163	5.3327	5.5750	6.3421
0.95	4.4286	4.4400	4.5246	4.9018	5.2042	5.6456	6.1734
0.98	4.3342	4.3504	4.4671	4.9550	5.5823	5.8638	6.2557

Note: The frictional pressure loss is increasing with increasing Taylor number for concentric annulus (*e*=0). This does not mean that we have an increase in pressure loss, but that the change is caused by an decrease in flowrate. The Reynolds number used by Escudier et al. (2000, 2002) can be expressed by:

$$Re = (1+\epsilon^2)^{\frac{1-n_{pl}}{2}} \cdot Re_0 \qquad \text{.....(30)}$$

Where $$Re_0 = \frac{\rho U^{2-n_{pl}} . D_H^{n_{pl}}}{K_{pl}} \qquad \text{.....(31)}$$

Epsilon is defined as:

$$\epsilon = \frac{wR_I}{U} \qquad \text{.....(32)}$$

Both the Reynolds number and the Taylor number are dependent on epsilon which changes with flow rate and rotation speed. As such, in order to keep the Reynolds number constant in the above data, the flow rate must be changed for each new Taylor number. Figure LIII shows how the Reynolds number changes with rotation speed for a specific case with specified constant flow rate, density, wellbore geometry and rheological parameters.

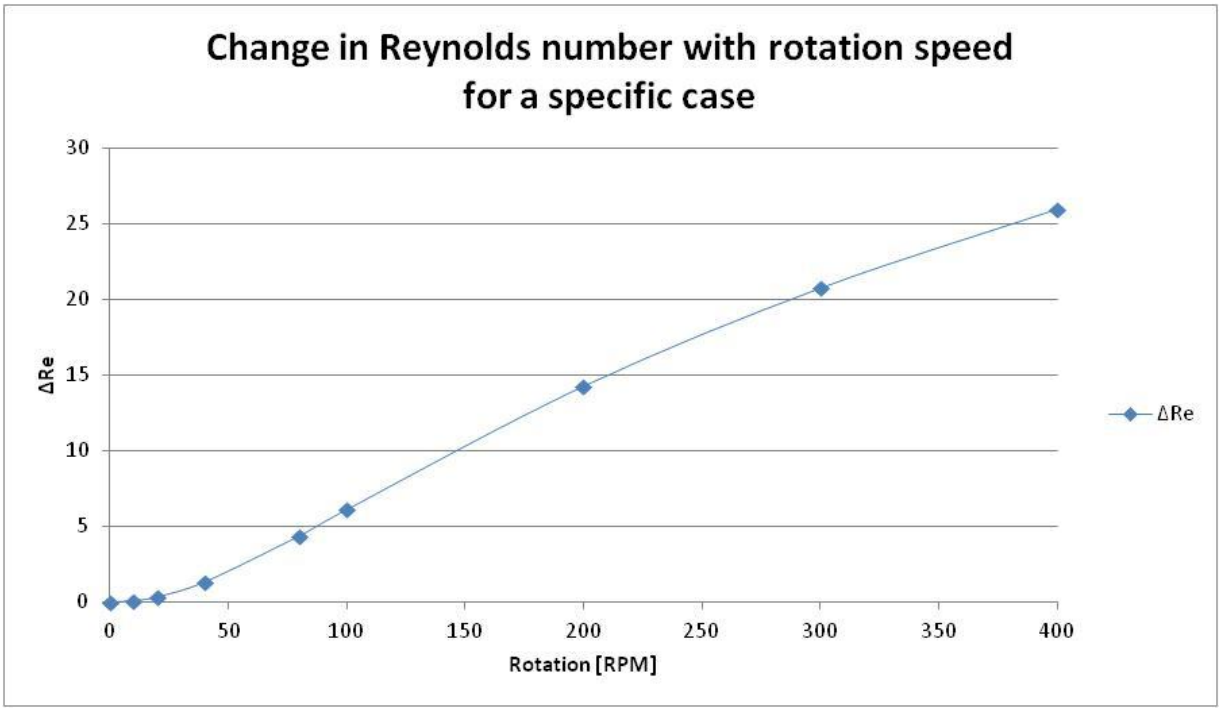

Figure LIII- Change in Reynolds number with rotation speed for a specific case

Appendix D – Program code of the new model

The program code is here displayed, but not in its completeness. Areas where the code has been limited are denoted with a […] sign.

```
// YPL Eccentric Annuli.cpp : Defines the entry point for the console application.
//

//*************************************************************************//
//*    Name:         YPL
                                  *//
//* Purpose:  to determine frictional pressure loss in pipe & con. annuli *//
//*                          under laminar flow conditions with pipe rotation
                                                  *//
//* Author:          Henrik Næsgaard      with advisor Dr. Ramadan Ahmed
                                                        *//
//* Date:            July 2012
                               *//
//*
                                                 *//
//*************************************************************************//

//     Da:                  Annular diameter
//     Dp:                  Drill pipe diameter
//     Ro:                  Annular radius
//     Ri:                  Drill pipe radius
//     dpdz:          Pressure gradient
//     Q_Exact:       Exact flow rate
//     Q:                   Approx. flow rate
//     Ty:                  Yield stress
//     PV:                  Plastic viscosity
//     a:                   Inner plug radius
//     b:                   Outer plug radius

//     Ref:           Non-Newtonian Flow and Heat Transfer

//--Headers-------------------------------------------------------------------

#include "stdafx.h"
#pragma once
#include <stdio.h>
#include <tchar.h>
#include <iostream>
#include <fstream>
#define _USE_MATH_DEFINES //added last
#include <math.h>
#include <stdlib.h>
#include <iomanip>

using namespace std;

double YPL_Exact_dpdz_max
(double,double,double,double,double,double,double,double,double);          // 9 inputs
(Da,Dp,Ty,Q, m,K,dpdz_max,Den,M)
double YPL_Exact_dpdz_min (double,double,double,double,double);     //5 inputs
double YPL_Eccentric_Annulus (double,double,double,double,double,double,double,
double, double);     //9 inputs (Da,Dp,Ty,dpdz,m,K,Den,Q,RPM)
```

```
double ConcRot2(double, double, double, double, double, double , double,
double,double,double);  //10 inputs (Da, Dp, Ty,  dpdL_max, m,  K,
Den,Q,RPM,dpdz_or_Q)
double YPL_Exact(double,double,double,double,double,double,double,double); //8 inputs
(Da,Dp,Ty,dpdz, m,Den, K, M)
double Integral_M (double,double,double,double,double,double,double,double,double);
            //9 inputs
double Integral_M2 (double,double ,double ,double ,double ,double, double , double
,double) ;    //9 inputs (ro,Ri,Ty,dpdz,m,K,M,a_star,b_star)
double YPL_Exact2(double ,double ,double , double , double,double, double,double);
            //8 inputs (Da,Dp,Ty,dpdz,m,K,M,Den)

double pi=3.14159265;

const int Max=51;
const int Max_ANN=201;
double Dp,Da,Ro,Ri,K,m,dpdz=0.000000001,Ty,Rel_Ecc,Yi,xi,yi,xii,yii;
double Qi,Xi,Delta_Teta,Ecc,Teta,Xi1,Xi2,A,B,C,Q;
double ri,ro,da,dp,Xii,Yii,Xii1,Xii2,Dh,U,fRe,ratio3,dpdz_new3,f3,fRe3;
double Area,A1,A2,dpdz_mod;
double
u[Max_ANN],r[Max_ANN],w[Max_ANN],Den,p[Max_ANN],dhdr[Max_ANN],dpdz_or_Q,Qr=0.0,Q_Total
=0.0;
int N=Max,i=1,Max_Input=100,ii=1;


int _tmain(int argc, _TCHAR* argv[])
{

[…]


//     Header Lines for the Output File

       outs  << "Program Outputs" <<"\n";
       outs  << "--------------------------------------------------------------" <<"\n";
       outs  << "Friction Pressure Loss, dp/dL [Pa/m]" <<"\n";


       ins.getline(EmptyLine,100); //Escaping Header Lines
       ins.getline(EmptyLine,100); //Escaping Header Lines
       ins.getline(EmptyLine,100); //Escaping Header Lines
//     ins.getline(EmptyLine,100); //Escaping Header Lines

//     program inputs

       ins >> dpdL_max;
       ins >> car; //Escaping Header Lines
       ins >> car; //Escaping Header Lines
       ins >> dpdL_min;
       ins >> car; //Escaping Header Lines
       ins >> car; //Escaping Header Lines
       ins >> Dp;
       ins >> car; //Escaping Header Lines
       ins >> car; //Escaping Header Lines
       ins    >> Da;
       ins >> car; //Escaping Header Lines
       ins >> car; //Escaping Header Lines
       ins >> K;
       ins >> car; //Escaping Header Lines
       ins >> car; //Escaping Header Lines
       ins >> Ty;
```

```
	ins >> car; //Escaping Header Lines
	ins >> car; //Escaping Header Lines
	ins >> m;
	ins >> car; //Escaping Header Lines
	ins >> car; //Escaping Header Lines
	ins >> Rel_Ecc;			//Change for several Rel_Ecc
	ins >> car; //Escaping Header Lines
	ins >> car; //Escaping Header Lines
	ins >> Den;
	ins >> car; //Escaping Header Lines
	ins >> car; //Escaping Header Lines
	ins >> RPM;				//Change for several RPM
	ins >> car; //Escaping Header Lines
	ins >> car; //Escaping Header Lines


	//cout <<"Convergence tolerance overview:\n\n"<<endl;
	//cout<<"The Q_mid loop : (fabs(Q-Q_mid)/Q>0.003) [Exception: for Q<0.0000092;
tolerance =0.031.]"<<endl;
	//cout<<"The YPL_Exact_dpdz_max loop : (fabs(Q-Q_mid)/Q>0.01)"<<endl;
	//cout<<"ConcRot2 RPM loop : (fabs(RPMmed-RPM)>0.01)"<<endl;
	//cout<<"YPL_Exact upo loop: (fabs(upo-upi)/upo > 0.0005)    "<<endl;
	//cout <<"YPL_Exact integral_Med loop:
(fabs(integral_Med)>0.0001)\n\n\n\n"<<endl;
	//cout<<"YPL_Exact s loop (integral_L & R loop):(s<1000000)"<<endl;


	cout<<"Registered input:"<<endl;
	cout<<"dpdL_max:\t"<<dpdL_max<<endl;
	cout<<"dpdL_min:\t"<<dpdL_min<<endl;
	cout<<"Dp:\t\t"<<Dp<<endl;
	cout<<"Da:\t\t"<<Da<<endl;
	cout<<"K:\t\t"<<K<<endl;
	cout<<"Ty:\t\t"<<Ty<<endl;
	cout<<"m:\t\t"<<m<<endl;
	cout<<"Rel_Ecc:\t"<<Rel_Ecc<<endl;//Change for several Rel_Ecc
	cout<<"Den:\t\t"<<Den<<endl;
	cout<<"RPM:\t\t"<<RPM<<endl;


//-------



	while (ii<Max_Input)
	{


//		if(Dp>Da) {cout <<"Pipe diameter should be less than the diameter of the
annulus"<<"\n";break;};

		Q=0.0;
		Qr=0.0;

		ins >> Q;

		cout<<"Q= "<<Q;
		cout<<"\nIf the simulation stops here (1 min), please specify a higher
maximum pressure drop in input"<<endl;
		//cin.get();
		//cin.ignore();
```

```
                if(Q==0.0) break;

                        //RPM=0;
                        //while (RPM<401)
                        //{ Rel_Ecc=0;

        //              while (Rel_Ecc<1.01)    //for (j=2;j<=10000000000000;j++)
        //{
[…]



                for (j=2;j<=10000000000000;j++)
                {

                        dpdz_max=j*dpdL_max;//Retaining the Original dpdL_max
                        if (j>2)
                        {cout <<"dpdz_max was increased to= "<<dpdz_max<<endl;}

                        dpdz_min=dpdL_min;


                        dpdz_or_Q=2;          //"2"  to return Q (not "1" to return dpdz)
                        Q_max=YPL_Eccentric_Annulus(Da,Dp,Ty,dpdz_max,m,K,Den,Q,RPM);


                        Q_min=0.0;


                        dpdz_mid=0.5*(dpdz_max+dpdz_min);


                        Q_mid=YPL_Eccentric_Annulus(Da,Dp,Ty,dpdz_mid,m,K,Den,Q,RPM);

                        if ((Q<Q_max)&&(Q>Q_min))
                        {       cout<<"\n\n\n\n##-----------------------------------------
-------------------#\n"<<endl;
                                cout<<"Entering Q_med loop with the following starting
values:\n"<<endl;
                                cout<<"dpdz_min= "<<dpdz_min<<"\t"<<"dpdz_max=
"<<dpdz_max<<"\n"<<endl;
                                cout<<"Q_min= "<<Q_min<<"\t"<<"Q_max= "<<Q_max<<"\n"<<endl;
                                cout<<"The desirable flowrate is "<<Q<<" [m^3/s].\n"<<endl;
                                cout<<"\n\nAt this point the calculations may take up to 5
minutes per flowrate. Press Enter to start"<<endl;
                                cout<<"\n##-----------------------------------------------
-------------#\n\n\n\n\n\n\n\n"<<endl;

                                //cin.get();
                                //cin.ignore();
                                break;}



                }

        //cout<<"The Q_mid loop : (fabs(Q-Q_mid)/Q>0.003) [Exception: for Q<0.0000092;
tolerance =0.031.]"<<endl;
                if (Q<0.0000092)            //Adjusting tolerance for small flow rates.
                        {Qmidtol=0.031;}
                else if (Q>0.0011)
```

```
                        {Qmidtol=0.005;}//History :[Adjusting tolerance for high flow
rates (fig 14).[0.06]]
                else
                        {Qmidtol=0.003;}

                while (fabs(Q-Q_mid)/Q>=Qmidtol)         //Was reduced to 0.003 because
of convergence for small flowrates. [was 0.0003 before].
                {


                        if (Q_mid<Q)
                        {
                                dpdz_min=dpdz_mid;
                        }
                        else if (Q_mid>Q)
                        {
                                dpdz_max=dpdz_mid;

                        }
                        else
                        {
                                {break;}
                        }

                        if ((fabs(Q-Q_mid)/Q)<best_tol)
                        {
                                best_Q_mid=Q_mid;
                                best_dpdz=dpdz_mid;
                                best_tol=fabs(Q-Q_mid)/Q;
                        }

                        tolprevious=fabs(Q-Q_mid)/Q;

                        if (fabs(dpdz_min-dpdz_max)/dpdz_max<0.000000000001)
                        {
                                cout<<"##-------------------------------------------------
------------------------##"<<endl;
                                cout<<"---------------------NO CONVERGENCE ALERT----------
--------------------------"<<endl;
                                cout<<"Q_mid loop is not converging. The final tolerance is
: "<<(Q-Q_mid)/Q<<"> "<<Qmidtol<<endl;
                                cout<<"\n The desired Q is: "<<Q<<" and the final Q is:
"<<Q_mid<<", with dpdz= "<<dpdz_mid<<endl;
                                cout<<"\n\n The best tolerance achieved was: "<<best_tol<<"
for Q: "<<best_Q_mid<<", which gives dpdz= "<<best_dpdz<<endl;

                                if (best_tol<((Q-Q_mid)/Q))
                                {
[…]

                                        cout<<" \n\n We will now accept the current
tolerance of: "<<best_tol<<endl;
                                        cout<<"##-------------------------------------------
------------------------------##"<<endl;
                                        cin.get();
                                        cin.ignore();
                                        dpdz_mid=best_dpdz;
                                        goto loop60;
                                }
                        }

                        dpdz_mid=0.5*(dpdz_max+dpdz_min);
```

```
                j=j+1;

                Q_mid=YPL_Eccentric_Annulus(Da,Dp,Ty,dpdz_mid,m,K,Den,Q,RPM);
                Qr=0.0;
                cout<< "\nQ_mid= "<<Q_mid<<"\n"<<endl;
                //cin.get();
                //cin.ignore();

        }




loop60:         outs  <<""<<endl;    /*reached loop60!*/


                Do=Ro*2;
                Di=Ri*2;
                delta=Ro-Ri;
                Dh=2*delta;
                k=Di/Do;
                e=Rel_Ecc;
                epsilon=vel_w*Ri/velocity_U;

        if ((m==1) && (Ty==0))            //Newtonian
        {
[…]



        else if ((m!=0) && (Ty==0.0))     //If Power Law
        {

                flow_N=m;
                shearz=(1+2*flow_N)/(3*flow_N)*12*velocity_U/(Do-Di);
                sheareggz=vel_w*Di/(Do-Di);
                shearegz=sqrt(pow(sheareggz,2)+pow(shearz,2));
                vis=K*pow(shearegz,(m-1));

        }

        else          //if YPL
        {

                sheareggz=vel_w*Di/(Do-Di);
                s_rate_wall_min=0;
                s_rate_wall_max=3000;

                        while (fabs(s_rate_wall_mid-shearegz)>0.0001)  //iteration
to find the shear rate at the wall
                        {
[…]

                                while (fabs(left_side-right_side)>0.00001)
        //iteration to find N (flow behaviour index)--//
                                {
                                        flow_N=(N_max+N_min)/2;
                                        left_side=3*flow_N/(2*flow_N+1);
```

```
                                        right_side=(3*m/(2*m+1))*(1-(1/(m+1))*x-
(m/(m+1))*pow(x,2));
                                              if (left_side>right_side)
                                              {N_max=flow_N;}
                                              else
                                              {N_min=flow_N;}

                                        cout << "Approximation N= "<<flow_N<<endl;

                                  }

                            shearz=(1+2*flow_N)/(3*flow_N)*12*velocity_U/(Do-Di);
                            sheareggz=sqrt(pow(shearegg,2)+pow(shearz,2));

                                  if (s_rate_wall_mid>sheareggz)
                                  {s_rate_wall_max=s_rate_wall_mid;}
                                  else
                                  {s_rate_wall_min=s_rate_wall_mid;}

                            cout << "Approximation shear rate=
"<<s_rate_wall_mid<<endl;
                            }

                      vis=Ty/sheareggz+K*pow(sheareggz,(m-1));

               }


               if ((RPM!=0)  && (e!=0))    //Inertia
               {
[…]
                      dpdz0=fRe0/Re/(delta/(Den*pow(velocity_U,2)));


                      outs<< "RPM="<<RPM<<", Q= "<<Q<<", Re= "<<Re<<", Ta= "<<Ta<<", e=
"<<e<<", k= "<<k<<", N= "<<flow_N<<", m= "<<m<<endl;

                      outs <<"\ndpdz0=         "<<setw(8)<<dpdz0<<endl;
                      outs <<"dpdz(EZ)=     "<<setw(8)<<dpdzEZ<<endl;
                      //outs <<"dpdz(EZOLD)=     "<<setw(8)<<dpdzEZOLD<<endl;
                      outs <<"dpdz(ALL)=    "<<setw(8)<<dpdzALL<<endl;
                      outs <<"\nf*Re(0)=    "<<fRe0<<" (inertia= "<<CALC5<<")."<<endl;
                      outs <<"f*Re(EZ)=   "<<fReEZ<<" (inertia= "<<CALCEZ<<")."<< endl;
                      //outs <<"f*Re(EZOLD)=   "<<fReEZOLD<<" (inertia=
"<<CALCEZOLD<<")."<< endl;
                      outs <<"f*Re(ALL)=  "<<fReALL<<" (inertia= "<<CALCALL<<").\n"<<
endl;

                      outs <<"                      ----------------------------"<<endl;
               }
               else
               {
                      Re0=Den*pow(velocity_U, (2-m))*pow(Dh,m)/K;
                      Ta0=pow(Den*pow(vel_w,(2-m))/K,2)*pow(Dh,(2*m+1))*pow(Ri,(3-
2*m))/8;
                      f0=(delta/(Den*pow(velocity_U,2)))*dpdz_mid;
                      fRe0=Re0*f0;

                      outs<< "RPM= "<<RPM<<", Q= "<<Q<<", Re= "<<Re0<<", Ta= "<<Ta0<<",
e= "<<e<<", k= "<<k<<", N= "<<flow_N<<", m= "<<m<<endl;
                      outs <<"\ndpdz=         "<<setw(8)<<dpdz_mid<<endl;
                      outs <<"\nf*Re= "<<fRe0<<" (no inertia)."<<endl;
```

```
            outs <<"                        ----------------------------"<<endl;

        }
        ////--------------------------------//
        ////--Adding inertial correlation---//
        ////--------------------------------//
        ////--------------------------------//
        //
        //
        //delta=Ro-Ri;

        //if ((RPM!=0) && (Rel_Ecc!=0))
        //{    Do=Ro*2;
        //Di=Ri*2;
        //k=Di/Do;


        //
        //if ((m==1.0) && (Ty==0.0))            //If Newtonian
        //{flow_N=1;
        //shearz=(1+2*flow_N)/(3*flow_N)*12*velocity_U/(Do-Di);
        //sheareggg=vel_w*Di/(Do-Di);
        //shearegggz=sqrt(pow(sheareggg,2)+pow(shearz,2));
        //vis=K;}

        //else if (Ty==0.0)                     //If Power-Law
        //{flow_N=m;
        //shearz=(1+2*flow_N)/(3*flow_N)*12*velocity_U/(Do-Di);
        //sheareggg=vel_w*Di/(Do-Di);
        //shearegggz=sqrt(pow(sheareggg,2)+pow(shearz,2));
        //vis=K*pow(shearegggz,(m-1));}

        //else                                          //If Yield-Power Law
        //{
        //sheareggg=vel_w*Di/(Do-Di);
        //s_rate_wall_min=0;
        //s_rate_wall_max=2000;

        //while (fabs(s_rate_wall_mid-shearegggz)>0.0001)      //iteration to find
the shear rate at the wall
        //{
        //N_max=10;
        //N_min=0;
        //left_side=4;
        //right_side=1;
        //s_rate_wall_mid=(s_rate_wall_min+s_rate_wall_max)/2;
        //tavgwall=Ty+K*pow(s_rate_wall_mid,m);
        //x=Ty/tavgwall;

        //while (fabs(left_side-right_side)>0.0001)    //iteration to find N
(flow behaviour index)--//
        //     {
        //     flow_N=(N_max+N_min)/2;
        //     left_side=3*flow_N/(2*flow_N+1);
        //     right_side=(3*m/(2*m+1))*(1-(1/(m+1))*x-(m/(m+1))*pow(x,2));
        //           if (left_side>right_side)
        //           {N_max=flow_N;}
        //           else
        //           {N_min=flow_N;}

        //     cout << "Approximation N= "<<flow_N<<endl;
```

```
//     }

//     shearz=(1+2*flow_N)/(3*flow_N)*12*velocity_U/(Do-Di);
//     sheareggz=sqrt(pow(sheareggg,2)+pow(shearz,2));

//            if (s_rate_wall_mid>sheareggz)
//            {s_rate_wall_max=s_rate_wall_mid;}
//            else
//            {s_rate_wall_min=s_rate_wall_mid;}

//     cout << "Approximation shear rate= "<<s_rate_wall_mid<<endl;
//}
//vis=Ty/sheareggz+K*pow(sheareggz,(m-1));

//}
//

//Ta=pow((Den*vel_w/vis),2)*Ri*pow(delta,3);
//e=Rel_Ecc;
//k=Ri/Ro;
//Re=2*Den*velocity_U*delta/vis;


      //ratio1=(0.00310885523*pow(Ta,0.52969735)*pow(e,13.7405522490094)*pow(k,0.74089
4085000067)+0.00183744081469697*pow(Ta,0.422732122055)+0.134970897434195*pow(e,0.02716
79067304634)+0.885415188859763*pow(k,0.0365556735));
            //dpdz_new1=dpdz_mid*ratio1;
            //f1=(delta/(Den*pow(velocity_U,2)))*dpdz_new1;
            //fRe1= f1*Re;

            //ratio2= (Ta/(326.3241732+0.083509798*Ta))*pow(e,4)-(18.16303975*(1-
pow(M_E,(-0.00021292*Ta))))*pow(e,3)+(9.802592633*(1-pow(M_E,(-
0.00018711*Ta))))*pow(e,2)+((-844.527052+Ta)/(-6228.20441-
0.00001666199437183*pow(Ta,2)))*e+0.000000000008350803443965*pow(Ta,2)+1.00441693;
            //dpdz_new2=dpdz_mid*ratio2;
            //f2=(delta/(Den*pow(velocity_U,2)))*dpdz_new2;
            //fRe2= f2*Re;


      //ratio3=0.00329310640951*pow(Ta,0.5134199717008)*pow(e,13.77227319684)*pow(k,0.
4901473398117)+0.003047147558474*pow(Ta,0.3992850426045)+0.7810230709819*pow(e,0.01291
718768449)+0.2012184381386*pow(k,-0.1482018269417);
            //dpdz_new3=dpdz_mid*ratio3;
            //f3=(delta/(Den*pow(velocity_U,2)))*dpdz_new3;
            //fRe3= f3*Re;

            //if ((m!=1) && (e!=0) && (RPM!=0))            //Shear-thinning for Non-
Newtonian
            //     {ratio_corrected=-
5.46529194015294*pow(m,0.677511212440706)*pow(k,0.175431290011059)*pow(Re,-
0.0431128272184168)*pow(e,0.0334253221710951)*pow(Ta,0.0329103387692092)-
0.705238095395905+0.692122792036371*pow(m,0.189984630249854)+1.01923882081454*pow(k,0.
342584488166501)+1.15007947784265*pow(Re,0.11386121750756)+0.900052286671447*pow(e,0.0
707691600064183)+1.08627131247515*pow(Ta,-
0.012296989400382)+0.982743446469727*pow(Re,0.0401438271019898);
            //     fRe3= fRe3/ratio_corrected;
            //     f3=fRe3/Re;
            //     dpdz_new3=f3/(delta/(Den*pow(velocity_U,2)));}

            //if (Ta>50000)
            //           {outs <<" Attention: Taylor number is higher than 50 000,
no correct solution as of yet!"<<endl;}
```

```
              //

              //outs  << "dpdz_new (1)= "<<dpdz_new1 <<", dpdz_new(2)= "<<dpdz_new2<<",
dpdz_new(3)= "<<dpdz_new3<<"\n";
              //outs  << "f*Re (1)= "<<fRe1 <<", f*Re(2)= "<<fRe2<<", f*Re(3)=
"<<fRe3<<".   [f1= "<<f1<<", f2= "<<f2<<", f3= "<<f3<<"]\n";
              //outs <<"Ratio(1) = "<<ratio1<<",  Ratio(2)= "<<ratio2<<", Ratio(3)=
"<<ratio3<<", Ratio(3)_corrected= "<<ratio_corrected<<endl;
              //outs  <<"with Ta= "<<Ta<<", k= "<<k<<", e= "<<e<<", Re= "<<Re<<", vis=
"<<vis<<", N= "<<flow_N<<", w= "<<vel_w<<",and velocity= "<<velocity_U<<"\n\n" <<endl;

              ////--------------------------------//
              ////--Adding inertial correlation---//
              ////----------END-------------------//
              ////--------------------------------//
              //}

       cout <<"Simulation done for e="<<Rel_Ecc<<".\n"<<endl;

       //if (Rel_Ecc>0.94)
       //{Rel_Ecc=Rel_Ecc+0.03;}
/*     else */
       //if (Rel_Ecc>0.75)
       //{Rel_Ecc=Rel_Ecc+0.05;}
       //else
       //{Rel_Ecc=Rel_Ecc+0.1;}
       //}

       //RPM=RPM+50;

       //if (RPM==0)
       //{RPM=100;}
       //else if (RPM==100)
       //{RPM=200;}
       //else if (RPM==200)
       //{RPM=300;}
       //else if (RPM==300)
       //{RPM=360;}
       //else if (RPM==360)
       //{RPM=400;}
       //else if (RPM==240)
       //{RPM=300;}
       //else if (RPM==300)
       //{RPM=360;}
       //else
       //{RPM=500;}
       //}

       m=m+0.05;
       }

       }

       return 0;

}



//---------------------------------------------------------------

       double YPL_Eccentric_Annulus (double Da,double Dp,double Ty,
```

```
                                        double dpdz, double m,double K,double Den,double
Q,double RPM)
       {


              Delta_Teta=pi/(N-1);

              Teta=-pi/2;

              Qi=0.0; i=1;

              while (i<N)
              {

                     A=1+pow(tan(Teta),2); B=-2*Ecc*tan(Teta); C=pow(Ecc,2)-pow(Ro,2);

                     Xi1=(-B+sqrt(pow(B,2)-4*A*C))/2/A;

                     Xi2=(-B-sqrt(pow(B,2)-4*A*C))/2/A;

                     if (Xi1>Xi2) {Xi=Xi1;} else {Xi=Xi2;}

                     Yi=Xi*tan(Teta);

                     xi=fabs(Ri*cos(Teta));

                     yi=Ri*sin(Teta);

                     Teta=Teta+Delta_Teta;

                     A=1+pow(tan(Teta),2); B=-2*Ecc*tan(Teta); C=pow(Ecc,2)-pow(Ro,2);

                     Xii1=(-B+sqrt(pow(B,2)-4*A*C))/2/A;

                     Xii2=(-B-sqrt(pow(B,2)-4*A*C))/2/A;

                     if (Xii1>Xii2) {Xii=Xii1;} else {Xii=Xii2;}

                     Yii=Xii*tan(Teta);

                     xii=fabs(Ri*cos(Teta));

[…]

                     dpdz_mod=pow(Ri/Ro,0.27*Rel_Ecc)*dpdz;

                     if (RPM==0.0)
                     {      //8 inputs (Da,Dp,Ty,dpdz,m,K,M,Den)

                            Qi=Qi+YPL_Exact2(da, dp, Ty, dpdz_mod,  m, K,  RPM,
Den)*Delta_Teta/(2*pi);
                     }
                     else
                     {
                            Qi=Qi+ConcRot2(da, dp, Ty, dpdz_mod,  m, K,  Den,
Q,RPM,dpdz_or_Q)*Delta_Teta/(2*pi);
                     }

                     //cout<<"Qi is equal to : "<<Qi<<"     "<<i<<endl;

                     i=i+1;
```

```
		}


		Q_Total=2*Qi; // Qi is for only half of the annulus


		return Q_Total;
	}


//-----------------------------------------------------------------


double YPL_Exact_dpdz_min (double Dp,double Ty,double Q, double m,double K)
{


	double pi=3.141592654,Ri,A,B,C,dpdz;
	double Tw,Tw_min,Tw_max,Tw_med,U,Area,f,D;
	int i=0,j=1;

//  calculation


	Ri=Dp/2;

	Area=pi*pow(Dp,2)/4;


		if(Q==0.0) {goto loop10;}

		U=Q/Area; A=8*U/Dp;  B=4*m/(3*m+1); C=2*m/(1+2*m);

		D=2*pow(m,2)/((1+m)*(1+2*m)); Tw_min=Ty; Tw_max=1000000;

		for (i=1;i<=100000;i++)
		{
			Tw_med =(Tw_min + Tw_max)/2;

			f = pow(Tw_med - Ty,1/m+1)/pow(K,1/m)/pow(Tw_med,3) * B *
(pow(Tw_med,2)
				+ C * Tw_med * Ty + D * pow(Ty,2)) - A;
[…]
			}

			if (fabs(Tw_max - Tw_min)/Tw_med < 0.01)
			{
				Tw=Tw_med;


				dpdz=4*Tw/Dp;


			}

		}


	loop10: cout <<"  ";

	return dpdz;
```

```
}
	double YPL_Exact_dpdz_max (double Da,double Dp,double Ty,
				double Q, double m,double K, double dpdz_max,
double Den, double M)

					// 9 inputs (Da,Dp,Ty,Q, m,K,dpdz_max,Den,M)
	{


		double dpdz_min, dpdz_mid, Q_min,Q_max,Q_mid;

		dpdz_min=YPL_Exact_dpdz_min(Da,Ty,Q,m,K);

		Q_min=YPL_Exact(Da,Dp,Ty,dpdz_min,m,Den,K,0.0);//8 inputs (Da,Dp,Ty,dpdz,
m,Den, K, M)

		//dpdz_max=1000000000;

		Q_max=YPL_Exact(Da,Dp,Ty,dpdz_max,m,Den,K,0.0);//8 inputs (Da,Dp,Ty,dpdz,
m,Den, K, M)

[…]

			if (Q_mid<Q)
			{
				dpdz_min=dpdz_mid;

				Q_min=YPL_Exact(Da,Dp,Ty,dpdz_min,m,Den,K,0.0);//8 inputs
(Da,Dp,Ty,dpdz, m,Den, K, M)

				if (Q_min>Q) {Q_min=Q-fabs(Q_min-Q);} // adjusting the
location of Q_min
			}
			else
			{
				dpdz_max=dpdz_mid;

				Q_max=YPL_Exact(Da,Dp,Ty,dpdz_max,m,Den,K,0.0); //8 inputs
(Da,Dp,Ty,dpdz, m,Den, K, M)

				if (Q_max<Q) {Q_max=Q+fabs(Q_max-Q);} // adjusting the
location of Q_max
			}

			Q_mid=0.5*(Q_min+Q_max);

			dpdz_mid=0.5*(dpdz_max+dpdz_min);

		}

		loop10: cout <<"  ";

		return dpdz_mid;
	}


//*************************************************************************//
//*    Name:         Return Q for given dpdz and M (ConcRot Self)
                                        */
//* Purpose:  to be implemnted in YPL Eccentric flow as YPL_Exact for rotation
concentric flwo                                                        *//
```

```
//* Author:          Henrik Naesgaard with advisor Dr.Ramadan Ahmed
                                                                  *//
//* Date:            July 2012
                              *//
//*
                                                  *//
//*************************************************************************//

//     Da:                  Annular diameter
//     Dp:                  Drill pipe diameter
//     Ro:                  Annular radius
//     Ri:                  Drill pipe radius
//     dpdz:          Pressure gradient
//     Q:                   flow rate
//     Ty:                  Yield stress
//     PV:                  Plastic viscosity
//     a:                   Inner plug radius
//     b:                   Outer plug radius
//     a_star:              dpdz* = -dpdz
//     b_star:
//     R_star:              radius r from the center where the axial stress vanishes
//     T:                   applied torque per length

//     Ref:           Non-Newtonian Flow and Heat Transfer

//--Headers-------------------------------------------------------------------

//10 inputs (Da, Dp, Ty,  dpdz, m,  K, Den,Q,RPM,dpdz_or_Q)
double ConcRot2 (double Da,double Dp,double Ty,
                                    double dpdz, double m,double K,double Den,double
Q,double RPM,double dpdz_or_Q)
{
int N=Max_ANN,i=1,ii=1,j=0;
double Qmed=0,Qprevious=0,RPMprevious=0;
double RPMmin=0, RPMmax=0,RPMmed=0, M_min=0.00, M_max=2.0, M_med, temp=0,enterloop30;
//M_max is 0.07Nm/m and M_min is 0.0Nm/m by default. Changed to M_max=2.0Nm/m for
conventional.

ofstream outs;
outs.open("out.dat");

outs  << "        i    "<< " r[m]  "<< " u[m/s]  "
         << " w[rpm]  " << "    p[Pa]  " << "\n";



//--------------------RPM_med LOOP-----------------------------------------------
//-------------------------------------------------------------------------------

if (RPM==0)
{Qr=YPL_Exact(Da,Dp,Ty,dpdz,m,Den,K,0.0);}//8 inputs (Da,Dp,Ty,dpdz, m,Den, K, M)
else
{      while (fabs(RPMmed-RPM)>0.5)            //Changed from 0.00001 to 0.01. Changed
from 0.01 to 0.11 for big annulii and high Ta number. Same reason, changed from 0.11
to 0.5.
       {

       Qr=0.0;

       i=i+1;
       //Debug:
       //cout<< "i= "<<i<<endl;
```

```
	M_med=0.5*(M_max+M_min);

	Qmed=YPL_Exact(Da,Dp,Ty,dpdz,m,Den,K,M_med);//8 inputs (Da,Dp,Ty,dpdz, m,Den, K,
M)

	//DEBUG:
	//cout<<"Qmed=\t"<<Qmed<<endl;

	RPMmed=w[0]/2/pi*60;
	//cout<<"\nApproximation RPM:"<<RPMmed<<"\n";
	//cin.get();


[…]


	if ((fabs(RPMprevious-RPMmed)<0.1) && (fabs(RPMmed-RPM)>0.5) && (i>28.0))
	{enterloop30=0.0;}

	RPMprevious=RPMmed;		//Save previous RPM value


loop30:	if (enterloop30==0)
		{
			if (RPMmed>RPM)
		{	M_max=0.9*M_max, M_min=0.0, M_med=0.0,i=0,j=j+1;
		/*	cout << "Qmed is not converging for the given torque (M_max
decreased to:"<<M_max<<")"<<endl;*/
		}
			else
		{	M_max=1.1*M_max, M_min=0.0,M_med=0.0,i=0,j=j+1;
			/*cout << "Qmed is not converging for the given torque (M_max
increased to:"<<M_max<<")"<<endl;*/
		}

		}

		if (j>20)
			//this is done to prevent to go into an endless loop of increasing
torque if tmax<ty several times. This is especially true for luids with high yield
stress.
		{/*cout<<"There seems to be no flow, Qr=0.0 is returned"<<endl;*/
		return Qr=0.0;}

	}
}

//--------------------END RPM_med LOOP-----------------------------------------
//-----------------------------------------------------------------------------


	if (w[0]/2/pi*60!=0)
	{/*cout<<"\nConvergence for RPM="<<w[0]/2/pi*60<<". Necessary applied torque was
"<<M_med<<" [Nm/m]."<<endl;*/
	Qr=YPL_Exact(Da,Dp,Ty,dpdz,m,Den,K,M_med);  //8 inputs (Da,Dp,Ty,dpdz, m,Den, K,
M)
	/*cout <<"\nReturning Qr="<<Qr<<"."<<endl;*/
	}
	else
	{/*cout <<"\nReturning Qr="<<Qr<<"."<<endl;}*/
	//cin.get();
```

```
	//cin.ignore();
	}

	return Qr;

}



//*************************************************************************//
//*    Name:         Exact YPL annular flow
                    *//
//* Purpose:  to determine frictional pressure loss in annuli                    *//
//*                         under laminar flow conditions
                          *//
//* Author:          Ramadan Ahmed
                          *//
//* Date:            Oct 2005
Upgraded July 2012 by Henrik Næsgaard
                                        *//
//*
                                                *//
//*************************************************************************//

//8 inputs (Da,Dp,Ty,dpdz, m,Den, K, M)

	double YPL_Exact(double Da,double Dp,double Ty,
                                    double dpdz, double m,double Den, double K, double
M)

	{

//		const int Max_ANN=201;
		double a_max,a,b,AA,BB,CC,Twi,Two,ri[Max_ANN],r_mid,upi,upo;
		double
C1i,C2i,C3i,delta_r,ro[Max_ANN],C1o,C2o,C3o,Beta,integral_Med=5,upo_tol;
		double ui,uo,Qi,Qo,Qp,up,Tw_min,Tw_max,Ro,Ri,b_star_Med;
		double pi=3.141592654,a_star,b_star,integral,r_med;
		double integral_L,integral_R,b_star_Min,b_star_Max,b_star_L,b_star_R;
		double alpha,dudr,R_star,shear_rate,dwdr;

//		double shear_rate,alpha;
		int N_ANN=Max_ANN,z,s;

		Ro=Da/2; Ri=Dp/2;

		Tw_min=Ty;

		a_max=Ro-2*Ty/dpdz; ///Changed from :a_max=Ro-2*Ty/dpdz;

		Tw_max=(Ty*a_max+0.5*dpdz*(pow(a_max,2)-pow(Ri,2)))/Ri;

		if (Tw_max<=Tw_min)
		{
			Q_Total=0.0;
			goto loop10;
		}

		AA=0.5*dpdz; BB=Ty;

		Beta=0.5*dpdz*(pow(Ro,2)-pow(Ri,2))/Ro;
```

```
                upi=2.0;upo=1.0; //initilization

                if (Q<0.000004)
                {upo_tol=0.0026672;}
                else
                {upo_tol=0.0005;}

                while (fabs(upo-upi)/upo > upo_tol)            //Change history:
[0.0001],[0.0005]
                {

                        Twi=0.5*(Tw_min+Tw_max); Two=Beta-Twi*Ri/Ro;

                        CC=-(0.5*dpdz*pow(Ri,2)+Twi*Ri);

                        a=(-BB+sqrt(pow(BB,2)-4*AA*CC))/2/AA;

                        b=2*Ty/dpdz+a;

                        C1i=-0.5*dpdz/K; C2i=Ri/K*(Twi+0.5*dpdz*Ri); C3i=Ty/K;

                        C1o=0.5*dpdz/K;      C2o=Ro/K*(Two-0.5*dpdz*Ro);C3o=Ty/K;

                        ri[0]=Ri; ri[N_ANN-1]=a; ro[0]=Ro; ro[N_ANN-1]=b;

                        upi=0.0;upo=0.0,Qi=0.0,Qo=0.0,ui=0.0,uo=0.0;

                        delta_r=(a-Ri)/(N_ANN-1);

                        for (z=1;z<=N_ANN-1;z++)
                        {
//                              u_old=ui;

                                ri[z]=ri[0]+z*delta_r;

                                r_mid=0.5*(ri[z-1]+ri[z]);

                                ui=ui+pow((C1i*r_mid+C2i/r_mid-C3i),1/m)*delta_r;

                                Qi=Qi+pi*(pow(ri[z],2)-pow(ri[z-1],2))*ui;

                        }

                        delta_r=(Ro-b)/(N_ANN-1);

[…]

                }

                up=0.5*(upi+upo);

                Qp=pi*(pow(b,2)-pow(a,2))*up;

                Q_Total=Qi+Qo+Qp;



                //     pipe rotation section ----------------------------------------------
---------
```

```
	R_star=pow(pow(Ri,2)+2*Twi*Ri/dpdz,0.5);

	a_star=dpdz;

	b_star=dpdz/2*pow(R_star,2);

	integral=Integral_M(Ro,Ri,Ty,dpdz,m,K,M,a_star,b_star);

	//if (integral==0.0)
	//	{cout<<"At this point integral was returned to be equal to 0.0, thus
after a long wait (s loop), we might not get convergence."<<endl;
	//	cout<<"integral set to 0.00000001 for convergence";
	//	integral=0.00000001;
	//	cin.get();
	//	cin.ignore();}

	s=1; Qr=0.0;

	if (integral==0.0)
	{
		cout<<"At this point integral was returned to be equal to 0.0, thus
skipping s-loop."<<endl;
		i=1000000;
		b_star_Min=0;
		b_star_Max=10;
		//cin.get();
		//cin.ignore();
	}


	while (s<1000000)
	{

		s=s+1;
		//cout<<"s: "<<s<<" and integral= "<<integral<<endl;
		b_star_L=b_star+s*0.01*b_star;
		b_star_R=b_star-s*0.01*b_star;

		integral_L=Integral_M(Ro,Ri,Ty,dpdz,m,K,M,a_star,b_star_L);
		integral_R=Integral_M(Ro,Ri,Ty,dpdz,m,K,M,a_star,b_star_R);

[…]

	}

	while (fabs(integral_Med)>0.0001) //Changed from 1E-14 to 1E-12.
	{
		b_star_Med=   0.5*(b_star_Min + b_star_Max);

		//cout<<"integral_med = "<<integral_Med<<endl;

		integral_Med=Integral_M(Ro,Ri,Ty,dpdz,m,K,M,a_star,b_star_Med);

		if (integral_Med > 0)
		{
			b_star_Max = b_star_Med;
		}
		else
		{
			b_star_Min = b_star_Med;
		}
	}
```

```
//     Axial Velocity Profile ----------------------------------------------------

       b_star = b_star_Med;

       delta_r=(Ro-Ri)/(N_ANN-1);

       r[0]=Ri; u[0]=0.0;dudr=0.0;

       for (z=1;z<=N_ANN-1;z++)
       {

              r[z]=r[z-1]+delta_r;

              r_med=0.5*(r[z]+r[z-1]);

              alpha=pow(pow(M/(2*pi*pow(r_med,2)),2)
                     +pow(b_star/r_med-a_star*r_med/2,2),0.5);


              if (alpha>Ty)
              {

                     shear_rate=pow((alpha-Ty)/K,1/m);
              }
              else
              {
                     shear_rate=0.0;
              }

              dudr=shear_rate/alpha*(b_star/r_med-a_star*r_med/2);

              u[z]=u[z-1]+dudr*delta_r;

              Qr=Qr+(u[z]+u[z-1])*pi*r_med*delta_r;

       }

//     Angular Velocity Profile ---------------------------------------------------

       r[N_ANN-1]=Ro;dwdr=0.0,w[N_ANN-1]=0.0;

       for (z=1;z<=N_ANN-1;z++)
       {

              r[N_ANN-1-z]=r[N_ANN-z]-delta_r;

              r_med=0.5*(r[N_ANN-1-z]+r[N_ANN-z]);

              alpha=pow(pow(M/(2*pi*pow(r_med,2)),2)
                     +pow(b_star/r_med-a_star*r_med/2,2),0.5);
[…]

              dwdr=M*shear_rate/(2*pi*pow(r_med,3)*alpha);

              w[N_ANN-1-z]=w[N_ANN-z]+dwdr*delta_r;

              dhdr[N_ANN-1-z]=r_med*Den*pow(0.5*(w[N_ANN-z]+w[N_ANN-1-z]),2);

       }
```

```
//     Pressure Distribution Profile ------------------------------------------------
--

       r[N_ANN-1]=Ro;p[0]=0.0;

       for (z=1;z<=N_ANN-1;z++)
       {

       p[z]=p[z-1]+dhdr[z-1]*delta_r;


       }


       dpdz=0.0;

       loop10: return Qr;


       }


//*************************************************************************//
//*    Name:         Integral_M
                                  *//
//* Purpose:  to determine the value of integral given by Eq. 3.11         *//
//* Author:          Ramadan Ahmed
                         *//
//* Date:            Oct 2005
Upgraded July 2012 by Henrik Næsgaard
                                      *//
//*
                                                 *//
//*************************************************************************//

       double Integral_M (double Ro,double Ri,double Ty,double dpdz,
              double m,double K, double M, double a_star,double b_star)
       {

//            const int Max_ANN=2001;

              double pi=3.141592654,integral=1.0;
              double shear_rate,alpha,delta_r,r_med;
              int N_ANN=Max_ANN,z;


              delta_r=(Ro-Ri)/(N_ANN-1);

              integral=0.0,r[0]=Ri;

[…]

                     r_med=0.5*(r[z]+r[z-1]);

                     alpha=pow(M/(2*pi*pow(r_med,2)),2)
                            +pow(b_star/r_med-a_star*r_med/2,2);

                     alpha=pow(alpha,0.5);

                     if (alpha>Ty)
                     {
                            shear_rate=pow((alpha-Ty)/K,1/m);
```

```
                }
                else
                {
                        shear_rate=0.0;
                }

                integral = integral+shear_rate/alpha*(b_star/r_med-
a_star*r_med/2)*delta_r;          //Coleman and Noll, Equation 3.12

        }

        return integral;
    }



    double YPL_Exact2(double Da,double Dp,double Ty,
                                double dpdz, double m,double K, double M,double
Den)
    {

//          const int Max=201;
            double a_max,a,b,AA,BB,CC,Twi,Two,ri[Max],r_mid,upi,upo;
            double
C1i,C2i,C3i,delta_r,ro[Max],C1o,C2o,C3o,Beta,integral_Med,integral_Med_tol;
            double ui,uo,Qi,Qo,Qp,up,Tw_min,Tw_max,Ro,Ri,b_star_Med;
            double pi=3.141592654,a_star,b_star,integral,r_med;
            double integral_L,integral_R,b_star_Min,b_star_Max,b_star_L,b_star_R;
            double alpha,dudr,R_star,shear_rate,dwdr;

//          double shear_rate,alpha;
            int N=Max,j,i;

            Ro=Da/2; Ri=Dp/2;

            Tw_min=Ty;

            a_max=Ro-2*Ty/dpdz;

[…]

            AA=0.5*dpdz; BB=Ty;

            Beta=0.5*dpdz*(pow(Ro,2)-pow(Ri,2))/Ro;

            upi=2.0;upo=1.0; //initilization

            while (fabs(upo-upi)/upo > 0.0001)
            {

                    Twi=0.5*(Tw_min+Tw_max); Two=Beta-Twi*Ri/Ro;

                    CC=-(0.5*dpdz*pow(Ri,2)+Twi*Ri);

                    a=(-BB+sqrt(pow(BB,2)-4*AA*CC))/2/AA;

                    b=2*Ty/dpdz+a;

                    C1i=-0.5*dpdz/K; C2i=Ri/K*(Twi+0.5*dpdz*Ri); C3i=Ty/K;

                    C1o=0.5*dpdz/K;     C2o=Ro/K*(Two-0.5*dpdz*Ro);C3o=Ty/K;
```

```
                        ri[0]=Ri; ri[N-1]=a; ro[0]=Ro; ro[N-1]=b;

                        upi=0.0;upo=0.0,Qi=0.0,Qo=0.0,ui=0.0,uo=0.0;

                        delta_r=(a-Ri)/(N-1);

                        for (j=1;j<=N-1;j++)
                        {
//                              u_old=ui;

                                ri[j]=ri[0]+j*delta_r;

                                r_mid=0.5*(ri[j-1]+ri[j]);

                                ui=ui+pow((C1i*r_mid+C2i/r_mid-C3i),1/m)*delta_r;

                                Qi=Qi+pi*(pow(ri[j],2)-pow(ri[j-1],2))*ui;

                        }

                        delta_r=(Ro-b)/(N-1);

                        for (j=1;j<=N-1;j++)
                        {
//                              u_old=uo;

                                ro[j]=ro[0]-j*delta_r;

                                r_mid=0.5*(ro[j-1]+ro[j]);

                                uo=uo+pow((C1o*r_mid+C2o/r_mid-C3o),1/m)*delta_r;

                                Qo=Qo+pi*(pow(ro[j-1],2)-pow(ro[j],2))*uo;

                        }

                        upi=ui; upo=uo;

                        if(upi>upo) {Tw_max=Twi;} else {Tw_min=Twi;}

                }

                up=0.5*(upi+upo);

                Qp=pi*(pow(b,2)-pow(a,2))*up;

                Q_Total=Qi+Qo+Qp;



                //      pipe rotation section
[…]

        {
                cout<<"At this point integral was returned to be equal to 0.0, thus
skipping s-loop."<<endl;
                i=1000000;
                b_star_Min=0;
                b_star_Max=10;
                //cin.get();
```

```
                //cin.ignore();
        }


        while (i<1000000)
        {

                i=i+1;
                b_star_L=b_star+i*0.01*b_star;
                b_star_R=b_star-i*0.01*b_star;

                integral_L=Integral_M2(Ro,Ri,Ty,dpdz,m,K,M,a_star,b_star_L);
                integral_R=Integral_M2(Ro,Ri,Ty,dpdz,m,K,M,a_star,b_star_R);

                if(integral>0 && integral_L<0)
{b_star_Max=b_star;b_star_Min=b_star_L;break;}
                if(integral>0 && integral_R<0)
{b_star_Max=b_star;b_star_Min=b_star_R;break;}
                if(integral<0 && integral_L>0)
{b_star_Min=b_star;b_star_Max=b_star_L;break;}
                if(integral<0 && integral_R>0)
{b_star_Min=b_star;b_star_Max=b_star_R;break;}

        }

        integral_Med=1;
        integral_Med_tol=0.00000000000001;
        i=0;

        while (fabs(integral_Med)>integral_Med_tol)
        {
                b_star_Med=   0.5*(b_star_Min + b_star_Max);

                integral_Med=Integral_M2(Ro,Ri,Ty,dpdz,m,K,M,a_star,b_star_Med);

                if (integral_Med > 0)
                {
                        b_star_Max = b_star_Med;
                }
                else
                {
                        b_star_Min = b_star_Med;
                }

                i=i+1;
                if (i==60)
                {integral_Med_tol=integral_Med_tol*10;
                i=0;
                cout<<"\nIntegral_Med_tol was increased to: "<<integral_Med_tol<<endl;
                }
        }

//      Axial Velocity Profile ----------------------------------------------------

        b_star = b_star_Med;

        delta_r=(Ro-Ri)/(N-1);

[…]
                alpha=pow(pow(M/(2*pi*pow(r_med,2)),2)
                        +pow(b_star/r_med-a_star*r_med/2,2),0.5);
```

```
		if (alpha>Ty)
		{

			shear_rate=pow((alpha-Ty)/K,1/m);
		}
		else
		{
			shear_rate=0.0;
		}

		dudr=shear_rate/alpha*(b_star/r_med-a_star*r_med/2);

		u[j]=u[j-1]+dudr*delta_r;

		Qr=Qr+(u[j]+u[j-1])*pi*r_med*delta_r;

	}

//	Angular Velocity Profile ---------------------------------------------------

	r[N-1]=Ro;dwdr=0.0,w[N-1]=0.0;

	for (j=1;j<=N-1;j++)
	{

		r[N-1-j]=r[N-j]-delta_r;

		r_med=0.5*(r[N-1-j]+r[N-j]);

		alpha=pow(pow(M/(2*pi*pow(r_med,2)),2)
			+pow(b_star/r_med-a_star*r_med/2,2),0.5);


		if (alpha>Ty)
		{

			shear_rate=pow((alpha-Ty)/K,1/m);
		}
		else
		{
			shear_rate=0.0;
		}

		dwdr=M*shear_rate/(2*pi*pow(r_med,3)*alpha);

		w[N-1-j]=w[N-j]+dwdr*delta_r;

		dhdr[N-1-j]=r_med*Den*pow(0.5*(w[N-j]+w[N-1-j]),2);

	}

//	Pressure Distribution Profile ----------------------------------------------
--

	r[N-1]=Ro;p[0]=0.0;

	for (j=1;j<=N-1;j++)
	{

	p[j]=p[j-1]+dhdr[j-1]*delta_r;
```

```
	}


	dpdz=0.0;

	loop10: return Qr;

	}


//*************************************************************************//
//*    Name:         Integral_M
                                  *//
//* Purpose:  to determine the value of integral given by Eq. 3.11         *//
//* Author:          Ramadan Ahmed
                         *//
//* Date:            Oct 2005
Upgraded July 2012 by Henrik Næsgaard
                                     *//
//*
                                                  *//
//*************************************************************************//

	double Integral_M2 (double Ro,double Ri,double Ty,double dpdz,
		double m,double K, double M, double a_star,double b_star)
	{

//		const int Max=2001;

		double pi=3.141592654,integral=1.0;
		double shear_rate,alpha,delta_r,r_med;
		int N=Max,j;


		delta_r=(Ro-Ri)/(N-1);

[…]
			alpha=pow(M/(2*pi*pow(r_med,2)),2)
				+pow(b_star/r_med-a_star*r_med/2,2);

			alpha=pow(alpha,0.5);

			if (alpha>Ty)
			{
				shear_rate=pow((alpha-Ty)/K,1/m);
			}
			else
			{
				shear_rate=0.0;
			}

			integral = integral+shear_rate/alpha*(b_star/r_med-
a_star*r_med/2)*delta_r;

		}

		return integral;
	}
```

Appendix E – Error source for no convergence of low flowrates

Probably one of the biggest problems with the new model, or more specifically its program counterpart, is that for some specific scenarios with low flowrates, no convergence is achieved.

The main part of the program goes through an iterative loop to find the pressure loss that gives the desired flowrate. As seen in FFFF, the normal case with a solution will give a curve that shows a trend and a unique solution. This solution is the intersection between the blue (calculated flowrate) and the red line (desired flowrate).

In the case of no convergence, the problem that occurs is that the trend is irregular and we have several solutions, see FFFXXX.

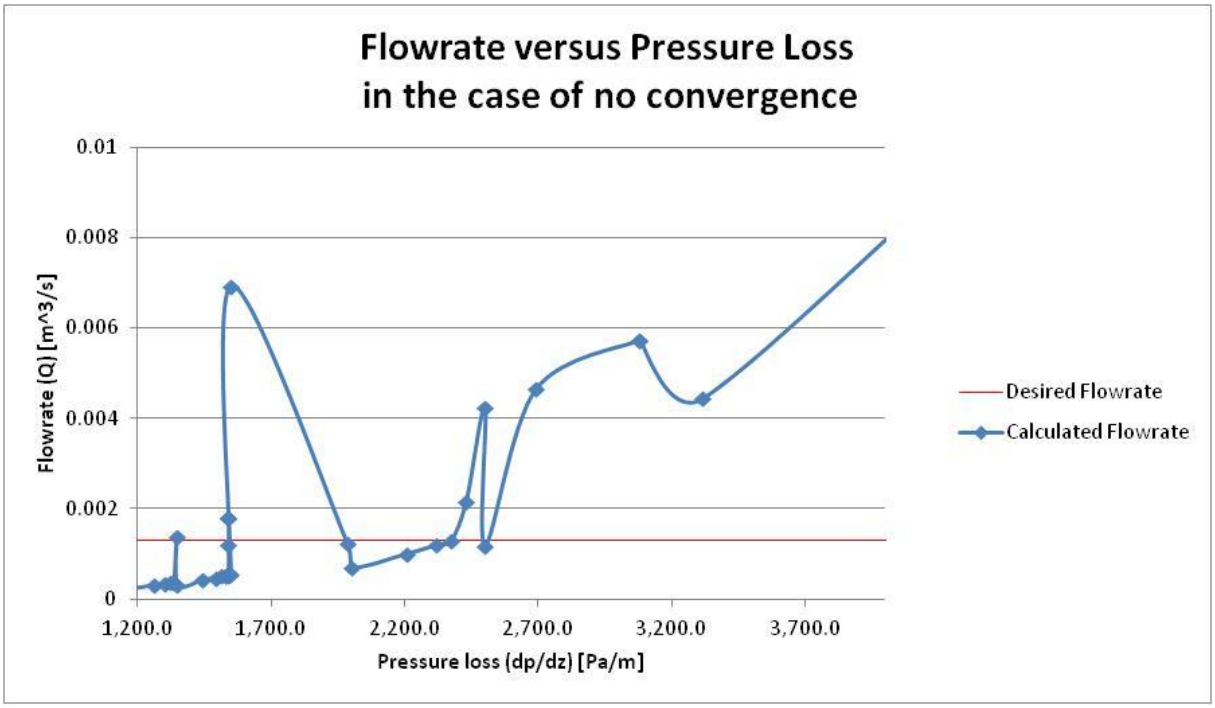

Figure LIV - Flowrate versus Pressure Loss in the case of no convergence

To better portray the irregularities, Table G shows the calculated flowrate for each pressure loss for the curve above. It shows that for a change in the eight decimal of the pressure loss, the flowrate may increase more than threefold before dropping down back to the expected numbers. The pressure loss of 1540.18262970 Pa/m is shown thrice, because the calculations were confirmed several times. No solution has been found for this problem yet.

Table G – Calculated flowrate against pressure loss in the case of no convergence

Pressure Loss [Pa/m]	Calculated Flowrate [m^3/s]
1492.10000000	0.000470
1516.10000000	0.000510
1528.10000000	0.000520
1534.20000000	0.000530
1537.20000000	0.000530
1540.10928082	0.000539
1540.17000000	0.000539
1540.17087904	0.000539
1540.17675437	0.000539
1540.18000000	0.000539
1540.18262953	0.000539
1540.18262960	0.000539
1540.18262969	0.000539
1540.18262970	0.001792
1540.18262970	0.001792
1540.18262970	0.001792
1540.18262975	0.000539
1540.18276485	0.000539
1540.18290000	0.000539
1540.18300000	0.000539
1540.20000000	0.000539
1540.23727012	0.000539